國立臺灣大學電機資訊學院光電工程學研究所

碩士論文

Graduate Institute of Photonics and Optoelectronics
College of Electrical Engineering and Computer Science
National Taiwan University

Master Thesis

光學透明化運用在人體離體與活體皮膚之倍頻影像術上的效用與機制

Investigate the Optical Clearing Effects and Mechanisms of *Ex Vivo* and *In Vivo* Human Skin with Glycerol Application by Harmonic Generation Microscopy

賴嘉泓

Jia-Hong Lai

指導教授：孫啟光 博士

Advisor: Chi-Kuang Sun, Ph.D.

中華民國 109 年 1 月

January 2020

doi:10.6342/NTU202000120

誌謝

沒想到一步一步這樣走著，也總算到了盡頭，這是一段漫長的日子，途中遇到的困難與挑戰沒有少過，也不斷地懷疑自己，整個碩士生涯都心裡都覺得心理壓力很大，有種看不見盡頭的感覺，一路走來，最想感謝的是自己，感謝自己的努力，感謝自己的堅持，感謝我自始自終沒有放棄。

謝謝孫啟光老師一路的悉心指導，給我機會與方向，讓我能夠成長，也提出了很多很好的看法，跳脫框架的思考，讓我看見不一樣的思維，一生受用。最後與老師密集討論論文與文章的日子，也讓我非常過癮，我們彼此討論著文章的邏輯架構，提出各自的想法，整合出最好的說法，一起期待文章的發表能有最好的結果，也謝謝廖怡華醫師一路上幫助我完成臨床試驗。

這漫長的日子中，做了好多的事情，從碩一開始學習如何建實驗室，碩二開始架系統、處理雷射，學習如何當個”工程師”，到之後碩三、碩四改成研究皮膚透明化、寫文章，學習如何當個”科學家”。在這裡的每一刻，都受到好多人的陪伴與幫助。碩一指導我研究方法與態度的鄭天佑博士，嚴謹以及有耐心地指導我，讓我在之後的碩士生涯能夠獨當一面。感謝實驗室助理 Rebecca，當我初期管理實驗室的時候常犯錯，受到蕾姊很多行政上的幫忙以及心理上的支持。感謝 Anatoly 與政翰學長教我對光、架雷射，也從他們的身上學到很多聰明且實用的小方法。謝謝 Bhaskar 在我們當初沒日沒夜建系統的時候一起努力，看到現在系統能成功運作，我非常感動。感謝李志昌博士指導我關於動物實驗的相關知識。感謝學長弈廷、從豈對我課業上的指導，還要特別感謝浩正在我最後做研究的時候，幫助我實驗、陪著我討論，也給了我很多的建議與支持，從浩正的身上，我學到很多。謝謝 Alicia 百忙之中抽空，協助我修改論文，在我寫論文的初期給了莫大的幫助。謝謝學長銘良，幫忙我處理臨床試驗的申請。謝謝我的同學，廷翰以及潘益，我們一起辛苦過來。謝謝最後一段時間陪我吃飯，一起承受很大壓力的好學弟承霖。謝謝實驗室夥伴，沈博、Sandeep、薈元、鵬瑞、沛哲、敏慈、政浩、勝澤，在這段時間的各種協助。

謝謝百仁男子天團: 柏淵、子揚、淶鈞、欣融、文杰、王鈞、翊誠、尹政、挺軒，

doi:10.6342/NTU202000120

有你們陪伴、鼓勵與打屁，讓這段時間能有一個情緒的出口。謝謝陪我打球的螢火蟲戰隊，長泰、正中。謝謝幫助我做人體實驗的所有好朋友們。然後要感謝我的女朋友彩瑄，在我這段努力畢業的日子裡面，不離不棄的陪伴我，知道這些日子對你來說也很艱難，也讓你委屈。你值得過更好的日子，我會更加努力。

最後要感謝我的父母支持，同年紀的孩子已經很多出外賺錢孝順父母了，我卻還不能讓你們享清福，也謝謝你們對我的決定，沒有過多的質疑以及否定，這段在外讀書的日子，陪伴你們的日子真的很少，我也會努力達成你們的期待，做個成功而且孝順的孩子，愛你們。

僅將此論文獻給所有給過我幫助的人們，謝謝!

doi:10.6342/NTU202000120

中文摘要

光學清潔法可用來提升光學顯微鏡的成像品質與深度。然而，由於缺乏影像的細節資訊，其運用在人體皮膚上的效果與機制仍未被完全了解。此研究中，我們使用倍頻顯微鏡，藉由結合三倍頻與二倍頻的高解析度影像，研究光學清潔法使用在離體與活體皮膚上的效用與機制。實行光學清潔法後，樣品內部的折射率均勻度提升，造成三倍頻影像強度在上表皮衰減，而二倍頻影像在下表皮的強度變化作為一個可靠的指標，顯示光學散射在上表皮的減少。結合這兩個影像技術，可以獲得更多關於光學清潔法的細節。

在離體皮膚的研究裡，我們將九位受試者分配到四種不同的實驗條件，分別將皮膚樣品浸泡或是表面塗抹上 100% 或是 50% 的甘油，研究在不同狀況下的光學清潔效果。在 50% 塗抹的實驗條件下，發現角質層扮演一個重要的關鍵，其光學清潔效果在厚角質層的皮膚樣品更為明顯。

過去光學清潔法在活體皮膚的研究中，使用在手臂內側與手掌的結果有很大的差異，在薄角質層的部位，效果非常薄弱。這些過去的活體皮膚研究也與我們的離體皮膚研究也發現一樣的結果。然而，許多的光學療法以及光學診斷都是運用在薄角質層的地方，光學清潔法使用在此類薄角質皮膚上的效果及機制仍需要被研究與了解。在此研究的活體皮膚部分，我們將 50% 甘油塗抹在手前臂內側，我們將八位受試者分配到四種不同的作用時間（15, 30, 90, 180 分鐘），發現光學清潔法的效果在 90 分鐘以內的效用不明顯，而在 180 分鐘作用後，在三個受試者中有兩位有明顯的效果，在此類薄角質層皮膚的部位，越長的作用時間，有越高的機率達成光學清潔的效用。

關鍵字：光學清潔法、活體皮膚、離體皮膚、甘油、三倍頻、二倍頻

doi:10.6342/NTU202000120

ABSTRACT

Imaging depth and quality of the optical microscopy can be enhanced by using the method of the optical clearing. However, the optical clearing effects and mechanisms in human skin remain largely unclear due to the lack of detailed image information. Here we investigate the optical clearing of the *ex vivo* and *in vivo* human skin by glycerol application. Harmonic generation microscopy, by combining second and third harmonic generation (THG) modalities, was utilized to retrieve high-resolution skin images. The THG image intensity in the epidermis is decreased due to the optical homogeneity after optical clearing, and the second harmonic generation (SHG) image intensity in the dermis is a beacon to confirm the reduction of the scattering in the epidermis layer. Combining these two image information, the details of the optical clearing effects can be well studied. For *ex vivo* experiment, nine different volunteers were separated into four different case types to study and unravel the optical clearing mechanisms. The 100% or 50% glycerol is applied on the skin by immersion or topical application. For the case type of 50% glycerol combined with the topical application, the method which can be used for the further *in vivo* or clinical research, SC acts the most important role. We observed stronger OC effect in thicker SC skin tissues.

For the previous *in vivo* human optical clearing studies, the effect between the volar forearm and palm showed different results. The optical clearing effect was found less

doi:10.6342/NTU202000120

effective in the skin area with thinner SC. The same result was also noted in our *ex vivo* experiment. However, it is essential to study the optical clearing on the skin with thinner SC, the area where the light therapeutic and dermatological diagnosis often focus on. In this study, we investigated the OC effect on the *in vivo* volar forearm by using 50% glycerol with topical application. For *in vivo* experiment, eight different volunteers were separated into four different applying time (15, 30, 90, and 180 minutes) to unravel the optical clearing mechanisms. The results showed that the optical clearing was less effective within 90 minutes application. After 180 minutes application, two of three cases were found the effect of the optical clearing. In the skin area with thinner SC, there was a higher probability to witness the optical clearing effects after a longer applying time.

Keywords: optical clearing, in vivo human skin, ex vivo human skin, glycerol, third-harmonic generation, second-harmonic generation.

doi:10.6342/NTU202000120

CONTENT

誌謝

中文摘要 i

ABSTRACT ii

CONTENT iv

LIST OF FIGURES vii

LIST OF TABLES xvi

Chapter 1 Introduction 1

1.1 Motivation 1

1.2 Thesis Scope 4

Chapter 2 Background Knowledge 6

2.1 The Skin 6

2.1.1 Skin Structure and Barrier Function of the Stratum Corneum 6

2.1.2 Glycerol and the Human Skin 8

2.2 Optical Clearing 9

2.2.1 Optical Clearing of the *Ex Vivo* Skin Experiments 10

2.2.2 Optical Clearing of the *In Vivo* Skin Experiments 16

2.2.2.1 Optical Clearing of *In Vivo* Rat Skin Experiments 17

2.2.2.2 Optical Clearing of *In Vivo* Human Skin Experiments 20

2.3 Basic Theory of Harmonic Generation 24

2.3.1 Second Harmonic Generation 24

2.3.2 Third Harmonic Generation 26

Chapter 3 Method and Materials of the *In vivo* and the *Ex Vivo* Optical Clearing Experiments 29

3.1 Experimental Protocol of the *Ex Vivo* Optical Clearing 29

doi:10.6342/NTU202000120

3.1.1 Skin Sample Preparation 32
3.1.2 Glycerol Solution Preparation 34
3.1.3 Skin Slide Preparation 34
3.1.4 Glycerol Solution Application with the Skin Tissue 35
3.2 System Set Up and Virtual Biopsy of the *Ex Vivo* Optical Clearing 36
3.2.1 Bright-field Imaging 36
3.2.2 Harmonic Generation Microscopy 37
3.2.3 THG and SHG imaging of the *Ex Vivo* Human Skin 39
3.3 Experimental Protocol of the *In Vivo* Human Skin Image Clearance 42
3.3.1 Scanning Region Selection and Preparation 43
3.3.2 Noninvasiveness and Photodamage Concern 45
3.3.3 THG and SHG imaging of *In Vivo* Human Skin 46
3.4 Analysis Methods of HGM Skin Image 47
3.4.1 Image Processing of HGM Image 47
3.4.2 Blinding 48
3.4.3 Thickness Analysis 50
3.4.4 Intensity Analysis 52
Chapter 4 Results of the *Ex Vivo* Optical Clearing 54
4.1 System Calibration by Using Gallium Nitrite 54
4.2 Bright-filed Image 56
4.3 Statistical Analysis of HGM Image and Representative HGM Images 58
4.3.1 Tissue Immersed by 100% Glycerol for 90 Minutes (E100-I90) 59
4.3.2 Tissue Immersed by 50% Glycerol for 90 Minutes (E50-I90) 65
4.3.3 Topically Applied by 50% Glycerol for 90 Minutes (E50-T90) 71
4.4 Summary of the *Ex Vivo* Optical Clearing Results 82

doi:10.6342/NTU202000120

Chapter 5 Discussion of the *Ex Vivo* Optical Clearing 84

5.1 Optical Clearing Effects and Mechanisms by Utilizing 100% Glycerol with the Tissue Immersion Technique 84

5.1.1 Bight-field Imaging 84

5.1.2 HGM Imaging 84

5.1.3 Skin Structure Analysis 86

5.2 100% Glycerol Immersion V.S. 50% Glycerol Immersion 86

5.3 50% Glycerol with Topical Application 88

5.4 The Relationship between the SC and the HGM Intensity Variation 90

5.5 Conclusion of the *Ex Vivo* Optical Clearing 94

Chapter 6 Results of the *In Vivo* Optical Clearing 96

6.1 System Calibration by Using Gallium Nitrite 99

6.2 Statistical Analysis of HGM Image and Representative HGM Images 101

6.2.1 Structure and HGM Intensity Analysis of Case I50-T15 101

6.2.2 Structure and HGM Intensity Analysis of Case I50-T30 104

6.2.3 Structure and HGM Intensity Analysis of Case I50-T90 110

6.2.4 Structure and HGM Intensity Analysis of Case I50-T180 115

6.3 Summary of the *In Vivo* Optical Clearing Results 123

Chapter 7 Discussion of the *Ex Vivo* Optical Clearing 125

7.1 Case I50-T180-1 125

7.2 Case I50-T180-3 127

7.3 Case I50-T30-1 127

7.4 Conclusion 128

Chapter 8 Summary 131

References 134

doi:10.6342/NTU202000120

LIST OF FIGURES

Fig. 2.1 The skin structure from the stratum corneum to the dermis. 8

Fig. 2.2 Simple physical picture of the SHG theory. 25

Fig. 2.3 Simple physical picture of the THG theory. 27

Fig. 3.1 Flow chart of whole *ex vivo* experiment. 32

Fig. 3.2 Human skin sample preparation (a) The original skin sample with fat tissue. (Red circle) (b) Remove the fat tissue under the dermal. (c) The skin sample was separate into two parts. The size of each part will be larger than 0.5*0.5 $mm2$ 34

Fig. 3.3 (a) iSpacer fix on the slide to form a space and watertight well. (b) & (c) Use clay to fix cover slip and slide together. (d) One of the finished slides with skin sample and water inside. 35

Fig. 3.4 (a) Skin sample was immersed into the glycerol solution. (b) We used a brush to make the skin surface covered by glycerol solution. 36

Fig. 3.5 Optical system setup. DBS: dichroic beam splitter; BPF: band-pass filter; PMT: photomultiplier tube. 39

Fig. 3.6 (a) A gallium nitrite (GaN) sample with some scotch (A1Z003) on it. (b) Imaged by bright light microscopy. (LEICA ICC50 HD). We choose the top of first letter “A” to image by our HGM. (c) & (d) The HGM images of the GaN before taking the image of the control group and taking the image of the glycerol group. There’s no big difference between each other. Laser power (after the objective lens): 20 mW, Average frame: 10 frames/frame. PMT setting: 400 V for SHG channel. 40

Fig. 3.7 (a) The slide fixed on the 2D stage which could manually adjust the scan area to get the image of different position. (b) Red circle: An objective lens. When

doi:10.6342/NTU202000120

we started to scan, it moved automatically to get a stack of images. 41

Fig. 3.8 Flow chart of whole *in vivo* experiment. 43

Fig. 3.9 (a) The waterproof tape (3M™ Tegaderm™) with the hole in the center to mark the position of the region of interest at the forearm. (b) Glycerol application for the *in vivo* experiment. We used second waterproof tape to seal the glycerol solution on the skin surface. 44

Fig. 3.10 (a) A volunteer was laying on the electric hospital bed. A red circle is the scanning head of our HGM system. (b) The details of the scanning head: Object lens (water immersion) was fixed on the system and covered by an adapter. This adapter not only separated the skin and objective lens to prevent from direct contact with each other by using coverslip but also kept water inside of it to create the water immersion condition for the *in vivo* experiment..... 47

Fig. 3.11 (a) Grayscale image of the THG signal. (b) Grayscale image of SHG image at the same skin depth of THG image. (c) Image after combining SHG and THG. (d) Color remapping of SHG and THG signal. (Green: SHG, Red: THG)..... 48

Fig. 3.12 The HGM images of human skin obtained at different depth with different skin structures. Here we defined the thickness of SC, the thickness of viable epidermis, the depth of the basal layer, the depth of the middle papillary dermis, and the depth of the top reticular dermis. Scale bar: 100 μm..... 52

Fig. 4.1 SHG images of GaN for system calibration. Left: The reference SHG image before taking the HGM skin image of the control group. Right: The SHG image before taking the HGM skin image of the glycerol group. (PMT setting: 400 Volt, Contrast: 400~4500, Illuminate power: 20 mW). It was only a little difference and indicates that the system condition remained the same. (a) Case E100-I90-1 (b) Case E100-I90-2 54

doi:10.6342/NTU202000120

Fig. 4.2 SHG images of GaN for system calibration. Left: The SHG image before taking the HGM skin image of the control group. Right: The reference SHG image before taking the HGM skin image of the glycerol group. (PMT setting: 400 Volt, Contrast: 400~4500, Illuminate power: 20 mW). It was only a little difference and indicates that the system condition remained the same. (a) Case E50-I90-1 (b) Case E50-I90-2 54

Fig. 4.3 SHG images of GaN for system calibration. Left: The reference SHG image before taking the HGM skin image of the control group. Right: The SHG image before taking the HGM skin image of the glycerol group. (PMT setting: 400 Volt, Contrast: 400~4500, Illuminate power: 20 mW). It was only a little difference and indicates that the system condition remained the same. (a) Case E50-T90-1 (b) Case E50-T90-2 (c) Case E50-T90-3 (d) Case E50-T90-4 55

Fig. 4.4 Bright field images taken by Leica ICC50 HD. Left: normal skin. Right: skin after immersed into 100% glycerol for 90 mins. The transmission light increased and the deeper hair became visible. Scale bar: 1 mm. (a) Case E100-I90-1 (b) Case E100-I90-2 56

Fig. 4.5 Bright field images taken by Leica ICC50 HD. Left: normal skin. Right: skin after immersed into 50% glycerol for 90 mins. The transmission light increased and the deeper hair became visible. (a) Case E50-I90-1 (b) Case E50-I90-2 57

Fig. 4.6 Bright field images taken by Leica ICC50 HD. Left: normal skin. Right: skin after topically applied with 50% glycerol for 90 mins. (a) Case E50-T90-1 (b) Case E50-T90-2 (c) Case E50-T90-3 (d) Case E50-T90-4 58

Fig. 4.7 Quantitative analysis and comparison of skin THG intensities at five different depths. Black: Case E100-I90-1 (control: N=8, glycerol: N=8); Red: Case E100-I90-2 (control: N=9, glycerol: N=9). *P <0.05; **P <0.01; *** P <0.001. C:

doi:10.6342/NTU202000120

control; G: glycerol..... 60

Fig. 4.8 Quantitative analysis and comparison of skin SHG intensities at three different depths. Black: Case E100-I90-1 (control: N=8, glycerol: N=8); Red: Case E100-I90-2 (control: N=9, glycerol: N=9). *P <0.05; ** P <0.01; *** P <0.001. C: control; G: glycerol..... 61

Fig. 4.9 *En face* skin image of Case E100-I90-1 (a) Glycerol-1 (b) Glycerol-2 (c) Control-1 (d) Control-2. Red: THG (Contrast setting: 600~10000). Green: SHG (Contrast setting: 600~4500). 63

Fig. 4.10 *En face* skin image of Case E100-I90-2 (a) Glycerol-1 (b) Glycerol-2 (c) Control-1 (d) Control-2. Red: THG (Contrast setting: 600~10000). Green: SHG (Contrast setting: 600~4500). 65

Fig. 4.11 Quantitative analysis and comparison of skin THG intensities at five different depths. Black: Case E50-I90-1 (control: N=6, glycerol: N=6); Red: Case E50-I90-2 (control: N=12, glycerol: N=12). *P <0.05; **P <0.01; *** P <0.001. C: control. G: glycerol. 67

Fig. 4.12 Quantitative analysis and comparison of skin SHG intensities at three different depths. Black: Case E50-I90-1 (control: N=6, glycerol: N=6); Red: Case E50-I90-2 (control: N=12, glycerol: N=12). *P <0.05; **P <0.01; *** P <0.001. C: Control. G: glycerol. 67

Fig. 4.13 *En face* skin image of Case E50-I90-1 (a) Glycerol-1 (b) Glycerol-2 (c) Control-1 (d) Control-2. Red: THG (Contrast setting: 600~10000). Green: SHG (Contrast setting: 600~8000). 69

Fig. 4.14 *En face* skin image of Case E50-I90-2 (a) Glycerol-1 (b) Glycerol-2 (c) Control-1 (d) Control-2. Red: THG (Contrast setting: 600~10000). Green: SHG (Contrast setting: 600~4500). 71

doi:10.6342/NTU202000120

Fig. 4.15 Quantitative analysis and comparison of skin THG intensities at five different depths. Black: Case E50-T90-1 (control: N=8, glycerol: N=8); Red: Case E50-T90-2 (control: N=10, glycerol: N=10). Blue: Case E50-T90-3 (control: N=9, glycerol: N=9). Magenta: Case E50-T90-4 (control: N=7, glycerol: N=7). *P <0.05; **P <0.01; *** P <0.001. C: control; G: glycerol 74

Fig. 4.16 Quantitative analysis and comparison of skin SHG intensities at three different depths. Black: Case E50-T90-1 (control: N=8, glycerol: N=8); Red: Case E50-T90-2 (control: N=10, glycerol: N=10). Blue: Case E50-T90-3 (control: N=9, glycerol: N=9). Magenta: Case E50-T90-4 (control: N=7, glycerol: N=7). *P <0.05; **P <0.01; *** P <0.001. C: control; G: glycerol. 74

Fig. 4.17 *En face* skin image of Case E50-T90-1 (a) Glycerol-1 (b) Glycerol-2 (c) Control-1 (d) Control-2. Red: THG (Contrast setting: 600~6000). Green: SHG (Contrast setting: 600~8000). 76

Fig. 4.18 *En face* skin image of Case E50-T90-2 (a) Glycerol-1 (b) Glycerol-2 (c) Control-1 (d) Control-2. Red: THG (Contrast setting: 600~10000). Green: SHG (Contrast setting: 600~4500). 78

Fig. 4.19 *En face* skin image of Case E50-T90-3 (a) Glycerol-1 (b) Glycerol-2 (c) Control-1 (d) Control-2. Red: THG (Contrast setting: 600~10000). Green: SHG (Contrast setting: 600~6000). 80

Fig. 4.20 *En face* skin image of Case E50-T90-4 (a) Glycerol-1 (b) Glycerol-2 (c) Control-1 (d) Control-2. Red: THG (Contrast setting: 600~8000). Green: SHG (Contrast setting: 600~6000). 82

Fig. 5.1 The variation of the THG intensity at the middle epidermis layer. We presented and compared the THG intensity variation at the middle epidermis layer of Case E100-I90-1 and Case E50-I90-2. C: control; G: glycerol. (a) In the Case of

doi:10.6342/NTU202000120

100% glycerol immersion (Case E100-I90-1), the THG intensity greatly reduced. (b) However, in the case of 50% glycerol immersion (Case E50-I90-2), the THG intensity greatly increased, opposite from (a). Scale bar = 100 μm. 88

Fig. 5.2 *En face* skin image of Case E100-T30-1 (a) Glycerol-1 (b) Glycerol-2 (c) Control-1 (d) Control-2. Red: THG (Contrast setting: 600~10000). Green: SHG (Contrast setting: 600~8000). 92

Fig. 6.1 SHG images of GaN for system calibration of Case I50-T15-1. Left: The reference SHG image before taking the HGM skin image of the control group. Right: The SHG image before taking the HGM skin image of the glycerol group. (PMT setting: 400 Volt, Contrast: 400~4500, Illuminate power: 20 mW). It is only a little difference and indicates that the system condition remained the same. 99

Fig. 6.2 SHG images of GaN for system calibration. Left: The reference SHG image before taking the HGM skin image of the control group. Right: The SHG image before taking the HGM skin image of the glycerol group. (PMT setting: 400 Volt, Contrast: 400~4500, Illuminate power: 20 mW). It is only a little difference and indicates that the system condition remained the same. (a) Case I50-T30-1 (b) Case I50-T30-2 99

Fig. 6.3 SHG images of GaN for system calibration. Left: The reference SHG image before taking the HGM skin image of the control group. Right: The SHG image before taking the HGM skin image of the glycerol group. (PMT setting: 400 Volt, Contrast: 400~4500, Illuminate power: 20 mW). It is only a little difference and indicates that the system condition remains the same. (a) Case I50-T90-1 (b) Case I50-T90-2 100

Fig. 6.4 SHG images of GaN for system calibration. Left: The reference SHG image before taking the HGM skin image of the control group. Right: The SHG

doi:10.6342/NTU202000120

image before taking the HGM skin image of the glycerol group. (PMT setting: 400 Volt, Contrast: 400~4500, Illuminate power: 20 mW). It is only a little difference and indicates that the system condition remained the same. (a) Case I50-T180-1 (b) Case I50-T180-2 (c) Case I50-T180-3 100

Fig. 6.5 Quantitative analysis and comparison of skin THG intensities at five different depths. Black (control: N=10, glycerol: N=10). 102

Fig. 6.6 Quantitative analysis and comparison of skin SHG intensities at three different depths. Black (control: N=10, glycerol: N=10). 102

Fig. 6.7 *En face* skin image of Case I50-T15-1 (a) Glycerol-1 (b) Glycerol-2 (c) Control-1 (d) Control-2. Red: THG (Contrast setting: 600~10000). Green: SHG (Contrast setting: 600~8000). 104

Fig. 6.8 Quantitative analysis and comparison of skin THG intensities at five different depths. Black: Case I50-T30-1 (control: N=10, glycerol: N=10); Red: Case I50-T30-2 (control: N=10, glycerol: N=10). **P <0.01; *** P <0.001. C: control; G: glycerol. 105

Fig. 6.9 Quantitative analysis and comparison of skin SHG intensities at three different depths. Black: Case I50-T30-1 (control: N=10, glycerol: N=10); Red: Case I50-T30-2 (control: N=10, glycerol: N=10). ** P <0.01. C: control; G: glycerol. .. 106

Fig. 6.10 *En face* skin image of Case I50-T30-1 (a) Glycerol-1 (b) Glycerol-2 (c) Control-1 (d) Control-2. Red: THG (Contrast setting: 600~15000). Green: SHG (Contrast setting: 600~10000). 108

Fig. 6.11 *En face* skin image of Case I50-T30-2 (a) Glycerol-1 (b) Glycerol-2 (c) Control-1 (d) Control-2. Red: THG (Contrast setting: 600~10000). Green: SHG (Contrast setting: 600~8000). 110

Fig. 6.12 Quantitative analysis and comparison of skin THG intensities at five

doi:10.6342/NTU202000120

different depths. Black: Case I50-T90-1 (control: N=6, glycerol: N=6); Red: Case I50-T90-2 (control: N=6, glycerol: N=6). *P <0.05. C: control; G: glycerol. 111

Fig. 6.13 Quantitative analysis and comparison of skin SHG intensities at three different depths. Black: Case I50-T90-1 (control: N=8, glycerol: N=8); Red: Case I50-T90-2 (control: N=9, glycerol: N=9). C: control; G: glycerol. 111

Fig. 6.14 *En face* skin image of Case I50-T90-1 (a) Glycerol-1 (b) Glycerol-2 (c) Control-1 (d) Control-2. Red: THG (Contrast setting: 600~15000). Green: SHG (Contrast setting: 600~8000) 113

Fig. 6.15 *En face* skin image of Case I50-T90-2 (a) Glycerol-1 (b) Glycerol-2 (c) Control-1 (d) Control-2. Red: THG (Contrast setting: 600~10000). Green: SHG (Contrast setting: 600~8000) 115

Fig. 6.16 Quantitative analysis and comparison of skin THG intensities at five different depths. Black: Case I50-T180-1 (control: N=7, glycerol: N=7); Red: Case I50-T180-2 (control: N=9, glycerol: N=9). Blue: Case I50-T180-3 (control: N=10, glycerol: N=10). *P <0.05; *** P <0.001. C: control; G: glycerol 117

Fig. 6.17 Quantitative analysis and comparison of skin SHG intensities at three different depths. Black: Case I50-T180-1 (control: N=7, glycerol: N=7); Red: Case I50-T180-2 (control: N=9, glycerol: N=9). Blue: Case I50-T180-3 (control: N=10, glycerol: N=10). *P <0.05. C: control; G: glycerol. 117

Fig. 6.18 *En face* skin image of Case I50-T180-1 (a) Glycerol-1 (b) Glycerol-2 (c) Control-1 (d) Control-2. Red: THG (Contrast setting: 600~10000). Green: SHG (Contrast setting: 600~8000) 119

Fig. 6.19 *En face* skin image of Case I50-T180-2 (a) Glycerol-1 (b) Glycerol-2 (c) Control-1 (d) Control-2. Red: THG (Contrast setting: 600~15000). Green: SHG (Contrast setting: 600~8000) 121

doi:10.6342/NTU202000120

Fig. 6.20 *En face* skin image of Case I50-T180-3 (a) Glycerol-1 (b) Glycerol-2 (c) Control-1 (d) Control-2. Red: THG (Contrast setting: 600~15000). Green: SHG (Contrast setting: 600~8000) 123

doi:10.6342/NTU202000120

LIST OF TABLES

Table 3.1 Three different case types of the *ex vivo* optical clearing. 32

Table 3.2 Four different cases of the *in vivo* optical clearing. 43

Table 4.1 Skin structure analysis results of case E100-I90. (*P <0.05, ** P <0.01, *** P <0.001) 59

Table 4.2 The lateral HGM skin images at six different depths of the control group and the glycerol group. Red: THG (Contrast setting: 600~10000). Green: SHG (Contrast setting: 600~4500). 62

Table 4.3 The lateral HGM images of the control group and the glycerol group at different depths. Red: THG (Contrast setting: 600~10000). Green: SHG (Contrast setting: 600~4500). 63

Table 4.4 Skin structure analysis results of Case E50-I90. (*P <0.05, ** P <0.01, *** P <0.001) 66

Table 4.5 The lateral skin images of the control group and the glycerol group. We choose different skin layers to display the images. Red: THG (Contrast setting: 600~10000). Green: SHG (Contrast setting: 600~8000). 68

Table 4.6 The lateral skin images of the control group and the glycerol group. We choose different skin layers to display the images. Red: THG (Contrast setting: 600~10000). Green: SHG (Contrast setting: 600~4500). 70

Table 4.7 Skin structure analysis results of all studied cases. (*P <0.05, ** P <0.01, *** P <0.001) 72

Table 4.8 Case E50-T90-1: The lateral skin images of the control group and the glycerol group. Different skin layers images were presented. Red: THG (Contrast setting: 600~6000). Green: SHG (Contrast setting: 600~8000). 75

Table 4.9 Case E50-T90-2: The lateral skin images of the control group and the

doi:10.6342/NTU202000120

glycerol group. Different skin layer images were presented. Red: THG (Contrast setting: 600~10000). Green: SHG (Contrast setting: 600~4500). 76

Table 4.10 Case E50-T90-3: The lateral skin images of the control group and the glycerol group. Different skin layers images were presented. Red: THG (Contrast setting: 600~10000). Green: SHG (Contrast setting: 600~6000). 78

Table 4.11 Case E50-T90-4: The lateral skin images of the control group and the glycerol group. Different skin layers images were presented. Red: THG (Contrast setting: 600~8000). Green: SHG (Contrast setting: 600~6000). 80

Table 4.12 Skin structure analysis results of all studied cases. (*P <0.05, ** P <0.01, *** P <0.001) 82

Table 4.13 Statistical analysis result on the THG intensity variation after the glycerol application. (-: no significant difference, △: Increased significantly, ▽: Decreased significantly, *P <0.05, ** P <0.01, *** P <0.001) 82

Table 4.14 Statistical analysis result on the SHG intensity variation after the glycerol application. (-: no significant difference, △: Increased significantly, ▽: Decreased significantly, *P <0.05, ** P <0.01, *** P <0.001) 83

Table 5.1 Variation of skin structure, THG intensity, and SHG intensity after 100% glycerol topical application for 30 minutes. 90

Table 5.2 The lateral skin images of the control group and the glycerol group at different depths. Red: THG (Contrast setting: 600~10000). Green: SHG (Contrast setting: 600~8000). 91

Table 5.3 Mean SHG intensities (arbitrary unit) of all studied cases at the middle papillary dermis layer, top reticular dermis layer, and SHG maximum layer. *P <0.05, ** P <0.01, *** P <0.001. 93

Table 6.1 Skin structure analysis results of all studied cases. (*p<0.05, **p<0.01,

doi:10.6342/NTU202000120

***p<0.001)..... 101

Table 6.2 Case I50-T15-1: The lateral skin images at different skin layers of the control group and the glycerol group. Red: THG (Contrast setting: 600~10000). Green: SHG (Contrast setting: 600~8000). 102

Table 6.3 Skin structure analysis results of Case I50-T30. (*p<0.05, **p<0.01, ***p<0.001)..... 105

Table 6.4 Case I50-T30-1: The lateral skin images at different skin layers of the control group and the glycerol group. Red: THG (Contrast setting: 600~15000). Green: SHG (Contrast setting: 600~10000). 106

Table 6.5 Case I50-T30-2: The skin images at different skin depths of the control group and the glycerol group. Red: THG (Contrast setting: 600~10000). Green: SHG (Contrast setting: 600~8000). 108

Table 6.6 Skin structure analysis results of all studied cases. (*p<0.05, **p<0.01, ***p<0.001)..... 110

Table 6.7 Case I50-T90-1: The skin images at different depths of the control group and the glycerol group. Red: THG (Contrast setting: 600~15000). Green: SHG (Contrast setting: 600~8000)..... 112

Table 6.8 Case I50-T90-2: The skin images at different depths of the control group and the glycerol group. Red: THG (Contrast setting: 600~10000). Green: SHG (Contrast setting: 600~8000)..... 113

Table 6.9 Skin structure analysis results of all studied cases. (*p<0.05, **p<0.01, ***p<0.001)..... 116

Table 6.10 Case I50-T180-1: The skin images at different depths of the control group and the glycerol group. Red: THG (Contrast setting: 600~10000). Green: SHG (Contrast setting: 600~8000)..... 118

doi:10.6342/NTU202000120

Table 6.11 Case I50-T180-2: The skin images at different depths of the control group and the glycerol group. Red: THG (Contrast setting: 600~15000). Green: SHG (Contrast setting: 600~8000) 119

Table 6.12 Case I50-T180-3: The skin images at different depths of the control group and the glycerol group. Red: THG (Contrast setting: 600~15000). Green: SHG (Contrast setting: 600~8000) 121

Table 6.13 Skin structure analysis results of all studied cases. (*p<0.05, **p<0.01, ***p<0.001) 123

Table 6.14 Statistical analysis result on the THG intensity variation after the glycerol application. (-: no significant difference, △: Increased significantly, ▽: Decreased significantly, *p<0.05, **p<0.01, ***p<0.001) 123

Table 6.15 Statistical analysis result on the SHG intensity variation after the glycerol application. (-: no significant difference, △: Increased significantly, ▽: Decreased significantly, *p<0.05, **p<0.01, ***p<0.001) 124

doi:10.6342/NTU202000120

Chapter 1 Introduction

1.1 Motivation

Optical microscopy is a light-based technique with a resolving power that is much higher when compared to other conventional imaging techniques such as ultrasound, x-ray tomography, and MRI. Optical microscopy is able to provide resolution in the submicron range, enabling it to resolve the fine structure inside a tissue. Its application has been extended into neural science which successfully shows sensory information within the rat brain in distributed spatiotemporal patterns of neuronal activity [1]. Although capable of providing high-resolution parameters, its application of clinical study is still limited by the imaging depth. As light scattering and absorption introduce both light pulse broadening, defocusing, and decrement of intensity, it is likely that image quality and contrast will be compromised with increasing depth of imaging [2]. Thus, in order to overcome the depth limitation and enhance the image quality, researchers have attempted to reduce the scattering of tissue turbidity by matching the refractive index using various osmotic agents, a procedure known as optical clearing.

The optical clearing was first studied by Tuchin using human sclera in 1997 [3] and since then, it has been frequently studied for various tissues. Many types of optical clearing agents (such as glucose, glycerol, peg-400, and DMSO) were combined with

doi:10.6342/NTU202000120

different application methods (such as immersion, stratum corneum abrasion, injection, sonophoresis, micro-needle, and topical) to enhance optical clearing efficacy. Among these studies, skin optical clearing attracts high attention. The skin is the outermost organ of human, which acts as the barrier between organism and environment. Many skin diseases are related to morphological changes in the different skin layers. Early diagnosis of skin disease, studying age-related changes of morphology, and understanding drug delivery are essential in dermatology and cosmetology. However, the skin is a high scattering tissue that comprises multiple layers with a variation of refractive index. The turbid nature of the skin strongly decreases the imaging depth of the optical microscopy (OCT<2 mm [4], confocal<0.35 mm [5]). In order to increase the depth of investigation, the optical clearing technique of the skin was proposed. Although the effect and mechanisms of optical clearing have been studied by many different optical imaging techniques such as NIR spectrophotometer [3, 6-18], confocal microscopy [19-21], multi-photon microscopy [5, 22, 23], harmonic generation microscopy [5, 24], optical coherence tomography (OCT) [4, 9, 13, 15, 25-34], and Raman microscopy [35] in the past few decades, most of them focused on tissues *ex vivo* and rat *in vivo* imaging. The agents and methods which have proven effective for *ex vivo* tissue or *in vivo* rat have not yet been well applied for *in vivo* human studies due to the safety concerns, and for this reason, the optical clearing efficacy and mechanism remain unclear in human clinical

doi:10.6342/NTU202000120

examinations.

Glycerol is the mostly-used and well-studied optical clearing agent for tissue *ex vivo* and rat *in vivo* to provide a promising optical clearing effect. Glycerol solutions have been shown to improve the skin condition and it is also widely used in skin-care products due to its high hygroscopicity in keeping the skin hydrated. It is a low toxicity substance and applied for skin-care products (Glysolid Germany) at low concentrations (50%). While the skin optical clearing effect of glycerol has been studied in some *in vivo* human experiments using OCT and NIR spectrometer, most were unsafe due to invasive methods or inappropriate concentrations of glycerol, resulting in tissue damage. On the other hand, the optical clearing effect of low concentration (below 50%) glycerol due to the safety concern for noninvasive skin imaging is still unclear due to inconsistent results and insufficient data from the OCT images.

In this thesis, we aim to study the optical clearing of *ex vivo* and *in vivo* human skin by noninvasive harmonic generation microscopy (HGM). HGM microscopy provides a much higher resolution compared to OCT, which is most frequently used to study optical clearing. Sub-micron resolution and label-free characteristics of HGM make it a promising tool to image and resolve the different layers of *ex vivo* and *in vivo* human skin. Although the HGM is a useful tool for clinical imaging by combining the THG and SHG, there is no investigation about the clinical optical clearing by using HGM. We first

doi:10.6342/NTU202000120

addressed the optical clearing effects and its mechanisms using a combination of the second and third harmonic generation. This unprecedented approach will enable us to obtain more information to realize the optical clearing mechanism. We want to achieve the optical clearing of the *in vivo* human skin, expanding the application of the HGM in the clinical region.

This study will be initiated in *ex vivo* experiments using two concentrations of glycerol solutions (50% and 100%) by topical application or immersion. Human skin tissue will be imaged by HGM microscopy before and after the glycerol solutions application. At least six different stacks of the image at different positions of each human skin were collected and averaged to obtained quantitative and statistical information of optical clearing efficiency. The subcellular resolution of the HGM image also enables us to directly observe the morphology change and the thickness variation of each skin layer, providing more information to study the mechanism of the optical clearing. For the *in vivo* human experiment, the same experimental and analytical processes will be carried out but with only 50% glycerol topically on the human forearm due to the safety concern. As the final goal of optical clearing research is the *in vivo* application, this study serves as a guide for future research of *in vivo* optical clearing of the human skin.

1.2 Thesis Scope

In chapter 2, all necessary background knowledge of this study is included. First, we

doi:10.6342/NTU202000120

briefly introduce the skin structure of the human. Second, we review the investigations of the optical clearing on *ex vivo* and *in vivo* experiments. Third, we introduce the basic theory of the second harmonic generation and third harmonic generation.

In chapter 3, we perform all experiment methods and procedures of *ex vivo* and *in vivo* experiments. We summarize all the methods of sample preparation of *ex vivo* experiments in section 3.1, and the details of the *ex vivo* imaging are included in section 3.2. In section 3.3, first, we describe the details of *in vivo* human experiments preparation include the scanning region selection and the glycerol application. Second, we perform the methods of *in vivo* human imaging by utilizing HGM microscopy. In section 3.4, all analysis methods of the HGM images are included.

In chapter 4, we summarize the results of the *ex vivo* experiments. Afterward, we discuss the optical clearing effects and mechanisms of the *ex vivo* human skin in chapter 5.

In chapter 6, we summarize and discuss the results of the *in vivo* experiments. Afterward, we discuss the optical clearing effects and mechanisms of the *in vivo* human skin in chapter 7.

Chapter 8 is the summary of this thesis.

doi:10.6342/NTU202000120

Chapter 2 Background Knowledge

2.1 The Skin

2.1.1 Skin Structure and Barrier Function of the Stratum Corneum

Skin is the largest organ of the human body; approximately 16% of the total weight of the total body. Moreover, it is also one of the most important organs. As the outermost layer of the human body, its diverse functions help people to maintain daily life. It contains many different tissues, including blood vessels, nerves, glands, collagen fibers, and fat. The skin can basically be divided into three different layers, which are epidermis, dermis, and subcutaneous fat.[36] These layers work in concert to provide flexibility and strength. The epidermis is the first layer of the skin, and itself can be divided into stratum corneum (SC), and viable epidermis. The viable epidermis is the layer suited beneath the SC. It contains other sub-layers (stratum lucidum, stratum granulosum (SG), stratum spinosum and basal layer) in which the cells are at different stages of differentiation (Fig. 2.1). Actively dividing cells are present in the stratum basal to form the stratum granulosum (SG), stratum spinosum, and the stratum lucidum (only founded in the very thick epidermis of the palms and soles). There are two different types of granules formed at the viable epidermis. First is keratohyalin granules which is full of protein; the other one is lamellar bodies that contain lipids. The deposition of the dead cells without nuclei of the viable epidermis will transform into corneocytes and squames to form the outmost

doi:10.6342/NTU202000120

SC. The most important function of the SC is the barrier function. The SC can prevent water loss and protect the body against the fluctuations in temperature, radiation, chemical toxic. “Brick and Mortar” is the basic model of SC. The SC cells and keratin microfibrils formed the brick structure. The intercellular space which fulfills the lipid was called mortar. The motor is the main reason that water cannot pass through the skin from the human body [37]. The barrier function will be destroyed by the use of surfactant and soap. The repeated wash of the skin by human cleaning products will break the barrier function by dissolving the lipid in the SC [38]. Most of the cosmetic products contain the surfactant to enhance the absorbing efficiency of their products by decreasing the barrier function. For drug delivery, SC will also cause the problem. Although the mechanisms of the drug delivery through the skin still unclear, there is some evidence showing the use of some methods like laser skin abrasion, skin stretching, tape stripping, ultrasonic and penetration enhancer are valid [39].

Skin is a complex organ that contains many layers for multiple functions. For these different layers, each of them has different refractive indices. These variations of refractive index cause much random scattering. In 1995, J. G. Fujimoto group determination the refractive index by measuring the focal length shift based on OCT (center bandwidth: 1300 nm, bandwidth: 50 nm). They computed that: for in vitro dermis: 1.41, *in vivo* stratum corneum: 1.51 and *in vivo* epidermis: 1.34 [40].

doi:10.6342/NTU202000120

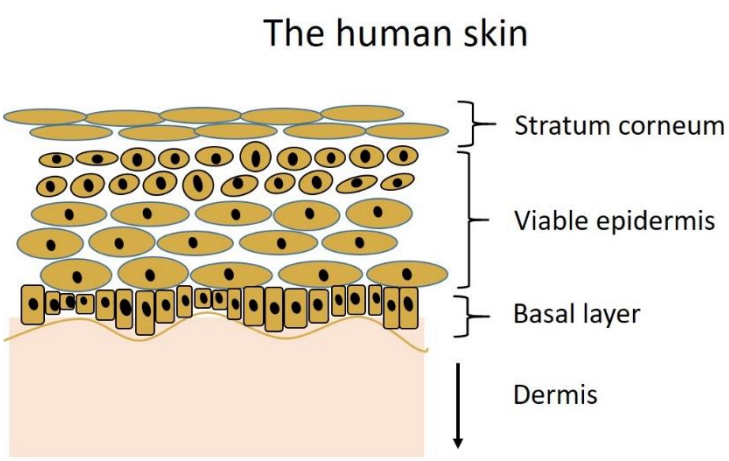

Fig. 2.1 The skin structure from the stratum corneum to the dermis.

2.1.2 Glycerol and the Human Skin

Glycerol or glycerin $[C_3H_5(OH)_3]$, is trihydroxy alcohol. It has three hydrophilic hydroxyl groups to provide high hygroscopicity and water solubility. Glycerol is also low toxic and widely used for the food industry, medicine, cosmetic products. For cosmetics, skincare products usually add glycerol because of its moisturizing and smoothing effects. There are lots of investigations to illustrate that after applying glycerol cream or solutions on the skin, the skin condition will be improved [41-43]. There is evidence showing that the glycerol solution will benefit the dry lower leg skin with 20-40% concentration. They also compared two different cases: high concentration with shorter treating time and lower concentration with longer treating time. The first one shows better improvement, proving that the total quantity of glycerol is the main factor in improving the skin condition. However, when the concentration is higher than 40% the skin improvement ability will saturate [42]. Glycerol will also help the skin to rebuild the barrier function of the stratum corneum. A study shows that after applying the tape stripping method to

doi:10.6342/NTU202000120

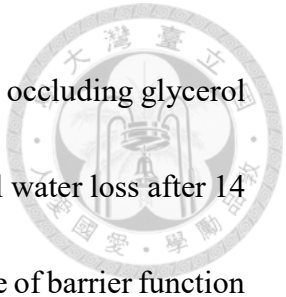

remove the stratum corneum, there is a significant difference between occluding glycerol and untreated case. The untreated case showed higher trans-epidermal water loss after 14 days compare to the occluded ones. The glycerol can accelerate the rate of barrier function recovery.

2.2 Optical Clearing

Currently, light-based diagnostic techniques have been widely developed, such as confocal microscopy, optical coherence tomography (OCT), two-photon fluorescence microscopy (TPFM), harmonic generation microscopy (HGM) and Raman microscopy. These optical microscopies can provide higher resolution and contrast images when compared to other conventional image techniques like x-ray computed tomography, MRI, ultrasound. It can provide submicron resolution to resolve the fine structure inside the tissues, expanding a new area for biomedical imaging. However, until this age, the application of optical microscopy is still limited because of the low imaging depth. Optical scattering originated from the turbid tissue decreases the contrast and the spatial resolution, as well as the imaging depth. In order to enhance the image contrast and depth of the optical microscopy, people are trying to reduce the optical scattering inside the tissue by replacing the interstitial fluid with various agents, which is called optical clearing.

To our best knowledge, the first research of optical clearing was published in 1994,

doi:10.6342/NTU202000120

originated from noninvasive monitoring the glucose concentration for human *in vivo* and in vitro [10, 11]. By using the near-infrared (NIR) light technique, they found that the concentration of glucose inside the human body affected the scattering coefficient. The higher the glucose concentration they used, the lower the light scattering inside the tissue. It was also found that the optical clearing mechanism not only depends on the refractive index matching. In 1996, Hanli Liu et al., used both the Mie and Rayleigh-Gans theory approximation to simulate scattering properties inside the liver tissue [12]. The calculations showed that the changes in scattering properties were affected by the cell size and volume fraction, osmolarity, and change of refractive index. These simulations were also correlated with the experiment results. After that, there are many investigations to study optical clearing by applying various agents and methods, trying to find out the most effective optical clearing agents for different tissues. Among them, the optical clearing of skin experiments attracts much intension.

2.2.1 Optical Clearing of the *Ex Vivo* Skin Experiments

The optical clearing technique was first studied by Tuchin in 1997, by immersing human sclera into optical clearing agents to reduce the scattering [3]. The method is to replace the interstitial fluid by some osmotic agents which are called optical clearing agents (OCAs) to make tissue transparent. The refractive index matching was convinced as the most important mechanisms to reduce the scattering inside the tissue. However, in

doi:10.6342/NTU202000120

different experiments of various tissues such as sclera[3], liver[12, 27, 44], muscle[45], tendon[27, 45], and the skin[5-9, 20-22, 24-27, 35, 46, 47], the results showed that there were more complicated mechanisms of the optical clearing. The optical clearing mechanisms and efficacy are still unclear and need more investigations. Among these tissues, the optical clearing of the skin is the most frequently studied by using different OCAs and imaging techniques. The final goal of the optical clearing is the *in vivo* application. The investigations of *ex vivo* tissue opened the door for further study of *in vivo* experiments.

Different optical clearing agents (OCAs), such as glycerol, polyethylene glycerol (PEG), the combined PPG- and PEG-based polymer mixture, sorbitol, glucose, dextrose, oleic acid, dimethyl sulphoxide (DMSO) were applied to study the optical clearing effect of the skin. Their chemical structure can classify these chemical agents as alcohols, sugars, organic acid, and organic solvents. In 2005, Cohi et al., studied the optical clearing potential of these different groups of solutions by diffuse reflectance and total light transmittance. The hydroxy-terminated clearing agents, named alcohol, demonstrated the highest optical clearing power. Their results suggested that only the hydrophilic clearing agents will diffuse into the skin [46]. Based on the research of the Cohi et al., the optical clearing potential of different alcohols (glycerol, PEG400, PEG200, 1,3-propanediol, 4,4-butanediol, 1-butanol) were studied by Dan Zhu et al [6]. The results showed that the

doi:10.6342/NTU202000120

optical clearing potential of these alcohols was related to the number of hydroxyl groups. The more hydroxyl groups an OCA had, the more effective optical clearing. In contrast, the refractive index and the molecular weight of these alcohols did not correlate with the degree of the optical clearing effect. Glycerol is the one of the most effective OCAs among these alcohols with its strongest dehydration power [46, 48].

Glycerol is the most popular and well-studied OCAs of the optical clearing. In this section, we discussed and summarized the previous studies related to the optical clearing of the *ex vivo* skin by using two different applying methods: (1) Tissue immersion technique: It is the primary and most widely used method for OCAs application. By using tissue immersion technique, glycerol solutions is able to diffuse into the tissue from the every surface, and achieve a promising optical clearing effect [5, 8, 9, 21, 22, 24, 27, 47]. (2) Topical application: There are some other studies used the topical application on the epidermal side by considering the barrier function of the stratum corneum [6, 7, 20, 25, 26, 35]. The method of topical application provides less optical clearing effects, but this kind of noninvasive method is proper for the further *in vivo* experiment and then clinical.

Vargas et al. studied the optical clearing of *ex vivo* rat skin by spectrophotometer and OCT in 1999 [9]. They immersed the rat skin tissue into the anhydrous glycerol to achieve the optical clearing. After 20 minutes of immersion, the transmittance intensity increased and the reflectance intensity decreased. The human hair was put under the rat skin tissue

doi:10.6342/NTU202000120

as the reference and took the OCT image. The skin appeared much darker at superficial layer and the hair under the skin became much brighter when comparing to the native skin. The shrinkage of the skin was also observed after the tissue immersion. Glycerol is a hyperosmotic agent that made water travel out of the cells. At the same time, glycerol traveled into the cells passively. However, the diffusion coefficient of the glycerol was much smaller than that of the water; less glycerol diffused into the tissue when compared with the water diffused out of it and resulted in the tissue shrinkage. The variation of the skin structure was also found to affect the scattering coefficient. The experiment results of the spectrophotometer correlate to the thickness of the skin. They hypothesized that the refractive index matching is the main but not only mechanism of the optical clearing. The next important factor should be dehydration.

In order to prove and find out how dehydration affects the optical clearing efficacy, Xiangqun Xu et al., used near-infrared reflectance spectroscopy (NIR) to determine the water content inside the skin tissue [49]. The optical clearing rate of the porcine muscle by 80% glycerol application was strongly correlated to the water desorption with the unchanged thickness. There are three different kinds of water inside the tissue, which are strong tightly bound water, less tightly bound water, and buck water. There are three different stages of the optical clearing. In the first stage, transmittance was enhanced and reflectance was reduced rapidly at the first minute as the result of a loss of the buck water.

doi:10.6342/NTU202000120

In the second stage, transmittance was enhanced and reflectance was reduced linearly during 1-10 minute as the result of a loss of the less tightly bound water. In the third stage, transmittance was enhanced and reflectance was reduced exponentially at the slowest rate during 10-30 minute as the result of a loss of the strong tightly bound water. In their research, glycerol showed a better optical clearing effect than that of the ethylene glycerol since that ethylene glycerol cannot introduce the third stage due to the lack of desorbing power. Dehydration was proved one of the most important mechanisms of optical clearing for porcine skin, human skin [24], rat skin [27]. In some cases, dehydration also changed the tissue structure. The collagen fibrils were found more densely packed after the glycerol application and the increased scattering as well as the image intensity.

The optical clearing of *ex vivo* skin by glycerol application has been studied by many optical imaging technique such as NIR spectroscopy [9, 27, 49], OCT [9, 26, 27, 47, 49], confocal microscopy(CM) [21, 24], two-photon fluorescence microscopy (TPFM) [5, 22, 23], Confocal Raman microscopy (CFM) [35], and second harmonic generation microscopy (SHGM) [5, 24]. These imaging techniques were used alone or combined to study the mechanisms and efficacy of optical clearing. In the most recent study by Tuchin in 2017, two different kinds of imaging techniques (Two-photon fluorescence microscopy and second-harmonic generation microscopy) were combined to study optical clearing quantitatively and qualitatively for *ex vivo* porcine skin. Two-photon excited auto-

doi:10.6342/NTU202000120

fluorescence originated from NAD(P)H, keratin, elastin, and melanin, while the second harmonic generation is due to the collagen response. By combining these two different image techniques, the high-resolution images from the epidermis to the dermis can be obtained. Depth dependent increments of TPF and SHG intensities for samples after one-hour immersion by different concentrations (40%, 60%, 100%) glycerol in comparison with the control sample were obtained. At least three different stacks of the image at different positions of each porcine skin were collected and average to obtained quantitative information of optical clearing efficiency. There was a trade-off between concentration and viscosity. High concentration glycerol provided a higher refractive index matching condition to reduce the scattering inside the skin. However, the high concentration glycerol could not penetrate far enough into the deep region due to its high viscosity. Low concentration glycerol was with higher penetration ability but provided insufficient clearing effect via the refractive matching mechanism. For two-photon measurements, 100% glycerol is the most effective in the depth from 25 μm to 100 μm and intensity was enhanced by a factor of 1.6. While 60% glycerol introduces a better optical clearing for two-photon in depth from 100 μm to 200 μm by a factor of 1.3 and for SHG in depth from 50 μm to 200 μm by a factor of 1.7. Optical clearing should be used with caution to improve the signals of TPFM and SHGM in the region of interest.

doi:10.6342/NTU202000120

2.2.2 Optical Clearing of the *In Vivo* Skin Experiments

Although there are many investigations to study the optical clearing effects and mechanisms of *ex vivo* skin tissue, there are quite different optical clearing efficacy between *ex vivo* and *in vivo* experiments. For *in vivo* experiments, the metabolism and blood circulation also affect the efficacy of optical clearing and OCAs cannot introduce the same optical clearing effect on the skin *in vivo* as that *ex vivo*. The strong barrier function of the stratum corneum makes substances hardly penetrate skins, and the optical clearing effects are not obvious by applying the OCAs on the surface in some previous study of *in vivo* experiments [14, 15, 33, 50]. As the results, many physical method such as injection[48, 51, 52] sonophoretic[33], electrophoretic[14], removal of SC[14, 29, 32, 53], laser ablation[18, 34, 54] and chemical methods such as chemical enhancer Thiazone [15, 54, 55] were applied to accelerating OCAs penetration into skin tissue. The basic theory for all these methods is reducing the barrier function and enhancing the penetration efficacy of OCAs by removing the SC or changing the skin condition. Most of these methods damaged the skin and were less desirable for the *in vivo* human clinical examination. Glycerol was proved the most effective optical clearing agent for the *ex vivo* experiments. However, for *in vivo* human experiments, the optical efficacy by topical application still remains unclear: First, the OCT images provide insufficient image information since it is unable to resolve the cellular morphology. Second, only one or two

doi:10.6342/NTU202000120

volunteers were studied in the most of these previous studies, and the results between each studies were inconsistent. Some of it achieved the optical clearing, but the others were not [14, 30, 31, 33, 50]. When applied the glycerol on the volar forearm [50] and dorsal hand [33], no observable optical clearing effect. In contrast, when applied the glycerol on the palm [13, 30] and finger [31], the scattering of the skin was reduced and enhanced the image intensity. The optical clearing of the *in vivo* human skin still needs more exploitation. There are still lack of the study cases and the results were strongly affected by the individual differences of the human. Due to above reasons, it is thus essential to investigate the optical clearing technique for *in vivo* application with glycerol, and some optical clearing experiments of *in vivo* rat and human skin have already been studied. In this section, the experimental results by using glycerol application of *in vivo* rat and *in vivo* human were presented.

2.2.2.1 Optical Clearing of *In Vivo* Rat Skin Experiments

In 2003, Vargas et al. studied the optical clearing effect by applying 100% and 75% glycerol topically on the rat dorsal skin [47]. They used the dorsal skin flap window to pull the skin away from the body and sutured to a vertical C-Clamp. The glycerol solution was occluded the epidermis side of the skin, and the Doppler optical coherence tomography image was taken from 0 to 30 minutes. The results showed that the image intensity and contrast of blood vessel were enhanced by using these two different

doi:10.6342/NTU202000120

concentrations glycerol. However, application of the 75% and 100% glycerol resulted in venule stasis for prolonged treatment times. In 2003, Tuchin and coworkers studied the back reflectance and micro-vascular system functioning at the action of osmotic agents [51]. Two different OCAs: 75% glycerol and 40% glucose, were injected into the rat. The results of 75% glycerol solution injection showed that the back reflectance reduced by 30% at the maximum and maintained for a long time. It was observed that 75% glycerol decreased the scattering but also caused hemolysis, dilation, and stasis in some micro-vessels. For 40% glucose, the back reflectance reduced 70% at the maximum but only remained for 1-3 minutes only. These two osmotic agents were used to improve the image depth by increasing the refractive index of the blood plasma to make it closer to the value of the erythrocyte cytoplasm, which is the main scatters of the blood. Glycerol acted as a better OCA due to its prolonged optical clearing effect. Based on the research of Vargas and Tuchin, the Dan Zhu group published two papers of the optical clearing by glycerol application of *in vivo* rat skin in 2008 and 2010 [48, 55]. In 2008, they studied the influence of glycerol with different concentrations (75%, 50%, 40%, 30%, and 20%) on skin optical clearing and morphological changed *in vivo* [48]. In order to find the best glycerol solutions concentration for *in vivo* application, the reflectance spectra were taken to monitor the optical clearing effect after different applying time (0 to 24 hours). The reflectance of the skin decreased after being injected withhigh concentration glycerol,

doi:10.6342/NTU202000120

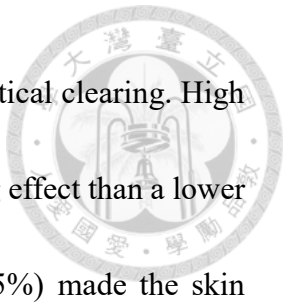

which meant scattering coefficient decreased and the skin became optical clearing. High concentration glycerol solution had a more prominent optical clearing effect than a lower one. However, high concentration glycerol solution (40%, 50%, 75%) made the skin suppurate and necrosis just like Vargas's work and low concentration (20%) solution showed little optical clearing effect. 30% glycerol solution was believed to be the ideal concentration for the rat skin optical clearing when there was a safety concern by injection. The reflectance was 0.8 and rose to the initial level in 10 minutes. In 2010, they studied optical clearing with the same experimental setup (optical clearing by injecting 20%, 30%, 75% glycerol solutions into rat dermis) but combined with more image techniques. SHG, NIR, TEM images were taken to get more information so that the mechanisms of optical clearing could be better studied [52]. The results showed that the variety of skin thickness affected the efficacy of optical clearing. After the glycerol solutions injection, the skin thickness decreased significantly and then increased with prolonged time. The results of the NIR spectrum correlated to the thickness measurement. When tissue shrank, the reflectance decreased also. In contrast, when tissue swelled, the reflectance increased. Thickness was one of the main factors that affected the scattering properties inside the skin. For SHG image observation, after immersing the sample into the 13M glycerol for 30mins, the SHG signal became much weaker and the bundle pattern was no longer be observed as the consequence of collagen dissociation. However, for the *in vivo* case of

doi:10.6342/NTU202000120

direct injection, no collagen dissociation was observed and the SHG signal was still strong. These results indicated that the optical clearing effects and mechanisms are different for *in vivo* and *ex vivo* applications.

2.2.2.2 **Optical Clearing of *In Vivo* Human Skin Experiments**

The first optical clearing experiment of *in vivo* human skin was studied in 1994 by John S. Maier et al. [11]. With the measurement of the NIR spectrometer, they found that the light scattering coefficient inside the human thigh decreased after the sub-dermal injection of the high concentration glucose. Since then, people who studied the optical clearing technique tried to find out the best optical clearing agents and methods to increase optical clearing efficacy for *in vivo* human experiments. Glycerol was found as the most effective optical clearing agent for *ex vivo* skin experiments [46, 48]. Although there are some investigations about *in vivo* human skin optical clearing by using OCT and NIR spectrometer, most of them used inappropriate concentration glycerol or delivery methods resulting in skin damage. The experimental results of these studies are also inconsistent and provide insufficient experimental data. The optical clearing techniques can achieve a promising optical effect by glycerol application for *in vivo* rat, while for *in vivo* human skin, it still unclear and need more exploration.

In 2000, optical clearing efficacy of 100% glycerol with gelatin and 40% glucose with gelatin were compared by three different applying methods (topical application,

doi:10.6342/NTU202000120

epidermis removal, and electrophoretic) by NIR reflectance microscopy [14]. The results indicated that the methods of topical application, epidermis removal, and electrophoretic would lead to the enhancement of optical clearing. Glycerol has better optical clearing efficacy when compared to the 40% glucose. The best optical clearing efficacy was obtained by using the electrophoretic administration glycerol from the anode, which could introduce nearly 20% reduction of the scattering signal. The topical application showed the minimal optical clearing among these methods, which could only introduce nearly an 8% reduction of the scattering signal for glycerol application.

In 2004, Xu et al. studied the optical clearing of *in vivo* human skin using OCT and spectrometer [13]. 80% glycerol was used as the clearing agents and topically applied on the palmar skin. The OCT and spectra were acquired respectively at the time intervals of 15, 30, 45, and 60 after the 80% glycerol applied topically on the skin surface. After 15 minutes, the upper layer of epidermis became more homogenous and the penetration depth was enhanced due to the refractive index matching as glycerol diffused into the skin. The clearing effect was maintained and saturated till 30minutes. After 30 minutes, the penetration depth was decreased, but the contrast started to be improved. The best optical clearing effect was obtained at 60 minutes with the maximum contrast. The skin layers of stratum corneum, viable epidermis and dermis were distinguished. In their study, the optical clearing was also studied by a spectrometer to acquire the scattering property

doi:10.6342/NTU202000120

of the skin. Within 45 minutes after application, the diffuse reflectance decreased with time up to 6% and then increased at the time interval from 45 minutes to 60 minutes. There was a compromise between optical clearing and contrast enhancement for the image. A substantial decrease in light scattering may actually decreased image contrast. It was likely that there is an optimal time period after the addition of the glycerol solution to increase the imaging depth as well as that it needed sufficient backscattering for contrast enhancement. In this study, only one data of optical clearing by glycerol application was performed. The method of topically applied with glycerol was also studied by Proskurin et al. at 2007 [31]. In this study, same as the Xu's research, only a data of a volunteer was performed. They applied 100% glycerol topically on the human finger. After 15 minutes application, the upper surface structures have similar resolution, whereas the deep vessel signal at ~1.5-1.7 mm was better resolved.

Although glycerol does lead to the optical clearing by topically applied in the above studies, there still some other researches do not agree with their results. In 2008, Xu et al. published another research of optical clearing on dorsal hands [33]. Two different methods were applied and compared to study the optical clearing effect. The treatments were topically applied with a 60% glycerol solution (as control) or a 60% glycerol in combination with 15 minutes of ultrasound (60% G/SP). It can be seen that the light penetration depth of the skin treated with 60% G/SP was gradually enhanced from 1.4

doi:10.6342/NTU202000120

mm to 2.5 mm at maximum (60minutes treatment). For the skin with 60% G (control), OCT imaging of the skin with only 60% glycerol applied topically has shown little enhancement in the imaging depth. This result has also been observed in the previous study in 2004 [50]. After applying 100% glycerol on the *in vivo* human forearm skin, there was not showing any enhancement of *in vivo* light penetration depth and contrast over 120 minutes. They suggested that it is extremely difficult for glycerol alone to permeate into viable skin and could not introduce the optical clearing.

There are still unclear optical clearing mechanisms and effects by topically applied glycerol on the *in vivo* human skin. The experiment results of previous studies are inconsistent, and only a few volunteer's data were taken. It is still questionable that if glycerol will penetrate through intact skin with the stratum corneum. In 2011, the optical clearing efficacy of 40% glycerol was studied by quantifying permeability using OCT. The measurements of 40% glycerol on the palm were carried out on four volunteers. In this study, the depth interval of 210-420 μm in the 1D OCT signal was chosen to calculate the attenuation coefficient. After the glycerol application, the attenuation coefficient started to decrease and then reached equilibrium after a long time of treatment. The decrement of the attenuation coefficient and the time of equilibrium were combined to calculate the permeability coefficient of 40% glycerol. The result indicated that 40% glycerol would diffuse into the skin from the surface with a permeability coefficient of

doi:10.6342/NTU202000120

$(1.67 \pm 0.04) \times 10^{-6}$ cm s^{-1} and decrease the attenuation coefficient by 12% at maximum.

Glycerol is the most effective optical clearing agent for the *ex vivo* experiment. However, its effects and mechanisms by topically applied on *in vivo* human skin are still unclear. The glycerol has a low molecular weight (<500 Da) to allow it diffuse into the human skin. Its permeability was also proved by using OCT. To sum up, these studies only provided low-resolution OCT images and insufficient data of a few volunteers to study the *in vivo* optical clearing. The effects and mechanisms of *in vivo* optical clearing by topically applied have not been well-studied in previous studies.

In this thesis, we aimed to explore the optical clearing effects and mechanisms by applying 50% glycerol topically on the *in vivo* human skin with high-resolution HGM microscopy. The skin image of different volunteers was analysis statistically, qualitatively, and quantitatively.

2.3 Basic Theory of Harmonic Generation

2.3.1 Second Harmonic Generation

The second harmonic is a second-order nonlinear optical process. Two photons inside the nonlinear materials with frequency ω will interact with each other to form a new photon with frequency 2ω. The process of SHG can be easily described by a simple

doi:10.6342/NTU202000120

physical picture. The atoms under the input field with frequency ω inside the materials will develop the oscillating dipole moment containing the component of 2ω (Fig. 2.2). When the relative phase of the incident light and the dipoles meet the phase condition, the radiated field of the dipole will add constructively to produce SHG radiation. Therefore, the SHG process does not involve any real-state transition and is known to leave no deposit energy inside the interacted matter (Fig. 2.2).

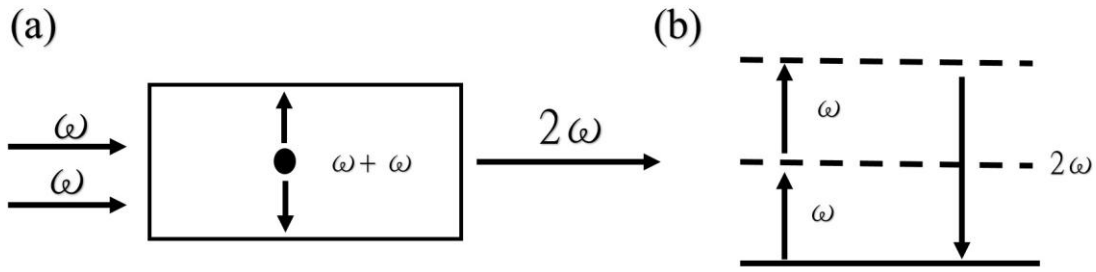

Fig. 2.2 Simple physical picture of the SHG theory.

The inversion symmetric on the second-order nonlinear response is quite important to produce SHG radiation. In centrosymmetric media, potential wells only have even powers of x (V(x)=V(-x)) and the nonlinear susceptibility $\chi^{(2)}$ must identically vanish. Therefore, only noncentrosymmetric structures like collagen fibers in biological tissue are capable of emitting SHG light. According to the theory of the Boyd (1992), the intensity of the SHG is proportional to the square of excitation intensity and the second-order nonlinear susceptibility:

$$I_{2\omega} \propto \left|\chi^{(2)}\right|^2 I_{\omega}^2$$

doi:10.6342/NTU202000120

The $I_{2\omega}$ is the radiated SHG intensity, $\chi^{(2)}$ is the second-order nonlinear susceptibility, and the I_{ω} is the intensity of the incident light. Base on the equation of Boyd, we know that the radiation SHG intensity is mainly affected by the excitation laser intensity and the tissue structure. The lateral and axial resolution of the SHG are given by Squier and Mu¨ ller [56]:

$$r_{lateral} = \frac{1}{\sqrt{2}} \frac{0.61\lambda}{NA}$$

$$r_{axial} = \frac{1}{\sqrt{2}} \frac{n\lambda}{NA^2}$$

where λ is the wavelength of the incident light, NA is the numerical aperture of the objective lens, n is the refractive index of the immersion media.

2.3.2 Third Harmonic Generation

The third harmonic is a third-order nonlinear optical process. Three photons inside the nonlinear materials with frequency ω will interact with each other to form a new photon with frequency 3ω. The process of THG can be easily described by a simple physical picture. The atoms under the input field with frequency ω inside the materials will develop the oscillating dipole moment containing the component of 3ω (Fig. 2.3). When the relative phase of the incident light and the dipoles meet the phase condition, the radiated field of the dipole will add constructively to produce THG radiation. Therefore, the same as the SHG, the THG process does not involve any real-state

doi:10.6342/NTU202000120

transition and is known to leave no deposit energy inside the interacted matter (Fig. 2.3).

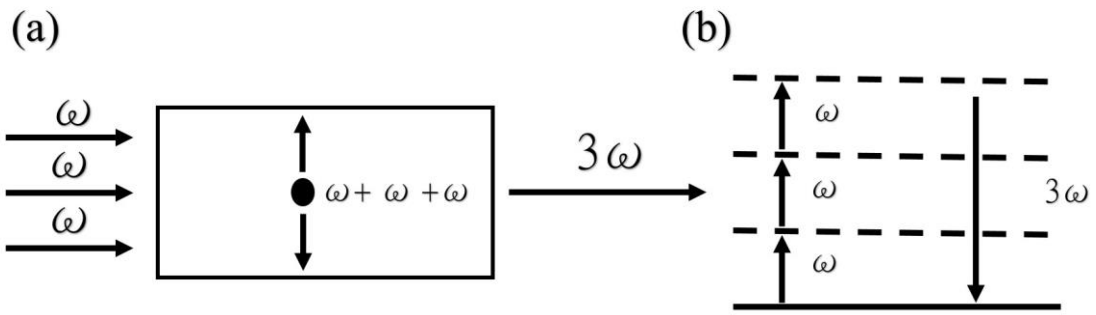

Fig. 2.3 Simple physical picture of the THG theory.

In contrast to SHG, which only allowed in noncentrosymmetric materials, the THG allowed in all materials due to its non-vanishing susceptibility. In bulk material, THG intensity is canceled due to the Gouy phase shift on both side of the focus, but still take place in the vicinity of the interface [57]. Due to its interface sensitivity characteristic, THG provides the capability of morphology imaging, such as the cell membranes. According to the theory of the Boyd (1992), the intensity of the THG is proportional to the cubic of excitation intensity and square of the third-order nonlinear susceptibility:

$$I_{3\omega} \propto \left|\chi^{(3)}\right|^2 I_{\omega}^3$$

The $I_{3\omega}$ is the radiated THG intensity, $\chi^{(3)}$ is the third-order nonlinear susceptibility, and the I_{ω} is the intensity of the incident light. The lateral and axial resolution of the THG are given by Squier and Mu¨ ller [56]:

$$r_{lateral} = \frac{1}{\sqrt{3}} \frac{0.61\lambda}{NA}$$

doi:10.6342/NTU202000120

$$r_{axial} = \frac{1}{\sqrt{3}} \frac{n\lambda}{NA^2}$$

where λ is the wavelength of the incident light, NA is the numerical aperture of the objective lens, n is the refractive index of the immersion media.

doi:10.6342/NTU202000120

Chapter 3

Method and Materials of the *In vivo* and the *Ex Vivo* Optical Clearing Experiments

In this chapter, all experiment methods and materials of the *ex vivo* human and the *in vivo* human skin optical clearing will be mentioned. In Section 3.1, we will show the protocol of *ex vivo* human skin experiments. Section 3.1 is divided into four different parts, which are skin sample preparation, glycerol solution preparation, slide preparation, and optical clearing agents (OCAs) application. Section 3.2 is all related to the HGM system set up and the virtual biopsy procedure of the *ex vivo* human skin tissue. The details of *in vivo* human skin experiments will be included in section 3.3. The analytical method of the skin thickness and signal intensity of the *ex vivo* and *in vivo* experiments are shown in section 3.4. The study protocol and safety risks associated with the glycerol applying on *ex vivo* and *in vivo* human skin and our harmonic generation microscopy were reviewed and approved by the institution review board (IRB) at National Taiwan University Hospital (No. 201804100DINA) and Taiwan Food and Drug Administration (TFDA). To make sure all information about the experiments were informed, volunteers who agree to participate in the experiment were required to provide consent.

3.1 Experimental Protocol of the *Ex Vivo* Optical Clearing

In chapter 2, we reviewed the studies of the *ex vivo* and the *in vivo* skin. Refractive

doi:10.6342/NTU202000120

index matching and the dehydration were considered as two most critical mechanisms that strongly affected the optical clearing efficiency. Different concentration glycerol solutions have different refractive indices as well as the dehydration power. Due to the above reasons, we studied optical clearing for the *ex vivo* human skin using two different concentration solutions, which are 100% and 50%. 100% glycerol provided a promising optical clearing effect in the previous studies of the *ex vivo* skin tissue. Even through it has been studied by various imaging techniques such as OCT (optical coherence tomography), NIR (near infrared) spectrometer, TPFM (two-photons fluorescence microscopy), and SHGM (second harmonic generation), this is the first time to study optical clearing effect and mechanisms by combining SHG (second harmonic generation) and THG (third harmonic generation). HGM (harmonic generation microscopy) is a promising technique that is useful in human clinical examination. However, for 100% glycerol, it usually followed the skin edema [14] and inflammation [6] in some previous studies and could not be applied for *in vivo* study. Here we also investigated the effect of 50% glycerol *ex vivo*. It is convinced that 50% glycerol is safe for human skin since it has been used for human skincare products ("Glysoild" from Germany). The results of *ex vivo* experiment by 50% glycerol application will also help our further research of the *in vivo* experiments.

The skin tissue will be immersed or topically applied by 100% or 50% glycerol.

doi:10.6342/NTU202000120

The tissue immersion technique is widely used for *ex vivo* tissue clearance. By using this method, optical clearing agents could penetrate from every surface of the tissue to achieve the most effective optical clearing effect. The optical clearing mechanisms by replacing the interstitial cell fluid into the glycerol solution could be studied. For human skin, the barrier function of the stratum corneum limits the penetration rate and efficiency of the OCAs. We also applied the glycerol topically on the skin surface. The optical clearing effect and mechanisms by considering the barrier function were also investigated.

It was well reported that glycerol would diffuse inside the *ex vivo* skin within 90 minutes to achieve the optical clearing by observing the skin images [4, 5, 9, 16, 20, 21]. In this study, we take these studies as references and select 90 minutes to study the optical clearing by tissue immersion. The reason is that we want to compare the optical clearing results with the previous studies but with different image technique (SHG+THG). Eight volunteers were separated into three different experimental conditions to study the optical clearing. (1) 100% glycerol immersion for 90 minutes (E100-I90). (2) 50% glycerol immersion for 90 minutes (E50-I90). (3) 50% glycerol applied topically on the skin surface for 90 minutes (E50-T90). (Table 6.2).

At last, a skin tissue was applied topically with 100% glycerol on the skin surface for 30 minutes (E100-T30) to double confirm the results and our hypothesis of the *ex vivo* optical clearing

doi:10.6342/NTU202000120

Table 3.1 Three different case types of the *ex vivo* optical clearing.

Case	Agent	Method	Application Time
E100-I90	100% Glycerol	Immersion	90 minutes
E50-I90	50% Glycerol+ 50% ddH_2O	Immersion	90 minutes
E50-T90	50% Glycerol+ 50% ddH_2O	Topical	90 minutes

In section 3.1, we presented all experimental setups of *ex vivo* human skin. After we got the fresh skin tissues from the NTU hospital, the skin tissue was pre-processed before imaging. We took bright-field and HGM images before (named: control) and after the glycerol application (named: glycerol). Before taking the HGM image of control and glycerol, we calibrated the HGM image system by test sample to maintain the system condition. The details of the bright-field imaging and system calibration were mentioned in section 3.2. Fig. 3.1 is the flow chart of the whole *ex vivo* experiment.

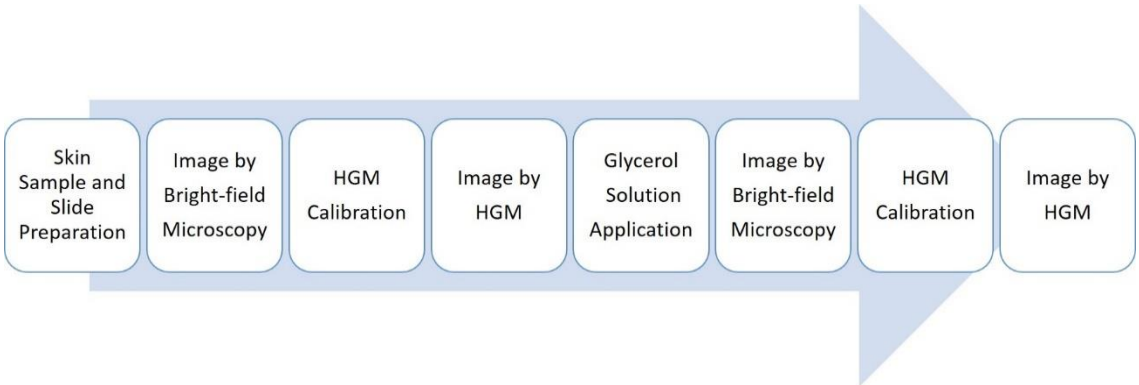

Fig. 3.1 Flow chart of whole *ex vivo* experiment.

3.1.1 Skin Sample Preparation

For skin surgery, to excise all lesion skin from the patient's body, the removed skin

doi:10.6342/NTU202000120

will follow little portions of nonlesion skin on edge. We chose the sample in which the nonlesion part is larger than 0.5*0.5mm^2on the surface area (Fig. 3.2). In the *ex vivo* research, the skin samples are not limited to the same area to maximize the studied cases. When the dermatologist finished the surgery, the part of healthy skin would be excised from the original skin and then stored in the saline to keep it from natural dehydration as well as to remove the surface blood. We got the fresh sample from the surgery room within one hour after the surgery. To keep the replication, we maintained the skin condition before every experiment by the following procedure.

First, the fat tissue under the dermal was removed. Second, when tissue was large enough (>1 mm^2 on the surface area), we cut the tissue into several parts and put into different bottles, which were fulfilled with saline. The bottles was stored inside the 4° refrigerator. Whenever new experiments start, we took the skin sample out from the 4° refrigerator. Before imaging, we soaked the skin sample in fresh saline and then left it under the room temperature for at least 30 mins to standardized the initial conditions of all samples in order to get reproducible results. To study the optical clearing of the fresh skin tissue, we finished the experiment within 24 hours after the skin was excised from the patient.

doi:10.6342/NTU202000120

Fig. 3.2 Human skin sample preparation (a) The original skin sample with fat tissue. (Red circle) (b) Remove the fat tissue under the dermal. (c) The skin sample was separate into two parts. The size of each part will be larger than 0.5*0.5 $\boldsymbol{mm^2}$

3.1.2 Glycerol Solution Preparation

We got glycerol from SIGMA-ALDRICH (Product Number: G2289) which meets USP testing specifications and safe for human experiments. For 100% glycerol experiments (E100-I90 and E100-T30), we used pure glycerol without any manipulation. While for 50% glycerol solutions, we used a pipette to mix glycerol with deionization water precisely to get a 50% glycerol solution (Volume to Volume). We mixed the glycerol and the deionization water one day before the experiment to make it stabilized, and stored in the small glass bottle and kept it under the room temperature.

3.1.3 Skin Slide Preparation

After excising the extra fat and blood of the skin, we fixed the skin tissue between the slide and coverslip before imaging. Since the skin is a thick tissue, it cannot be directly fixed between the slide and coverslip because it will cause too much pressure to make sample deform. To prevent the skin from deformation, we used iSpacers (Sun Jin Lab, part number: ISO011-0.5 mm deep, ISO012-1.0 mm deep) which are made from adhesive tapes in different thickness to create the space between coverslip and slide. Also, a sealed

doi:10.6342/NTU202000120

watertight well is formed to contain water in place to prevent evaporation. As long as we finished the skin sample preparation, we put the sample into the slide which already fulfilled with the water (Fig. 3.3).

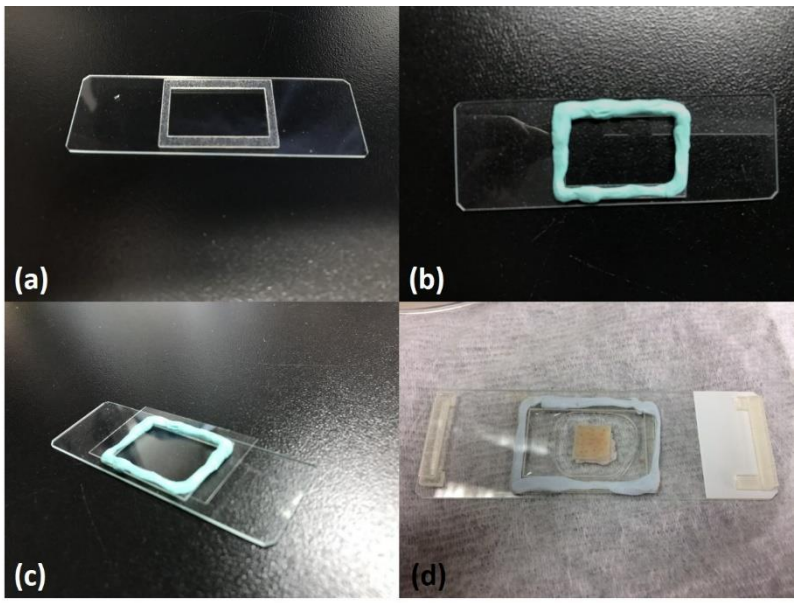

Fig. 3.3 (a) iSpacer fix on the slide to form a space and watertight well. (b) & (c) Use clay to fix cover slip and slide together. (d) One of the finished slides with skin sample and water inside.

3.1.4 Glycerol Solution Application with the Skin Tissue

Because of the barrier function of the stratum corneum, the penetration rate of glycerol is different when comparing two different applying methods (tissue immersion or apply topically on the skin surface). The optical clearing by tissue immersion is the most frequently used technique for *ex vivo* clearance. We directly put the sample inside a bottle which was filled with the glycerol solution and waited for a specific time to complete the clearing (Fig. 3.4). After we immersed the skin tissue into the bottle, the

doi:10.6342/NTU202000120

glycerol solution penetrated the skin through every surface of the skin.

For topical application, we used a brush to make the skin surface covered by a layer of glycerol solution. The function of the cotton under the skin tissue was to absorb the leaking solution from the edge of the skin, preventing the glycerol from being absorbed by the subdermal skin (Fig. 3.4). During the time interval of the glycerol application, the solution was added whenever it was evaporated or being absorbed by skin tissue.

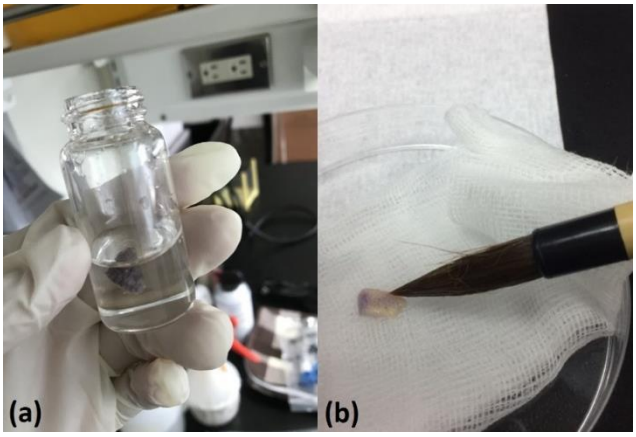

Fig. 3.4 (a) Skin sample was immersed into the glycerol solution. (b) We used a brush to make the skin surface covered by glycerol solution.

3.2 System Set Up and Virtual Biopsy of the *Ex Vivo* Optical Clearing

3.2.1 Bright-field Imaging

We used LEICA ICC50 HD, bright-field trans-illumination microscopy, to investigate the visual changes on the skin tissue before and after the optical clearing. The eyepiece was set on 10x/20 and combining with the 4x/0.10 objective lens to provide the 40 times magnified skin image. The skin images were taken before and after the glycerol application. The transmission ability of the propagating light could be observed by visual

doi:10.6342/NTU202000120

changes of the bright-field skin images. The more transmission light meant the less scattering and reflection light inside the tissue. However, for our reflected-illumination HGM microscopy, the THG intensity depends on multiple factors such as refractive index mismatching, the intensity of excitation light, and back-scattering of the emission signal. Bright-field imaging could provide information on the transmission ability of the propagating light. We combined these two imaging techniques to better understand how these factors affect the optical clearing

3.2.2 Harmonic Generation Microscopy

The system setup of the Harmonic Generation Microscopy (HGM) is shown in Fig. 3.5. A homemade femtosecond Cr:forsterite laser is used as a light source to provide 1260 nm at the central wavelength [58]. The light absorption and light scattering of the human skin at this wavelength is nearly minimum. The short time pulse (33 fs) of this laser makes it available to generate a strong harmonic generation at the focus point. The label-free and low photo-damage characteristics of the harmonic generation make it a good tool for a human clinical study. The double chirped mirror [58] is utilized to compensate for the dispersion of the system for the shortest pulse width. The telescope is used to collimate the laser light to maintain the beam size after a long traveling path. The excitation power of the laser can be adjusted and maintained via the ND wheel. The light guide, which is critical for the human clinical study, was able to move the scanning head conveniently to

doi:10.6342/NTU202000120

image different areas of the human. The 2D scanner is combined with a high resonate 8 kHz mirror and a galvanometer mirror to generate a 2D scan (Thorlabs Laser Scanning Essentials Kit). The scan lens and tube lens not only increase the beam size to make it fulfilled the back aperture of the objective lens but also form a 4f system to make tilted light go back to the back aperture of objective lens. The laser light is focused in the human skin by an objective lens (water immersion, NA 1.15). The SHG (630 nm) and THG (410 nm) signal will be generate at the focal point and the signal will be collected by the same objective lens (Olympus, UApoN340). The first dichroic beam splitter (DBS) (Thorlabs / DMLP900L) is used to reflect the signal which is collected by the objective lens and the second DBS (Thorlabs / DMLP505R) separate the signal of SHG (630 nm) and THG (410 nm). The signal of the SHG and THG will be detected by two individual photomultiplier tubes (PMTs). (Hamamatsu/R928 for SHG and Hamamatsu/R4220P for THG) with band-pass filters (BPF) inserted (Semrock FF02-617/73 for SHG and Semrock FF01-417/60). The objective lens is attached to a 3D step motor (Sigma Koki / TSDM40-15X) which can move an image plane manually to create 3D images.

doi:10.6342/NTU202000120

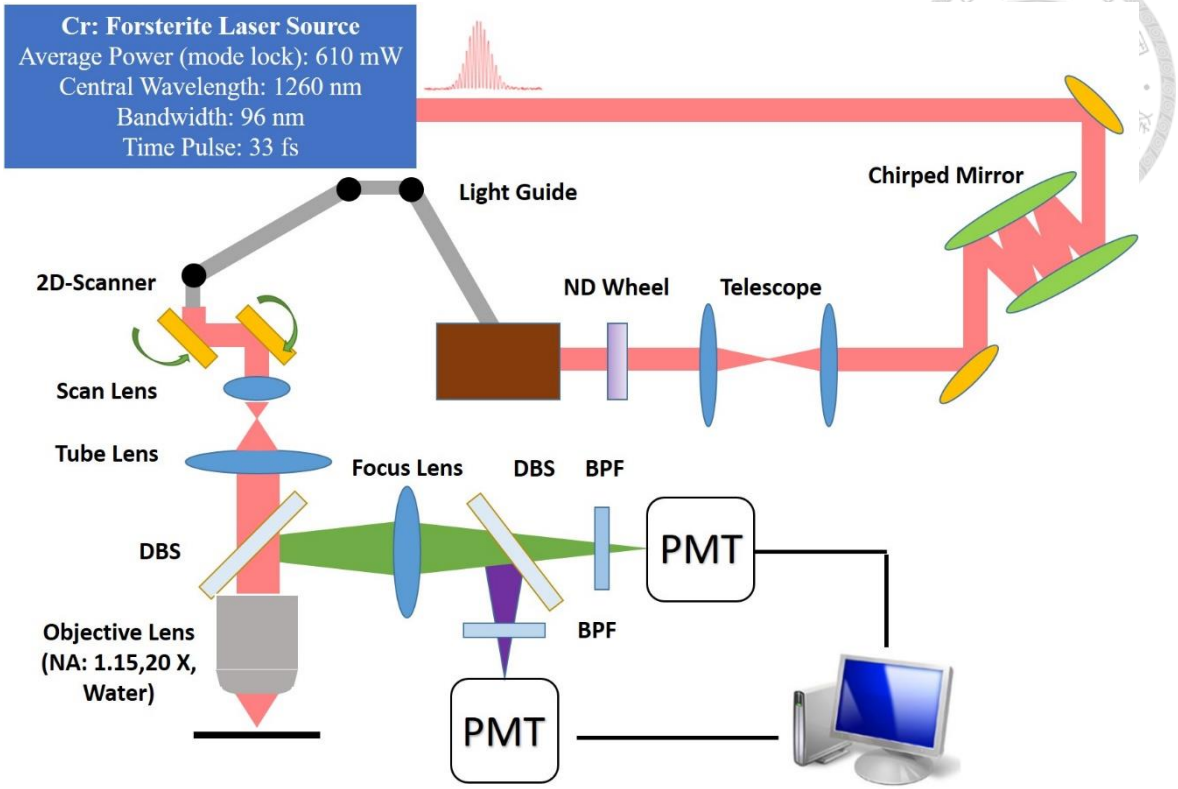

Fig. 3.5 Optical system setup. DBS: dichroic beam splitter; BPF: band-pass filter; PMT: photomultiplier tube.

3.2.3 THG and SHG imaging of the *Ex Vivo* Human Skin

We calibrated the HGM microscopy to make the operating conditions remain the same before and after the glycerol application by taking the images of a calibration sample (gallium nitrite grown on top of double-side polished sapphire substrate). The advantage of GaN is that it can generate very strong and stable SHG signal excited by our home-build Cr: forsterite laser (center wavelength: 1260 nm) when compared to a normal skin sample [59]. The scotch on the surface of gallium nitrite helped us to find out the same area to image. When the HGM system was ready for skin imaging, we took the HGM image of the calibrate sample as a reference. After that, we took the image of the normal skin as a control. Then, we took the image of the calibrate sample again to make the

doi:10.6342/NTU202000120

system before taking the skin with the glycerol application. We compared the image intensity and morphology of the calibrate sample to make them no difference by adjusting the HGM system (Fig. 3.6). This step is to ensure the intensity of the HGM skin images were affected by the inconsistency of the imaging system.

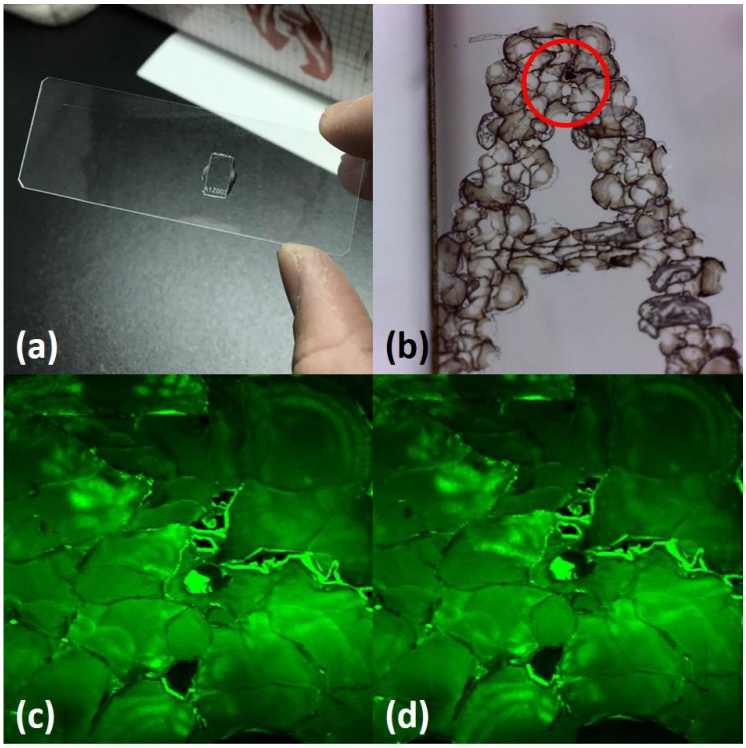

Fig. 3.6 (a) A gallium nitrite (GaN) sample with some scotch (A1Z003) on it. (b) Imaged by bright light microscopy. (LEICA ICC50 HD). We choose the top of first letter "A" to image by our HGM. (c) & (d) The HGM images of the GaN before taking the image of the control group and taking the image of the glycerol group. There's no big difference between each other. Laser power (after the objective lens): 20 mW, Average frame: 10 frames/frame. PMT setting: 400 V for SHG channel.

The best method to study the skin optical clearing is to observe the same location on the skin surface before and after the application of the glycerol. However, in each scan of the HGM, the image area of the skin is around 235*235 μm^2 at maximum (pixel number 512*512). The skin tissue we used for the HGM imagining was much larger than the

doi:10.6342/NTU202000120

scanning area. It was hard to find out the same location for imaging since it was quite similar morphology all around the skin tissue. Instead, we took a few different locations to study the overall changes after the glycerol application. For each skin sample, at least six stacks of depth scans were collected for statistical analysis. The number of stacks depended on the skin area to extract as much information as possible.

We fixed the slide on a 2-dimensional stage so that we could image the different locations on the skin sample by manually adjusting the 2D stage (Fig. 3.7). Once we started to scan the location after finding the region of interest, the objective lens was moved vertically and automatically to focus on different skin depth to get a stack of images (Fig. 3.7). One step for our Z-axis is 1.8 μm and a stack combined with 130 steps images which were related to different depth down to 200 μm. For a one-step image, 15 frames were averaged to form a new frame to enhance the SN ratio.

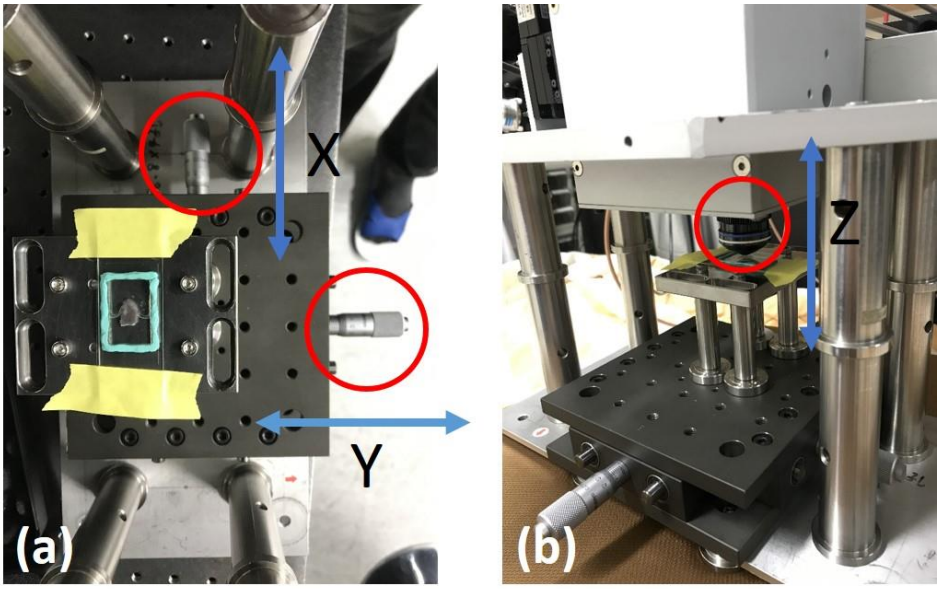

Fig. 3.7 (a) The slide fixed on the 2D stage which could manually adjust the scan area to

doi:10.6342/NTU202000120

get the image of different position. (b) Red circle: An objective lens. When we started to scan, it moved automatically to get a stack of images.

3.3 Experimental Protocol of the *In Vivo* Human Skin Image Clearance

In section 3.3, we will present our experimental protocol of the *in vivo* experiment by topical application. In previous studies, the glycerol solution was combined with some chemical [15] or physical [14, 32, 33] methods to enhance penetration. These methods usually break the skin surface like SC to enhance the penetration ability of the OCAs. However, the optical clearing effect and mechanisms of the topical application with noninvasive methods is still unclear due to the insufficient information of OCT images [30, 31, 33, 50]. Different from the *ex vivo* experiments, which can use an immersion or topically method to study the optical clearing, for noninvasive *in vivo* human optical clearing, we applied the glycerol solution topically to test the barrier function of the SC.

High concentration glycerol was found to make the skin edema in the published work [48] and cannot be used for *in vivo* human experiment. While for low concentration glycerol solution (< 50%), it is biocompatible and used as the content of the skincare product (Glysoild, Germany). We want to investigate the optical clearing effect and mechanisms by noninvasive topical application with 50% glycerol during four different time intervals (15, 30, 90, 180 minutes), named Case I50-T15, Case I50-T30, Case I50-T90, Case I50-T180. Fig. 3.8 is the flow chart of whole *in vivo* human experiments.

doi:10.6342/NTU202000120

Table 3.2 Four different cases of the *in vivo* optical clearing.

Case	Agent	Method	Application Time
I50-T15	50% Glycerol+ 50% ddH_2O	Topical	15 minutes
I50-T30			30 minutes
I50-T90			90 minutes
I50-T180			180 minutes

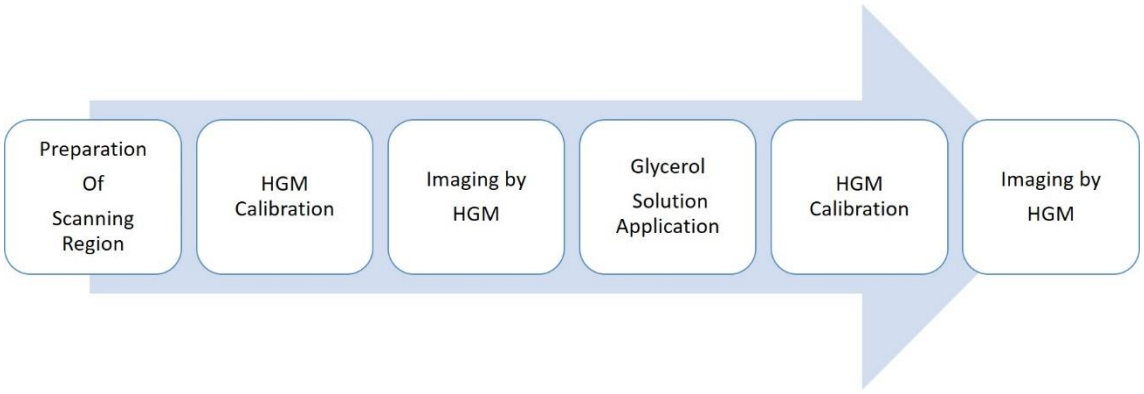

Fig. 3.8 Flow chart of whole *in vivo* experiment.

3.3.1 Scanning Region Selection and Preparation

For the *in vivo* human optical clearing, the effect between the volar forearm [50] and palm [13, 30] showed different results. The optical clearing effect was found less effective in the skin area with thinner SC. The same result was also noted in our recent study [60]. However, it is essential to study the optical clearing on the skin with thinner SC, the area where the light therapeutic and dermatological diagnosis often focus on. In this study, we investigated the OC effect on the *in vivo* volar forearm by using 50% glycerol with topical application.

doi:10.6342/NTU202000120

Volunteers were asked not to use the makeup or skincare products on the test area on the day of the experiment. Volunteers were asked to wash the test area using soap before the experiment to remove the dust and small particles. After that, we used 70% alcohol to clean the test area again to remove the extra oil. In order to make sure the image was acquired from the region of the interest on the forearm, we used the waterproof tape to mark the test region by a circle (Fig. 3.9), and take the HGM skin images as control.

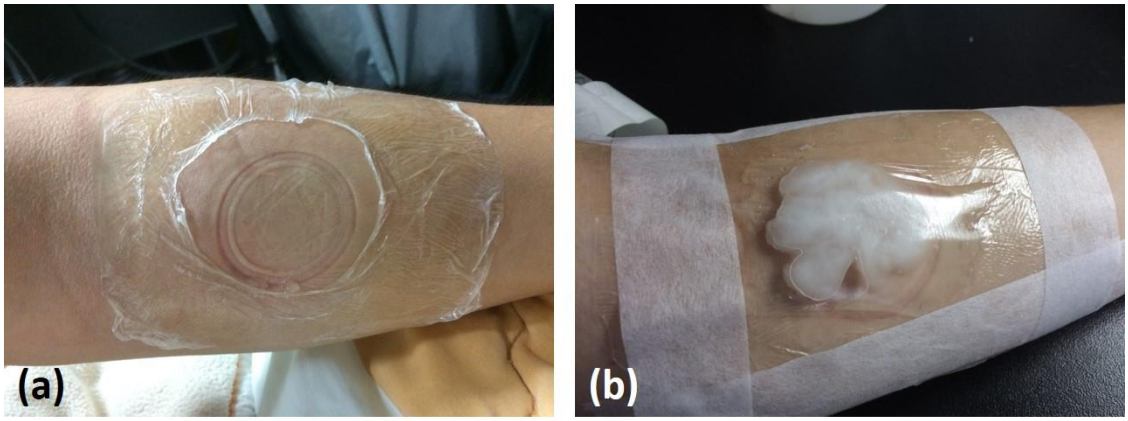

Fig. 3.9 (a) The waterproof tape (3M™ Tegaderm™) with the hole in the center to mark the position of the region of interest at the forearm. (b) Glycerol application for the *in vivo* experiment. We used second waterproof tape to seal the glycerol solution on the skin surface.

After finishing the HGM imaging of the control group, we applied 50% glycerol solution on the test area for a while and then took the HGM image again as the glycerol group to study the effect of the optical clearing. 50% glycerol is water-like solution that has low viscosity to make it hard to stay on the skin surface. In order to keep the glycerol solution on the skin surface as much as possible, cotton was soaked into the glycerol and then sealed on the skin surface by the waterproof tape. By using this method, the glycerol

doi:10.6342/NTU202000120

solution could stay on the skin surface for a long time without leaking or evaporating.

3.3.2 Noninvasiveness and Photodamage Concern

The safety issue is the most important concern for noninvasive clinical application. In this clinical study, the central wavelength of the femtosecond excitation light is 1260 nm with a 105-MHz repetition rate, 100-mW radiation corresponds to a pulse energy of 0.95 nJ. The superior viability performance of the Cr:F-based HGM has been noted in our previous studies.

In our previous mouse embryo study, the mouse embryo was kept under 10 minutes continuous scanning by using 1230 nm Cr:F-based laser with 140 mW average power (total exposure >29 J per embryo). The surviving rate between the imaged set and the non-imaged set were similar (imaged n = 9, blastocyst stage = 67%; non-imaged n = 10, blastocyst stage = 70%). For the advanced viability test, 6- to 8-week-old female ICR mice were illuminated by the femtosecond Cr:F laser with an average power of 120 mW (six embryos in a dish; 3 min per embryo; total exposure = 21.6 J per embryo). The blastocyst development rate of the HHGM-imaged embryos with laser exposure in this advanced study is 97.4% (n = 76 embryos: blastocyst stage = 74 embryos), while the rate of the embryos without HHGH-imaged is 97.1% (n = 70 embryos: blastocyst stage = 68 embryos) [61], no short-term embryonic damage can be found in our two studies. The 1230 nm Cr:F-based was proved will not affect the DNA expression or cloning process.

doi:10.6342/NTU202000120

For our in vivo experiments by using Cr:F-based HGM , the in vivo optical virtual biopsy of human skin has been performed on 21 healthy volunteers' forearms [61], and on 23 vitiligo patients [62], there were no inflammatory symptoms, no skin color change, no pigmentation, no wound, no blister formation, and no ulceration reported. Similar conclusions on the clinical study have been noted previously [63-65].

After the experiments, there was no observable photodamage and the volunteers did not feel uncomfortable. HGM imaging reveals no erythema, pigmentation, crust, or vesicular formation.

3.3.3 THG and SHG imaging of *In Vivo* Human Skin

Volunteers were asked to lie on the electric height-adjustable bed, put left arm on the cushion to make forearm face up and stay stable (Fig. 3.10). We adjusted the height of the electric hospital bed to make the scanning head contact on the skin surface of the forearm. This scanning head of the HGM system was designed for the *in vivo* human experiment (Fig. 3.10). An adapter was used to separates the skin and the objective lens by a coverslip to prevent direct contact with each other. During the scanning, the volunteer had to take a rest and try not to move the scanning region. Since we could not avoid the natural vibration from the volunteer for an *in vivo* experiment, the scanning time was decreased by reducing the average frame down to 10 frames/per frame compared to the *ex vivo* issue (15 frames/per frame). The laser power after the objective lens was adjusted to 100mW.

doi:10.6342/NTU202000120

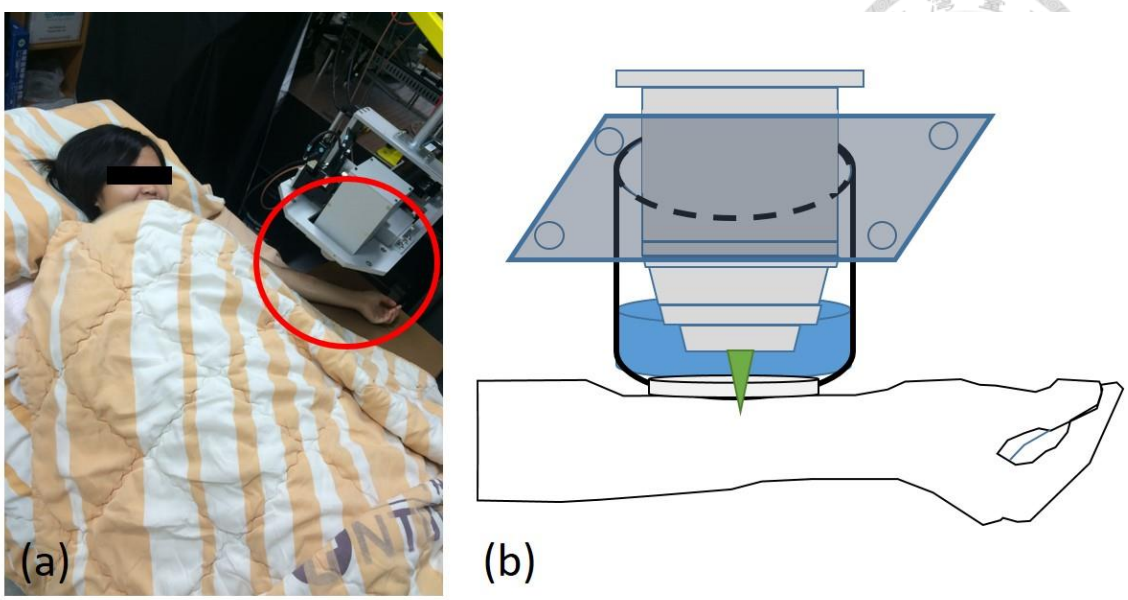

Fig. 3.10 (a) A volunteer was laying on the electric hospital bed. A red circle is the scanning head of our HGM system. (b) The details of the scanning head: Object lens (water immersion) was fixed on the system and covered by an adapter. This adapter not only separated the skin and objective lens to prevent from direct contact with each other by using coverslip but also kept water inside of it to create the water immersion condition for the *in vivo* experiment.

3.4 Analysis Methods of HGM Skin Image

3.4.1 Image Processing of HGM Image

The backscattering SHG and THG signal were detected by two photomultipliers separated by a dichroic mirror. For THG, it is allowed for all inhomogeneous materials, i.e., the interfaces. It can image different skin layers and the cells inside the epidermis (stratum corneum, stratum granulosum (SG), stratum spinosum, and basal layer). In contrast to THG, SHG can only be generated from non-centrosymmetric material, i.e., collagen fibers in dermis. By combining THG and SHG, the skin image of different structures from SC to the dermis can be obtained. The light intensity detected by PMT was remapped by 14-bit to form a grayscale image, from 0 (darkest) to 16383 (brightest).

doi:10.6342/NTU202000120

The skin morphology can be observed by a contrast of a grayscale image. We combined the THG and SHG images of the same skin depth into one image by using “Matlab”. The software “Image J” was also applied for our image processing and analyzing. In order to distinguish the SHG signal from the THG, two different false colors were used to present the signal of the SHG and THG, respectively. Green for SHG, and red for THG (Fig. 3.11).

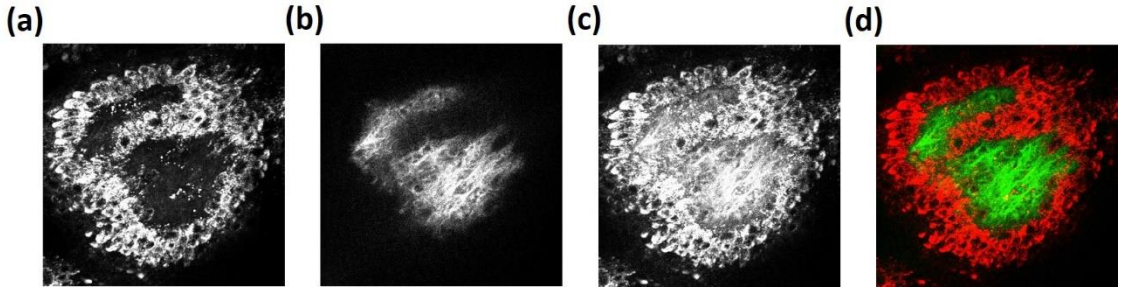

Fig. 3.11 (a) Grayscale image of the THG signal. (b) Grayscale image of SHG image at the same skin depth of THG image. (c) Image after combining SHG and THG. (d) Color remapping of SHG and THG signal. (Green: SHG, Red: THG)

3.4.2 Blinding

Scientific research bases on reliable data, yet data collection is often subjective. Subjectivity can cause bias, originates from common cognitive and sensory biases of all of us. For example, confirmation bias makes us detect and focus on the outcomes we believe. This tendency can cause observer bias during data collection and analysis. For life science research, it is essential that people should eliminate observer bias to make the results more reliable. However, blinding is not always possible in this research. Here we describe the level and method of blinding for our experiments.

doi:10.6342/NTU202000120

Since we are going to compare the image variation before and after the glycerol application from a volunteer, it impossible that the investigator is blinded during data collection. Instead, we choose the image area randomly before and after the glycerol application to prevent observer bias when assessing its outcome. It is an island shape on the skin surface (Fig. 3.11), and we choose the imaging area randomly by arranging the 2D-stage to make at least a half area covered by the skin image.

We take at least six stacks of images in different areas before and after the glycerol application with a volunteer. The skin stack image of a volunteer was stored in each specific folder. The first stack image of control was named C-01, and the first stack image after the glycerol application was named G-01. The other stacks were named by following this rule by C02, C03,…, G02, G03…, et al. Before we analyze the image data, all image stacks of a volunteer were renumbered by those who do not participate in the analyzation. For example, C01, C02, C03, G01, G02, and G03, were renamed randomly from 001 to 006. The relationship between the old names and new names were recorded on the paper, and the paper was put in sealed envelopes to make sure the researchers have no idea whether stack images are assigned to a treatment or control group.

After we finished the structure and thickness analysis of the HGM images (The analysis methods of HGM images will be mention in section 4.4.3 and 4.4.4), the envelope was unsealed to make the data blindness.

doi:10.6342/NTU202000120

3.4.3 Thickness Analysis

Thickness variation of the skin tissue after being introduced by optical clearing agents was proved as one of the most important optical clearing mechanisms in the previous studies. The shrinkage or swelling of tissue will affect the scattering coefficient [52]. Glycerol is a hyperosmotic agent that will make water travel out of the tissue and cells, leading to tissue shrinkage and the decrement of scattering inside the tissue. In this thesis, we also analyze the thickness variation of the skin tissue to study the optical clearing.

After the glycerol application, glycerol solution might diffuse into the skin and cause dehydration to make the skin shrink. However, the variation of thickness might be different in different layers of the skin and result in different optical clearing efficacy. Five different measurements of the skin were investigated, which are the thickness of SC, the thickness of the viable epidermis, depth of the basal layer, depth of the middle papillary dermis layer, and depth of the top reticular dermis layer. Since it is hard to distinguish the boundary of these five different structures, we defined and selected skin layers by the following rules.

Stratum corneum is the outmost layer of the skin, which is composed of dead, plate-like cells called corneocytes that lack nuclei and form a multilayer structure. In this area, strong scattering result in the strong back-reflection THG signal. The thickness of the SC

doi:10.6342/NTU202000120

is counted from the top layer of SC to the top layer of the viable epidermis. The brightest image contains the THG signal from the skin surface and the glass was selected and defined as the top of SC. There is the viable epidermis beneath the SC, in this area, the dark round nuclei of the HGM image start to appear and increase (white arrows in Fig. 3.12). The lack of the THG signal is coming from the homogeneous environment of the cells nuclei. The existence of the cells is the significant difference between SC and viable epidermis. When the number of the existing dark nuclei of the skin image is more than six, the layer will be defined as the top of the viable epidermis (or the bottom of SC).

The thickness of the viable epidermis is counted from the top layer of the viable epidermis to the basal layer. Basal layer is the deepest layer of the epidermis. It is a single layer that contains the basal cells and melanocytes, showing a strong THG signal of the cells. Beneath the basal layer, the SHG signal of the collagen (green color of the HGM image) in the dermis starts to show up. Dermis consists of connective fiber tissues. The dermis can be divided into the papillary dermis and the reticular dermis with different collagenous structures. The papillary dermis is tightly connected to the epidermis by the basal lamina and is composed of loose collagen fibers. In this area, the collagen fibers start to appear and show the strong SHG signal (green). Beneath the papillary dermis, the much thicker reticular dermis is composed of dense collagen fibers. We choose a skin layer that completely lacks the signal of basal lamina as the top of the reticular dermis.

doi:10.6342/NTU202000120

Since the papillary dermis is the area between the basal layer and the reticular dermis. We defined the central layer between the basal layer and the top reticular layer as the middle papillary dermis layer. The depth of reticular dermis is counted from the top of SC to the top of the reticular dermis.

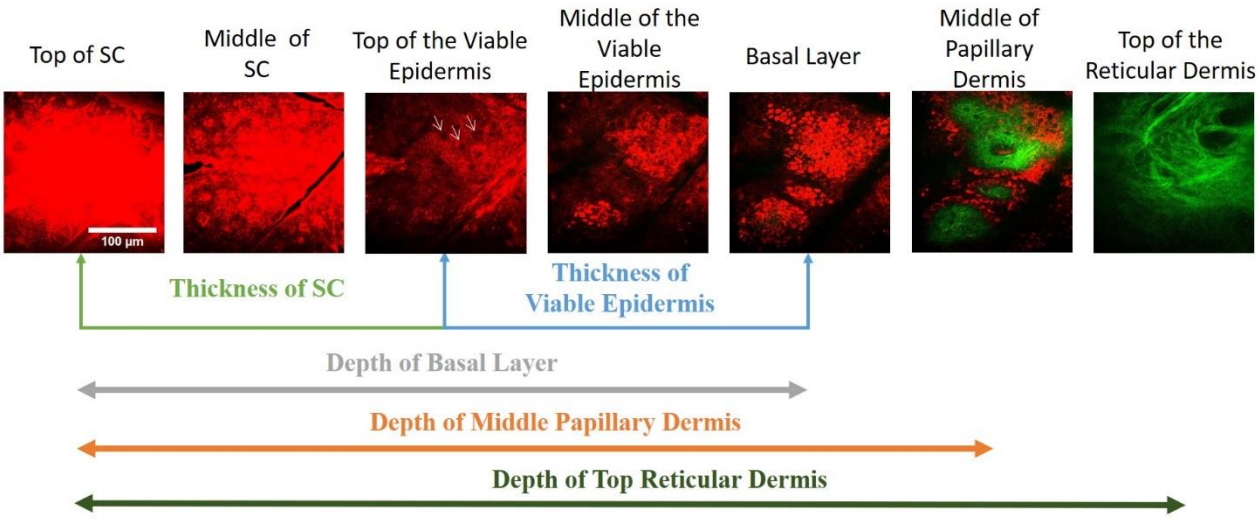

Fig. 3.12 The HGM images of human skin obtained at different depth with different skin structures. Here we defined the thickness of SC, the thickness of viable epidermis, the depth of the basal layer, the depth of the middle papillary dermis, and the depth of the top reticular dermis. Scale bar: 100 μm

3.4.4 Intensity Analysis

Intensity analysis: The intensity analysis in this study is quite different from the analysis that frequently used in some previous studies. Although provided with a stack of images at different skin depths, we are not going to compare the intensity at the same skin depth prior and after the glycerol application by plotting the depth-dependent intensity diagram. After the application of glycerol, layer depth will follow the variation of structures (for example, shrinkage), and it is unsuitable to compare the image intensity at

doi:10.6342/NTU202000120

the same depth since the image intensity will be affected by the shift of the layer depth. Based on the high 3D resolution and label-free characteristic of the HGM that enables us to distinguish different skin sub-layers, we implemented the position correction to achieve the image intensity comparison of the same skin structures before and after the glycerol application. We recorded and compared the average THG intensities of five different skin layers of the control group and the glycerol group, which were the bottom of stratum corneum, the middle layer of the viable epidermis, the basal layer, the middle layer of the papillary dermis, and the top layer of the reticular dermis. The average SHG intensities of three different depths were recorded, which were the middle layer of papillary dermis, the top reticular dermis, and the layer with the maximum SHG intensity.

The result of the skin thickness and the HGM image intensity was expressed as mean ± standard deviation. Independent sample t-test was used for comparisons between the control group and the glycerol group. Statistics were performed with the excel software (Microsoft office 2013), and $P < 0.05$ was considered statistically significant.

doi:10.6342/NTU202000120

Chapter 4 Results of the *Ex Vivo* Optical Clearing

4.1 System Calibration by Using Gallium Nitrite

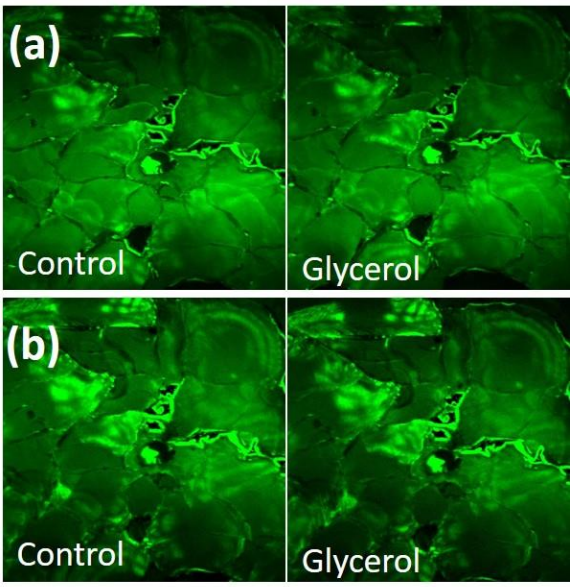

Fig. 4.1 SHG images of GaN for system calibration. Left: The reference SHG image before taking the HGM skin image of the control group. Right: The SHG image before taking the HGM skin image of the glycerol group. (PMT setting: 400 Volt, Contrast: 400~4500, Illuminate power: 20 mW). It was only a little difference and indicates that the system condition remained the same. (a) Case E100-I90-1 (b) Case E100-I90-2

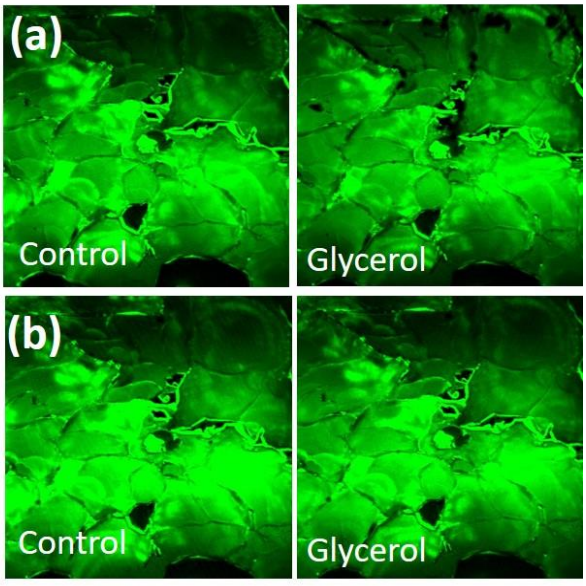

Fig. 4.2 SHG images of GaN for system calibration. Left: The SHG image before taking the HGM skin image of the control group. Right: The reference SHG image before taking

doi:10.6342/NTU202000120

the HGM skin image of the glycerol group. (PMT setting: 400 Volt, Contrast: 400~4500, Illuminate power: 20 mW). It was only a little difference and indicates that the system condition remained the same. (a) Case E50-I90-1 (b) Case E50-I90-2

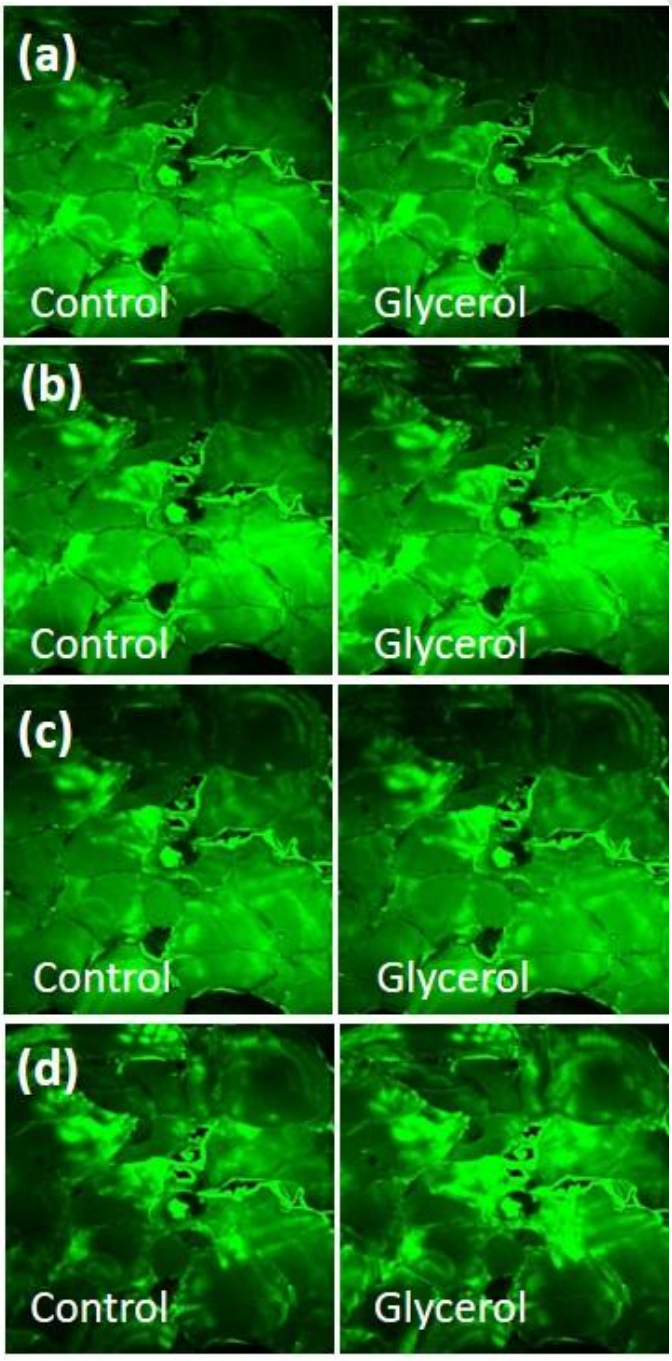

Fig. 4.3 SHG images of GaN for system calibration. Left: The reference SHG image before taking the HGM skin image of the control group. Right: The SHG image before taking the HGM skin image of the glycerol group. (PMT setting: 400 Volt, Contrast: 400~4500, Illuminate power: 20 mW). It was only a little difference and indicates that the system condition remained the same. (a) Case E50-T90-1 (b) Case E50-T90-2 (c) Case E50-T90-3 (d) Case E50-T90-4

doi:10.6342/NTU202000120

4.2 Bright-filed Image

There are two skin tissues used to study the optical clearing in case E100-I90, named E100-I90-1 (skin of scalp) and E100-I90-2 (skin of armpit). Fig. 4.4 shows bright light field trans-illumination microscopy images before (left) glycerol application and after (right) glycerol application. After we immersed the skin tissues into 100% glycerol for 90 minutes, the transparency of the skin was highly enhanced, and the hair inside the deeper skin became visible.

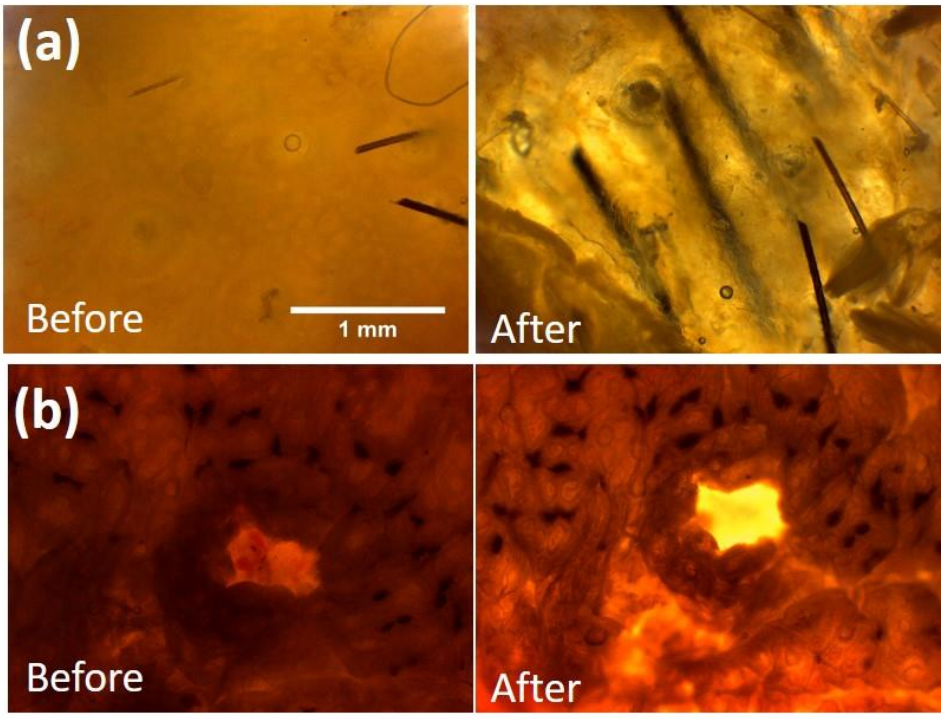

Fig. 4.4 Bright field images taken by Leica ICC50 HD. Left: normal skin. Right: skin after immersed into 100% glycerol for 90 mins. The transmission light increased and the deeper hair became visible. Scale bar: 1 mm. (a) Case E100-I90-1 (b) Case E100-I90-2

For 50% case type, after 90 minutes immersion, the hair inside the deep skin region became clearer and indicated that the transmittance of the skin was enhanced (Fig. 4.5).

doi:10.6342/NTU202000120

The results were similar to the results of 100% immersion but with less enhancements of the transmittance. Although it was only a half concentration when comparing the case E100-I90, it did alter the skin scattering property after 90 minutes immersion.

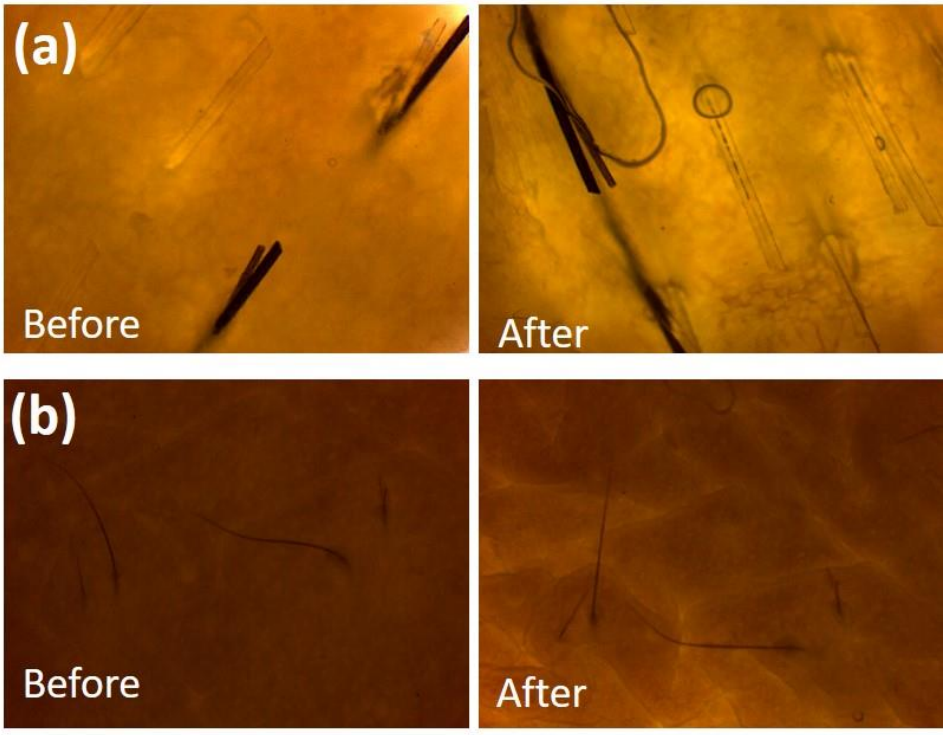

Fig. 4.5 Bright field images taken by Leica ICC50 HD. Left: normal skin. Right: skin after immersed into 50% glycerol for 90 mins. The transmission light increased and the deeper hair became visible. (a) Case E50-I90-1 (b) Case E50-I90-2

Fig. 4.6 shows the bright-field images before and after topically applied with the 50% glycerol. When comparing to the immersion cases, which the transmission light increased significantly after the glycerol application, for the case of 50% glycerol topically applied, the enhancement of the transmission light was not obvious.

doi:10.6342/NTU202000120

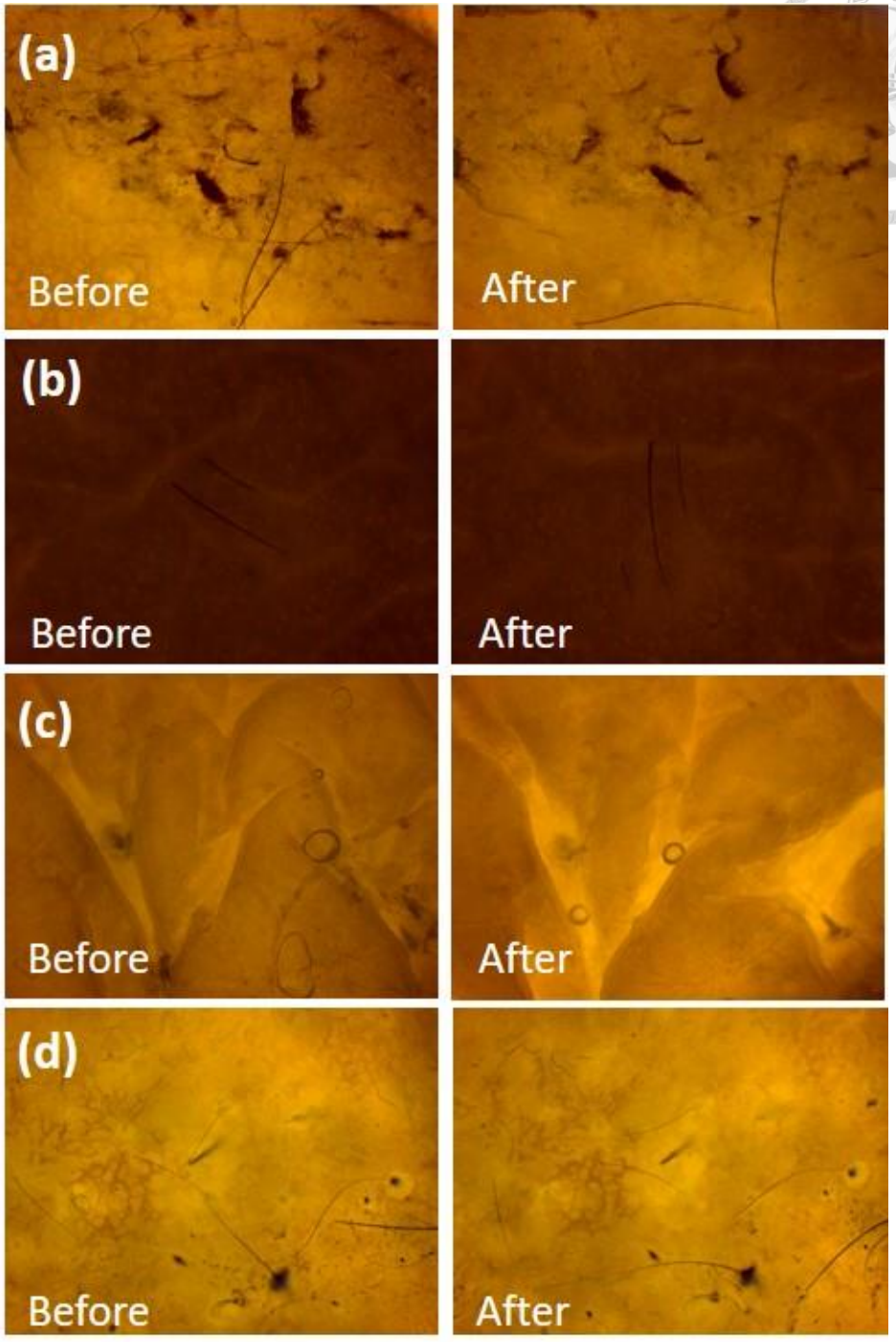

Fig. 4.6 Bright field images taken by Leica ICC50 HD. Left: normal skin. Right: skin after topically applied with 50% glycerol for 90 mins. (a) Case E50-T90-1 (b) Case E50-T90-2 (c) Case E50-T90-3 (d) Case E50-T90-4

4.3 Statistical Analysis of HGM Image and

doi:10.6342/NTU202000120

Representative HGM Images

In this section, we presented the analysis of HGM skin images. The optical clearing effects of the SHG and THG image were discussed. We took the stack images randomly on the skin surface to analyze effect of the optical clearing statistically. The number of positions depended on the size of the skin sample.

4.3.1 Tissue Immersed by 100% Glycerol for 90 Minutes (E100-I90)

In case-E100-I90-1, we took eight different positions for the control group, and another eight different positions for the glycerol group to image. In case E100-I90-2: nine different positions as a control group and another nine different positions as a glycerol group for HGM imaging. The thickness of the tissue was measured by observing the specific structure of the HGM images. Table 4.1 recorded the structure analysis results of Case E100-I90. For Case E100-I90-1, after 100% glycerol immersion, only the depth of the top reticular dermis layer was found with a significant difference, which increased by only 7%. In contrast, in the Case E100-I90-2, the skin shrank significantly at all layers. In previous studies, the anhydrous glycerol was proved to make the skin shrink [6, 7, 9]. However, we only found significant shrinkage of the skin in Case E100-I90-2. The skin of the armpit was softer than the skin of the scalp to make it shrink more severely.

Table 4.1 Skin structure analysis results of case E100-I90. (*P <0.05, ** P <0.01, *** P <0.001)

Depth or thickness change (μm)	Thickness of SC	Thickness of viable epidermis	Depth of basal layer	Depth of middle papillary dermis layer	Depth of top reticular dermis layer

doi:10.6342/NTU202000120

1	Control (N=8)	13.7±4.6	54.9±13.4	68.6±13.0	113.0±9.1	156.6±8.8
	Glycerol (N=8)	12.6±4.6	50.6±7.5	63.2±11.6	116.1±7.8	168.5±13.4*
2	Control (N=9)	30.0±2.4	29.2±3.5	59.2±3.9	114.2±6.7	167.8±13.3
	Glycerol (N=9)	21.6±4.5***	20.4±5.3***	42.0±4.2***	87.0±5.2***	131.0±10.5***

Fig. 4.7 and Fig. 4.8 showed the statistical analysis of the THG and SHG intensities in Case E100-I90. For THG, the average intensities reduced significantly at superficial levels (SC, and the viable epidermis) but increased significantly at deep levels (the reticular dermis) in Case E100-I90-1. While in Case E100-I90-2, the average THG intensities reduced significantly only at SC. For SHG, the average SHG intensities increased at all three different depths in both Case E100-I90-1 and Case E100-I90-2.

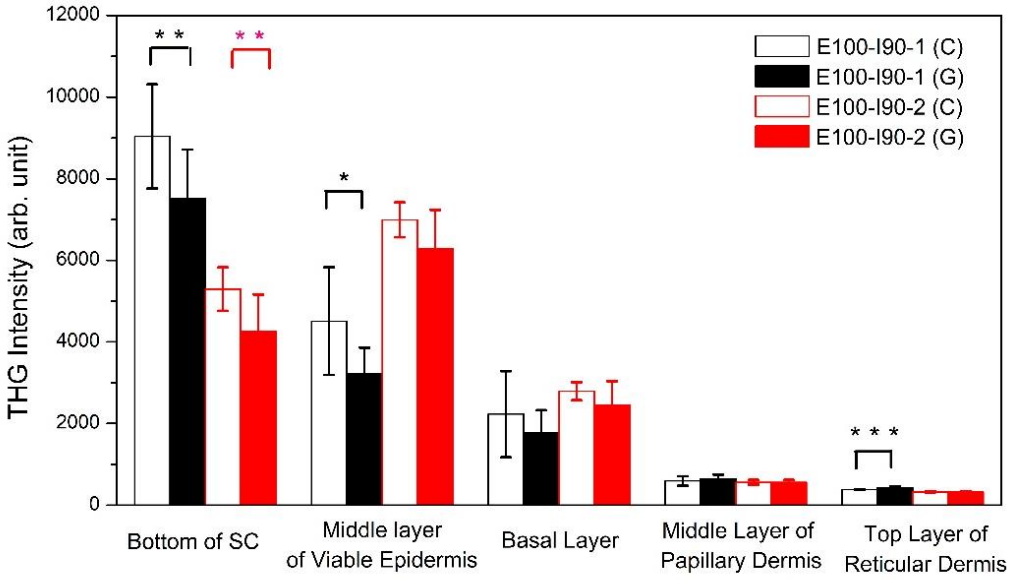

Fig. 4.7 Quantitative analysis and comparison of skin THG intensities at five different depths. Black: Case E100-I90-1 (control: N=8, glycerol: N=8); Red: Case E100-I90-2 (control: N=9, glycerol: N=9). *P <0.05; **P <0.01; *** P <0.001. C: control; G: glycerol.

doi:10.6342/NTU202000120

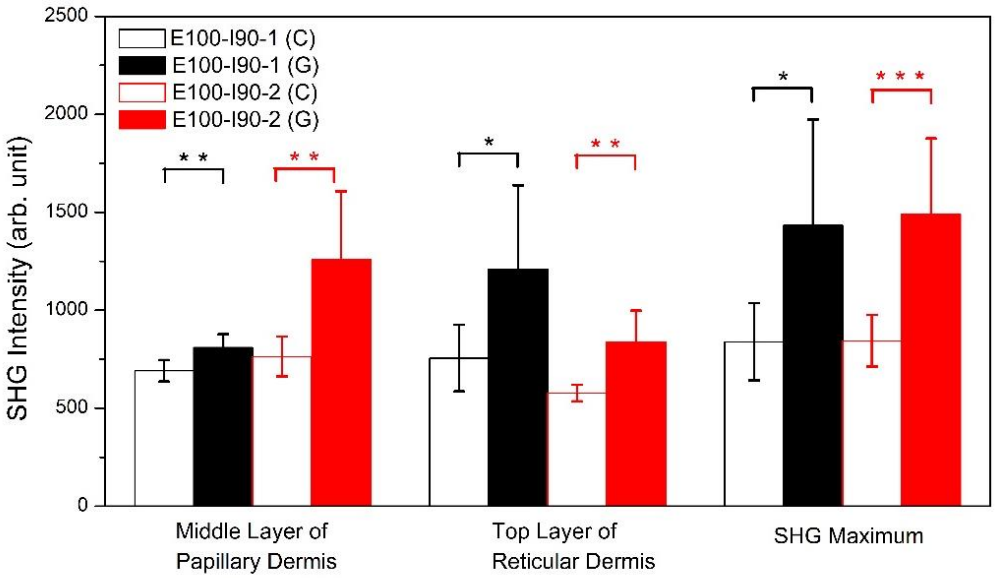

Fig. 4.8 Quantitative analysis and comparison of skin SHG intensities at three different depths. Black: Case E100-I90-1 (control: N=8, glycerol: N=8); Red: Case E100-I90-2 (control: N=9, glycerol: N=9). *P <0.05; ** P <0.01; *** P <0.001. C: control; G: glycerol.

Table 4.2 and Table 4.3 showed representative lateral HGM stack images at different skin layers before and after the glycerol application. Fig. 4.9 and Fig. 4.10 showed representative *en face* HGM stack images. In both cases, the THG (red) intensity and contrast at the epidermis decreased. While at the dermis, the SHG (green) intensity of the collagen strongly increased [61]. Similar to the Case E100-I90-1, the THG provided cell structure at the viable epidermis of the Case E100-I90-2 became less visible after the glycerol application, in contrast to the much-enhanced SHG intensity in the dermis [61]. The green signal at the sample surface was attributed to autofluorescence leakage due to residual dye from a marker pen.

doi:10.6342/NTU202000120

Table 4.2 The lateral HGM skin images at six different depths of the control group and the glycerol group. Red: THG (Contrast setting: 600~10000). Green: SHG (Contrast setting: 600~4500).

Case E100-I90-1				
	Glycerol-1	Glycerol-2	Control-1	Control-2
TOP	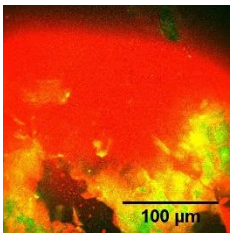	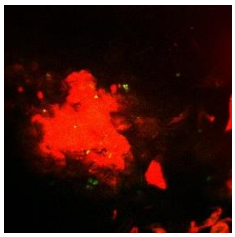	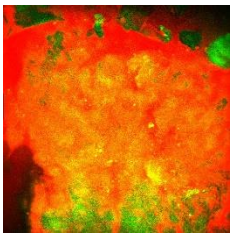	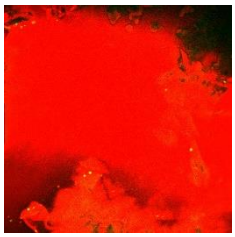
Bottom of SC	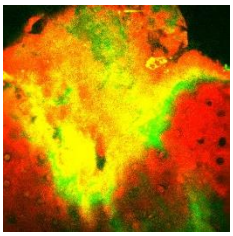	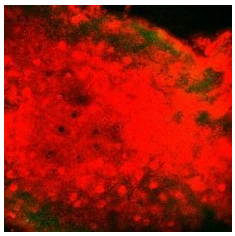	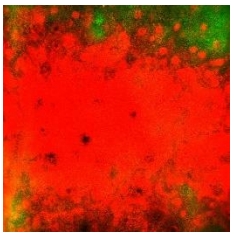	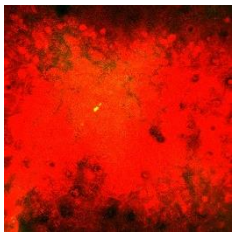
	16.2 μm	18 μm	10.8 μm	14.4 μm
Middle Layer of Viable Epidermis	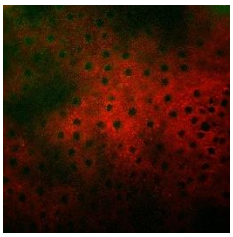	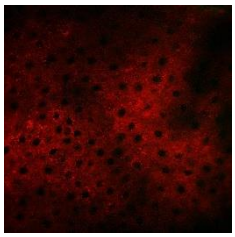	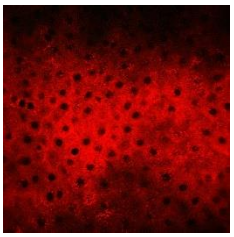	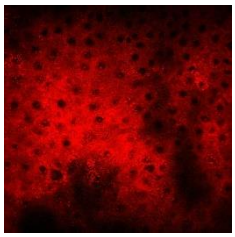
	45 μm	46.8 μm	32.4 μm	43.2 μm
Basal Layer	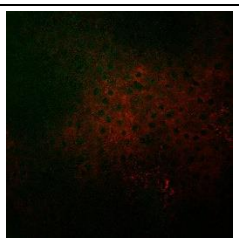	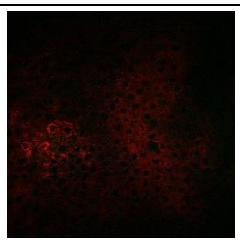	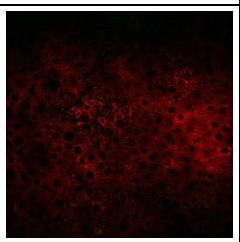	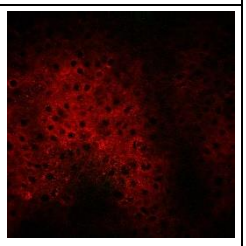
	73.8 μm	75.6 μm	73.8 μm	72 μm

doi:10.6342/NTU202000120

Middle Layer of Papillary Dermis	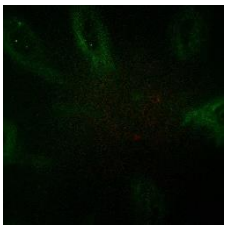	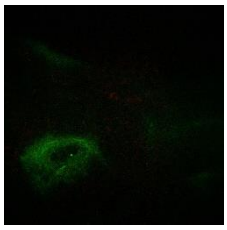	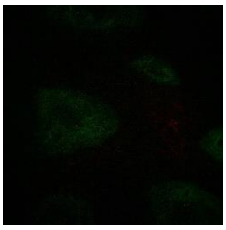	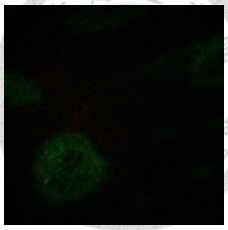
	120.6 μm	117 μm	118.8 μm	122.4 μm
Top Layer of Reticular Dermis	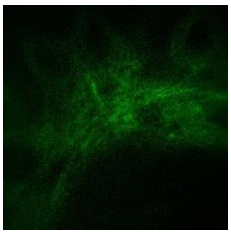	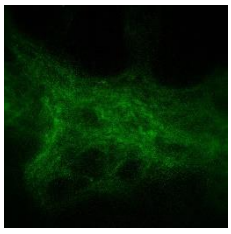	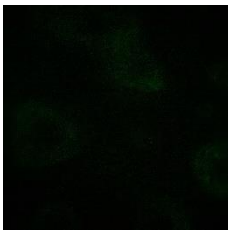	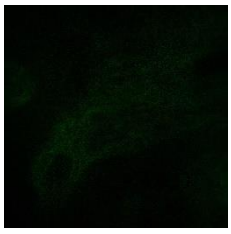
	167.4 μm	158.4 μm	162 μm	172.8 μm

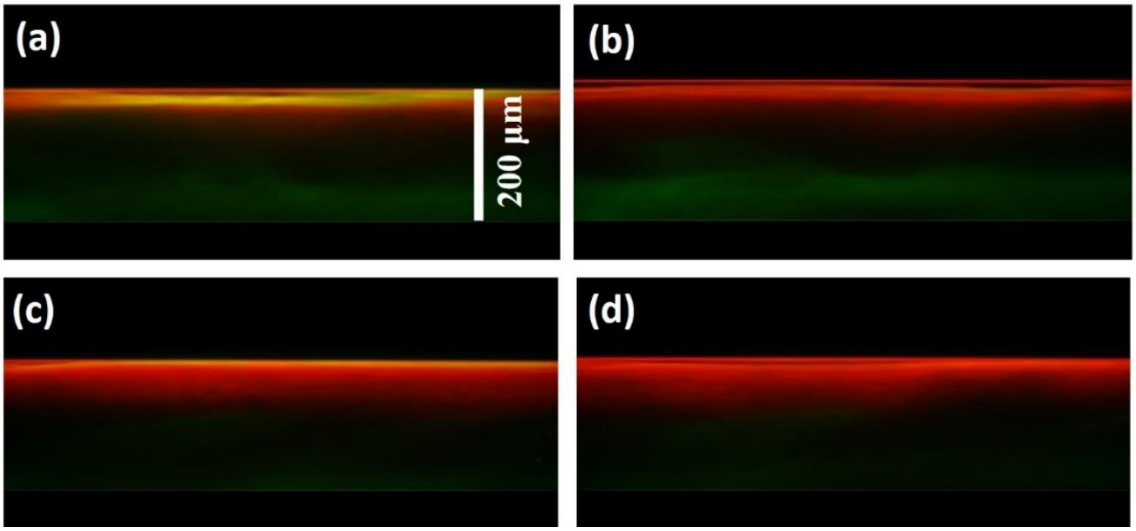

Fig. 4.9 *En face* skin image of Case E100-I90-1 (a) Glycerol-1 (b) Glycerol-2 (c) Control-1 (d) Control-2. Red: THG (Contrast setting: 600~10000). Green: SHG (Contrast setting: 600~4500).

Table 4.3 The lateral HGM images of the control group and the glycerol group at different depths. Red: THG (Contrast setting: 600~10000). Green: SHG (Contrast setting: 600~4500).

Case E100-I90-2				
	Glycerol	Glycerol	Control	Control

doi:10.6342/NTU202000120

TOP	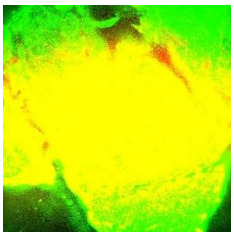	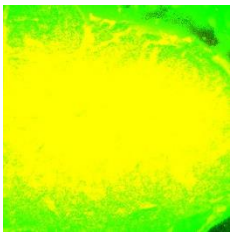		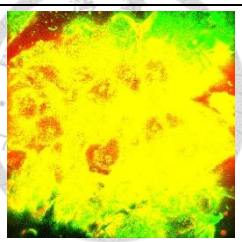
Bottom of SC	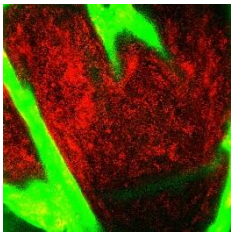	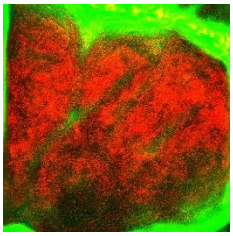	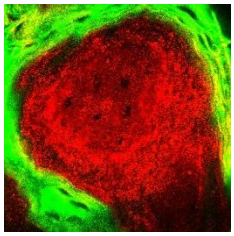	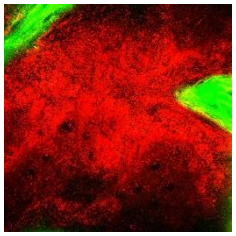
	23.4 μm	18 μm	30.6 μm	28.8 μm
Middle Layer of Viable Dermis	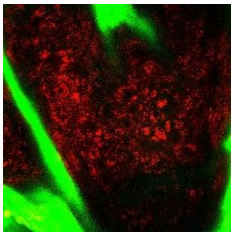	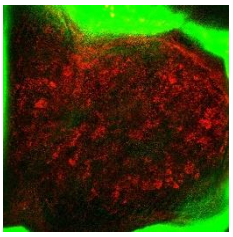	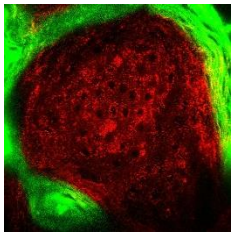	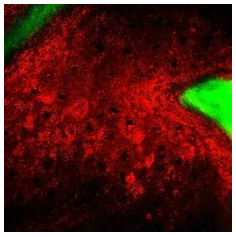
	32.4 μm	27 μm	43.2 μm	41.4 μm
Basal Layer	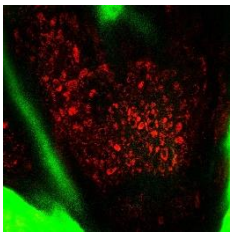	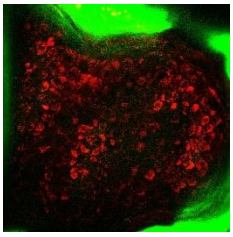	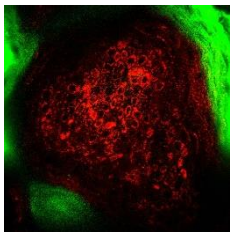	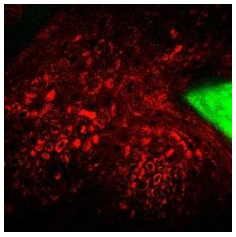
	41.4 μm	37.8 μm	57.6 μm	55.8 μm
Middle Layer of Papillary Dermis	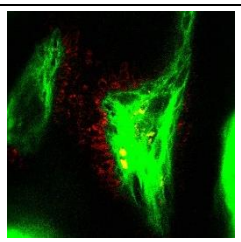	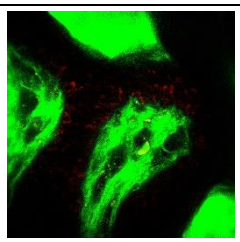	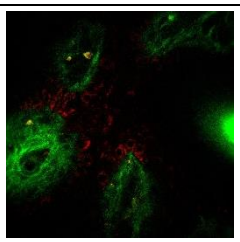	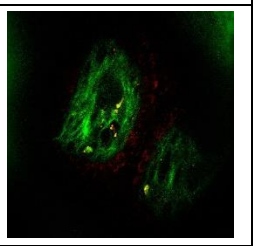
	81 μm	88.2 μm	113.4 μm	115.2 μm

doi:10.6342/NTU202000120

Top Layer of Reticular Dermis	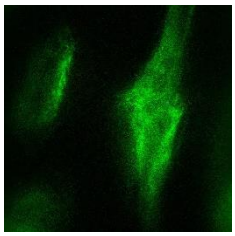	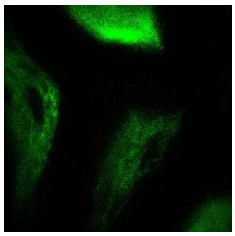	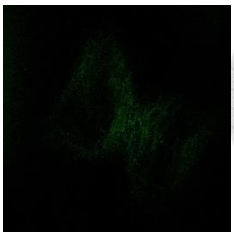	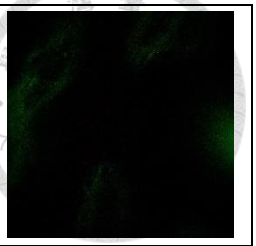
	120.6 μm	138.6 μm	171 μm	169.2 μm

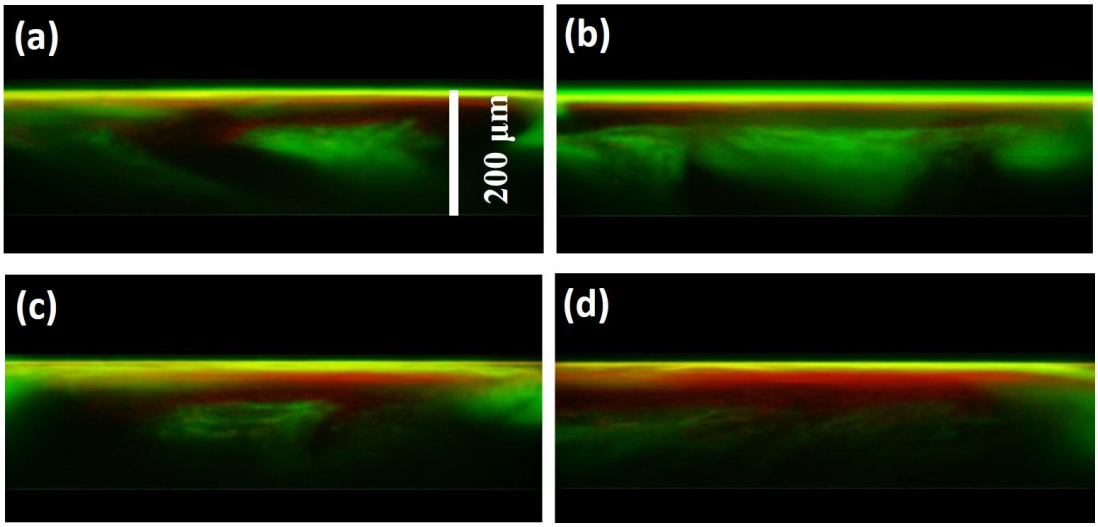

Fig. 4.10 *En face* skin image of Case E100-I90-2 (a) Glycerol-1 (b) Glycerol-2 (c) Control-1 (d) Control-2. Red: THG (Contrast setting: 600~10000). Green: SHG (Contrast setting: 600~4500).

4.3.2 Tissue Immersed by 50% Glycerol for 90 Minutes (E50-I90)

In case E50-I90-1, we randomly took six different positions as a control group and other six different positions as a glycerol group for HGM imaging. In case E50-I90-2, we randomly took twelve different positions as a control group and another twelve different positions as a glycerol group for HGM imaging. Table 4.4 recorded the structure analysis results of Case E50-I90. In the previous cases of the100% glycerol immersion, we found there is an entire shrinkage of the whole skin sample. While for the case of 50% glycerol,

doi:10.6342/NTU202000120

its dehydration power was less than the 100% glycerol and only the shrinkages of the SC were observed.

Table 4.4 Skin structure analysis results of Case E50-I90. (*P <0.05, ** P <0.01, *** P <0.001)

	Depth or thickness change (μm)	Thickness of SC	Thickness of viable epidermis	Depth of basal layer	Depth of middle papillary dermis layer	Depth of top reticular dermis layer
1	C (N=6)	12.0±3.4	15.3±3.7	27.3±4.8	66.6±10.4	108.0±30.9
	G (N=6)	7.5±1.4*	15.0±5.7	22.5±5.4	66.0±16.9	105.0±16.1
2	C (N=12)	30.6±3.0	27.8±5.8	58.4±4.5	109.1±5.1	158.7±10.1
	G (N=12)	18.0±3.5***	35.1±6.8**	53.1±8.3	120.8±4.4***	187.7±6.0***

Fig. 4.11 and Fig. 4.12 showed the statistical analysis of the THG and SHG intensities in Case E100-I90. In Case E100-I90-1, the average THG intensity at the bottom of SC, the middle layer of the viable epidermis, and the basal layer increased by nearly 11.4%, 15.1%, and 29.8%, separately (Fig. 4.11), but did not show the significant difference. At deeper layers, papillary dermis and reticular dermis, the average THG intensity increased significantly by nearly 2-fold and 2.4-fold. The SHG intensity at middle layer of the papillary dermis, the top layer of reticular dermis, and the SHG maximum all increased significantly by nearly 2.2-fold, 2.1-fold, and 3.28-fold. There were strong increments of the HGM intensity at the papillary dermis and the reticular dermis. In Case E100-I90-2, the THG intensities of the bottom of SC, the middle layer of the viable epidermis, the basal layer, and middle layer of the papillary dermis all increased significantly by nearly 36.2%, 37.3%, 40.8%, and 43%, separately (Fig. 4.11). At dermis, no significant difference of THG intensity was found. Fig. 4.12 recorded the SHG intensity at three different skin layers. The SHG intensity at the middle layer of papillary

doi:10.6342/NTU202000120

dermis, the top layer of reticular dermis, and the SHG maximum all increased significantly by nearly 15%, 49%, and 44%

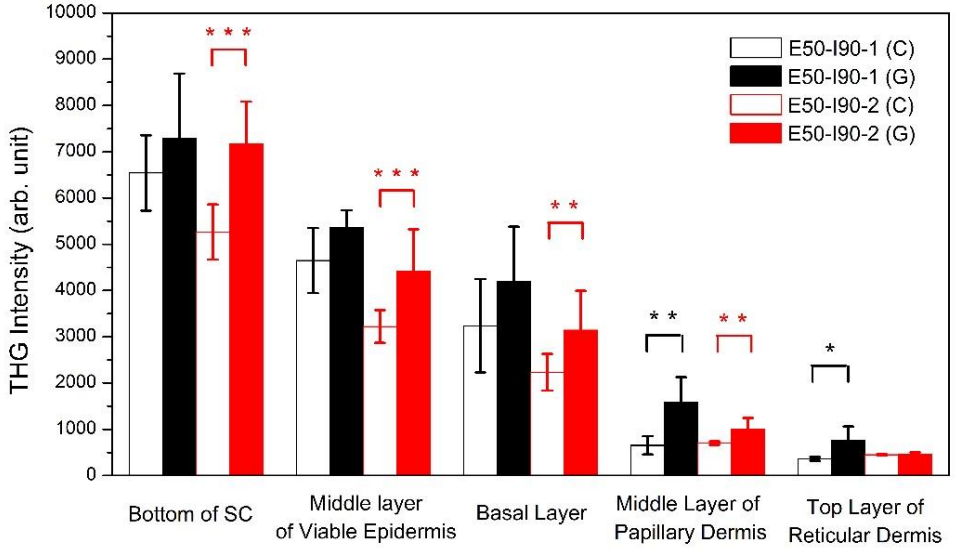

Fig. 4.11 Quantitative analysis and comparison of skin THG intensities at five different depths. Black: Case E50-I90-1 (control: N=6, glycerol: N=6); Red: Case E50-I90-2 (control: N=12, glycerol: N=12). *P <0.05; **P <0.01; *** P <0.001. C: control. G: glycerol.

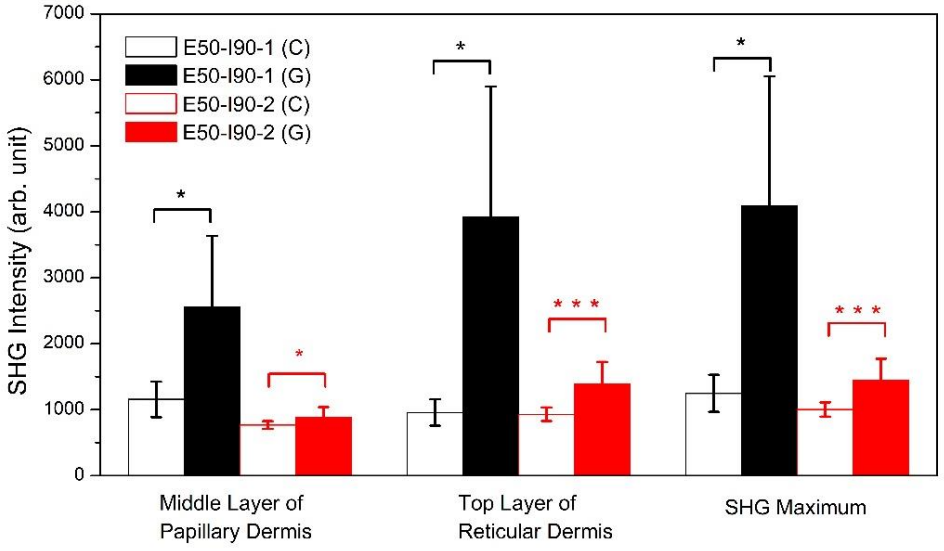

Fig. 4.12 Quantitative analysis and comparison of skin SHG intensities at three different depths. Black: Case E50-I90-1 (control: N=6, glycerol: N=6); Red: Case E50-I90-2

doi:10.6342/NTU202000120

(control: N=12, glycerol: N=12). *P <0.05; **P <0.01; *** P <0.001. C: Control. G: glycerol.

Table 4.5 and Fig. 4.13 show the skin images of the case E50-I90-1. We observed that the HGM intensities increased significantly at papillary dermis and reticular dermis.

Table 4.6 and Fig. 4.14 show the skin images of the case E100-I90-2. We observed that the HGM intensities increased significantly at both epidermis and dermis.

Table 4.5 The lateral skin images of the control group and the glycerol group. We choose different skin layers to display the images. Red: THG (Contrast setting: 600~10000). Green: SHG (Contrast setting: 600~8000).

Case E50-I90-1				
	Glycerol	Glycerol	Control	Control
TOP	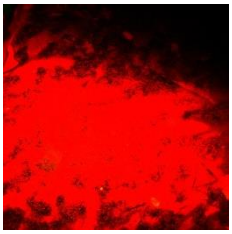	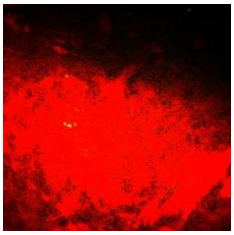	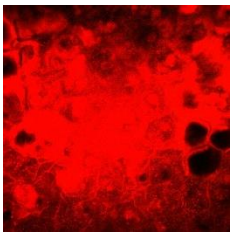	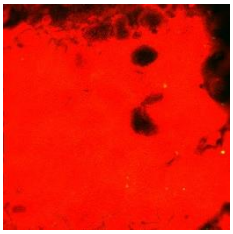
Bottom of SC	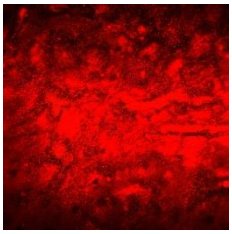	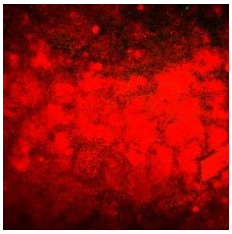	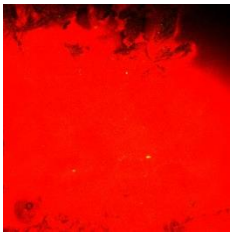	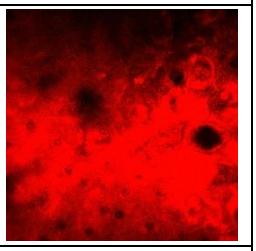
	9 μm	7.2 μm	7.2 μm	12.6 μm
Middle Layer of Viable Dermis	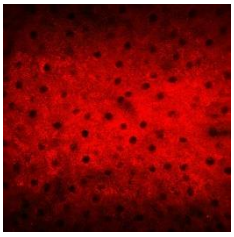	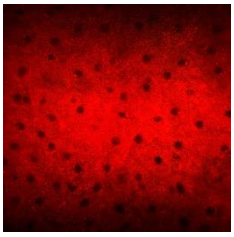	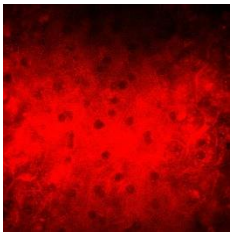	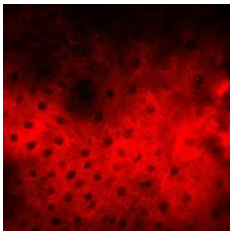
	19.8 μm	14.4 μm	14.4 μm	19.8 μm

doi:10.6342/NTU202000120

Basal Layer	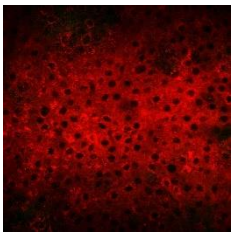	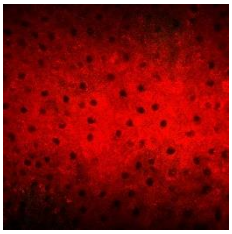	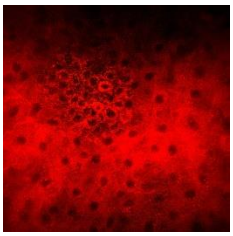	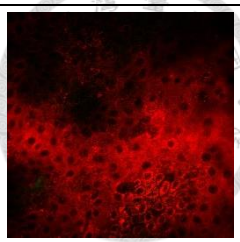
	28.8 μm	19.8 μm	18 μm	27 μm
Middle Layer of Papillary Dermis	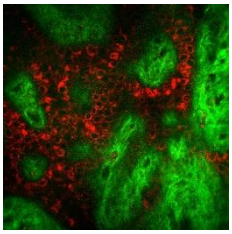	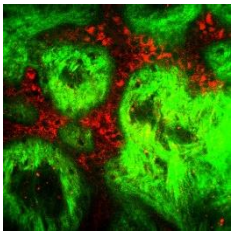	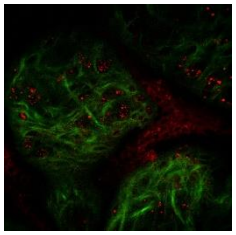	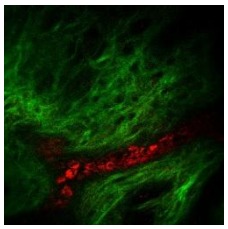
	55.8 μm	57.6 μm	50.4 μm	57.6 μm
Top Layer of Reticular Dermis	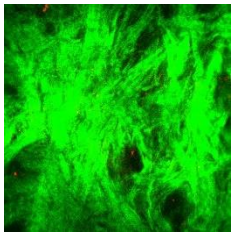	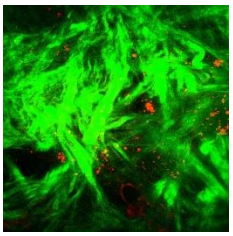	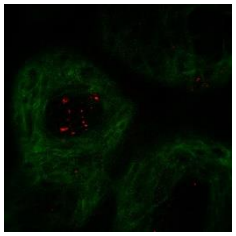	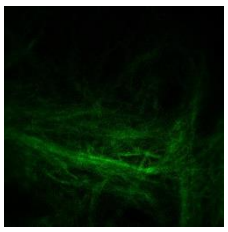
	81 μm	93.6 μm	82.8 μm	88.2 μm

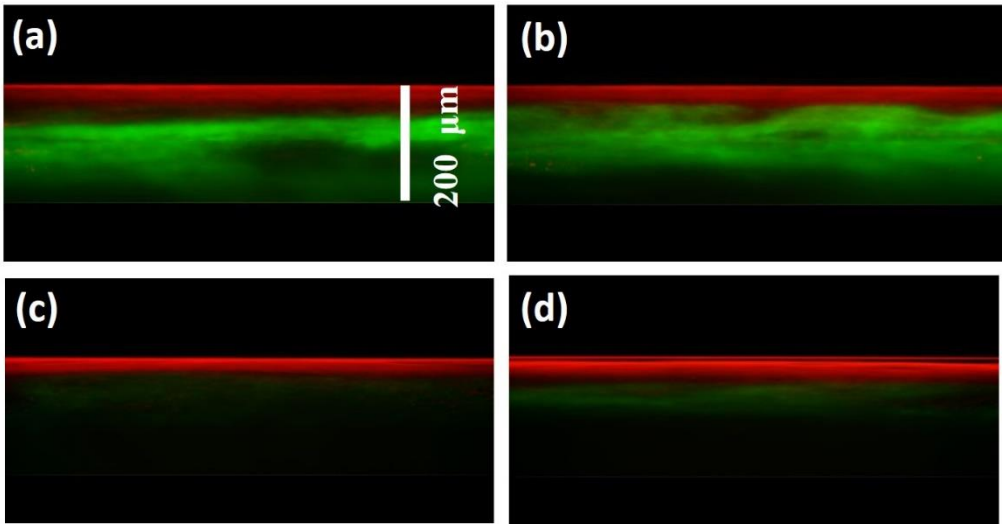

Fig. 4.13 *En face* skin image of Case E50-I90-1 (a) Glycerol-1 (b) Glycerol-2 (c) Control-1 (d) Control-2. Red: THG (Contrast setting: 600~10000). Green: SHG (Contrast setting: 600~8000).

doi:10.6342/NTU202000120

Table 4.6 The lateral skin images of the control group and the glycerol group. We choose different skin layers to display the images. Red: THG (Contrast setting: 600~10000). Green: SHG (Contrast setting: 600~4500).

Case E50-I90-2				
	Glycerol	Glycerol	Control	Control
TOP	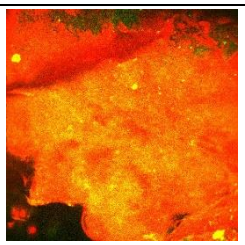	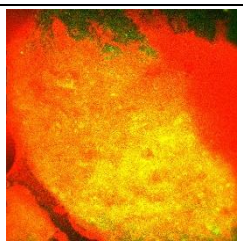	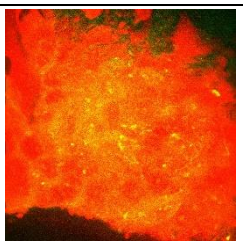	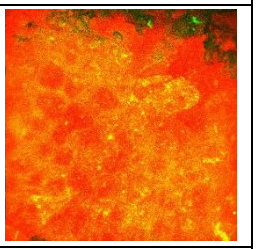
Bottom of SC	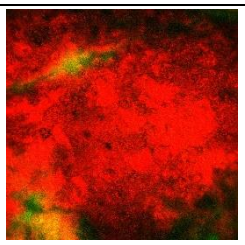	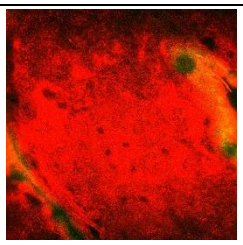	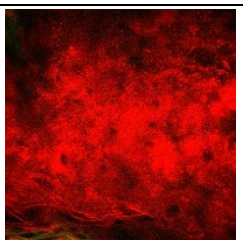	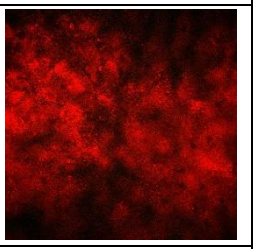
	19.8 μm	19.8 μm	30.6 μm	34.2 μm
Middle Layer of Viable Dermis	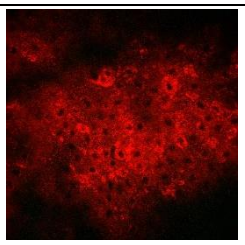	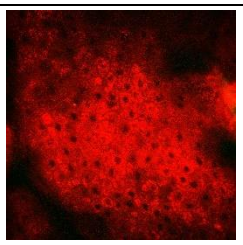	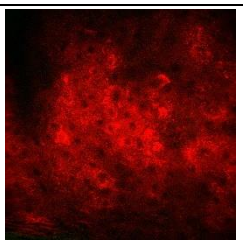	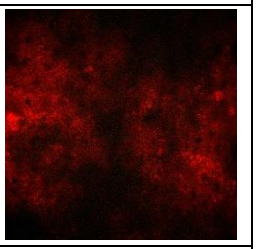
	41.4 μm	37.8 μm	45 μm	48.6 μm
Basal Layer	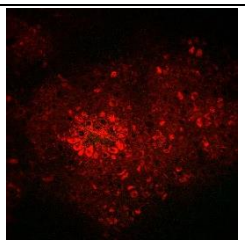	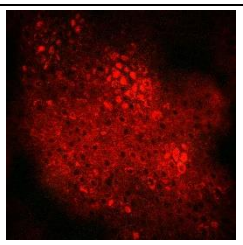	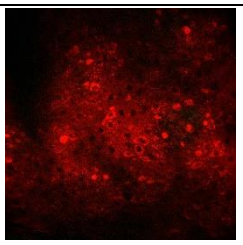	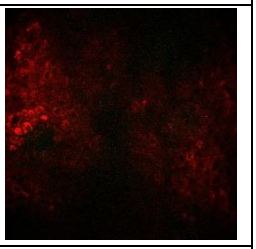
	63 μm	55.8 μm	57.6 μm	63 μm
Middle Layer of Papillary Dermis	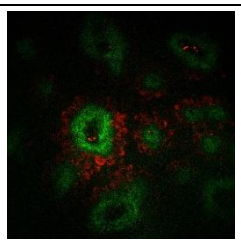	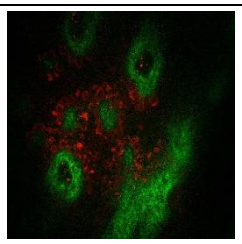	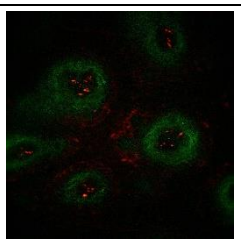	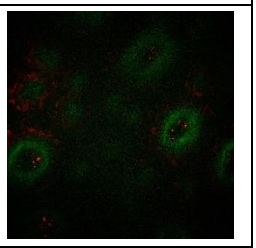

doi:10.6342/NTU202000120

	122.4 μm	118.8 μm	115.2 μm	106.2 μm
Top Layer of Reticular Dermis	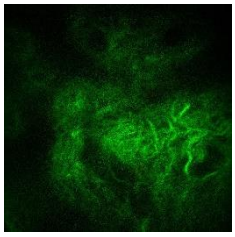	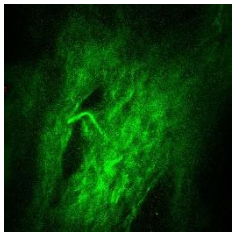	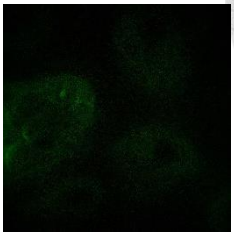	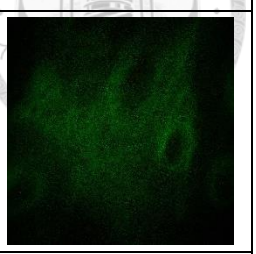
	180 μm	181.8 μm	171 μm	149.4 μm

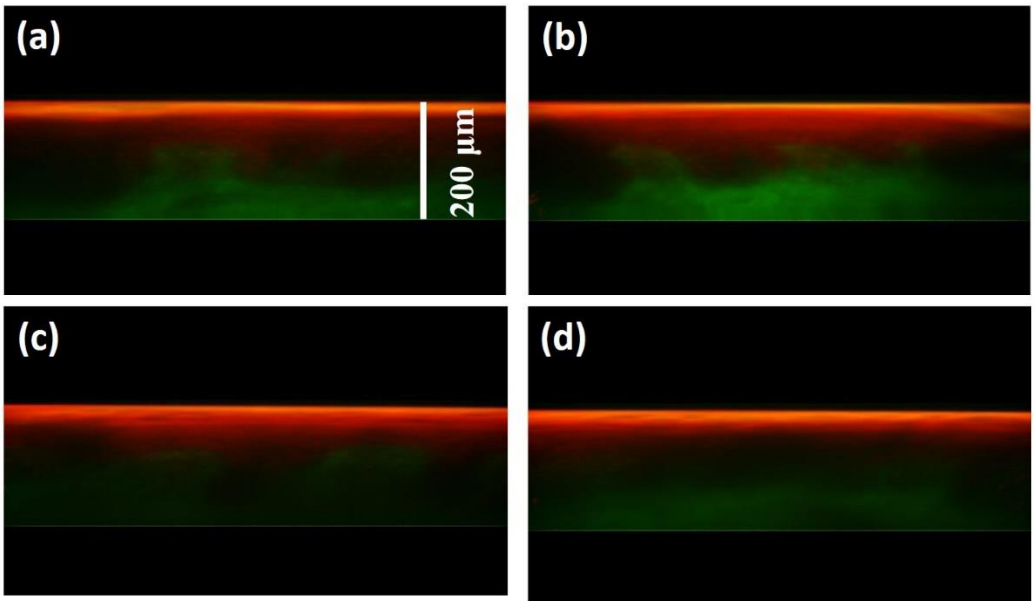

Fig. 4.14 *En face* skin image of Case E50-I90-2 (a) Glycerol-1 (b) Glycerol-2 (c) Control-1 (d) Control-2. Red: THG (Contrast setting: 600~10000). Green: SHG (Contrast setting: 600~4500).

4.3.3 Topically Applied by 50% Glycerol for 90 Minutes (E50-T90)

Table 4.7 shows the structure analysis of Case E50-T90. In case E50-T90-1: eight different positions as a control group and another eight different positions as a glycerol group for HGM imaging. The average thickness of the SC decreased significantly by nearly 40%. In the contrast, the average thickness of the viable epidermis increased significantly by 25%. The depth of the basal layer, the depth of middle papillary dermis layer, and the depth of the top reticular dermis layer remained the same. In Case E50-

doi:10.6342/NTU202000120

T90-2: ten different positions as a control group and another ten different positions as a glycerol group for HGM imaging. In this case, the thickness of SC decreased significantly by nearly 46%. In the contrast, the average thickness of the viable epidermis increased slightly by 14%. Since decrement of the SC thickness was much more than the increment of the viable epidermis thickness, the depth of the basal layer decreased significantly by nearly 15%. However, the depth of the middle papillary layer and of the top reticular dermis layer remained the same. In Case E50-T90-3: nine different positions as a control group and another nine different positions as a glycerol group for HGM imaging. In this case, the skin structure changed slightly and showing no significant difference. In Case E50-T90-4: seven different positions as a control group and another seven different positions as a glycerol group for HGM imaging. In this case, the thickness of SC, the thickness of viable epidermis, the depth of the basal layer, and the depth of middle papillary dermis all decreased significantly by nearly 45%, 13%, 32%, and 12%.

Table 4.7 Skin structure analysis results of all studied cases. (*P <0.05, ** P <0.01, *** P <0.001)

	Depth or thickness change (μm)	Thickness of SC	Thickness of viable epidermis	Depth of basal layer	Depth of middle papillary dermis layer	Depth of top reticular dermis layer
1	C (N=8)	22.1±4.8	33.8±6.1	55.8±6.3	95.4±5.4	134.1±12.7
	G (N=8)	13.3±1.6***	42.3±6.5*	55.6±7.0	94.1±9.0	132.3±12.6
2	C (N=10)	33.3±4.6	34.9±6.2	68.2±4.8	122.9±9.2	176.4±17.3
	G (N=10)	18.0±3.1***	40.1±6.0	58.1±5.8***	120.8±5.7	182.5±9.7
3	C (N=9)	12.2±2.0	53.8±12.4	66.0±10.8	93.4±15.1	120.4±13.7
	G (N=9)	13.0±1.5	57.2±7.8	70.2±8.3	92.2±12.2	113.4±17.6
4	C (N=7)	27.3±9.0	63.2±8.1	90.5±6.8	116.8±8.6	145.0±15.9
	G (N=7)	15.1±2.8***	55.5±7.0*	70.5±6.8***	102.6±7.8***	133.5±15.1

Fig. 4.15 and Fig. 4.16 showed the statistical analysis of the THG and SHG intensities in Case E50-T90. In Case E50-T90-1, the THG intensities of the epidermis did

doi:10.6342/NTU202000120

not show a significant difference. It seems that the THG intensities only depends on the depth. The thickness of SC was decreased and the average intensity of bottom of SC was increased. While at the middle layer of the viable epidermis, the basal layer, the papillary dermis, and the reticular dermis less or no shrinkage was observed and average THG changed slightly. However, at top of the reticular dermis and the SHG maximum, the average SHG intensity increased significantly by nearly 54% and 52%, separately. In Case E50-T90-2, the average THG intensities at all the epidermis and the papillary dermis increased significantly by nearly 65%, 28%, 26%, and 24%. While at reticular dermis, the average THG intensity remained the same and shows no shrinkage at this depth. The SHG intensity at three different depths. The SHG intensity at the reticular dermis and the maximum SHG intensity increased significantly by nearly 35% and 36%.

For Case E50-T90-3, the average THG intensities at the epidermis remained the same after the glycerol application. At the papillary dermis and the reticular dermis, the average THG and SHG intensities increased, but only the THG intensity at the papillary dermis increased significantly. In this case, it was less effectiveness after the glycerol application when comparing to other cases. For Case E50-T90-4, the THG intensities increased by nearly 43%, 66%, and 91% at the bottom of SC, middle layer of the viable epidermis, and the basal layer, separately. The THG intensity at the papillary dermis and the reticular dermis not showing the significant difference. Although the average SHG intensities all

doi:10.6342/NTU202000120

increased at three different depths, no significant difference was found.

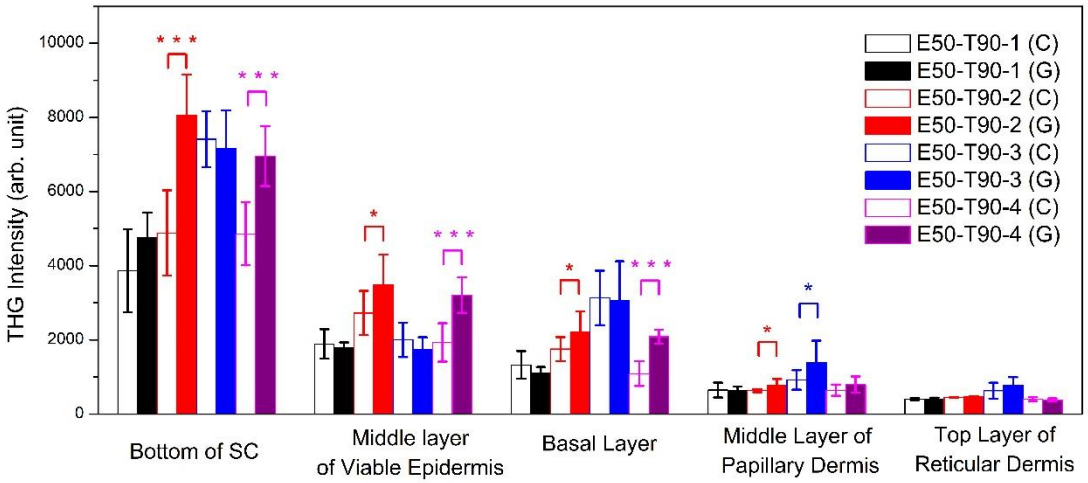

Fig. 4.15 Quantitative analysis and comparison of skin THG intensities at five different depths. Black: Case E50-T90-1 (control: N=8, glycerol: N=8); Red: Case E50-T90-2 (control: N=10, glycerol: N=10). Blue: Case E50-T90-3 (control: N=9, glycerol: N=9). Magenta: Case E50-T90-4 (control: N=7, glycerol: N=7). *P <0.05; **P <0.01; *** P <0.001. C: control; G: glycerol

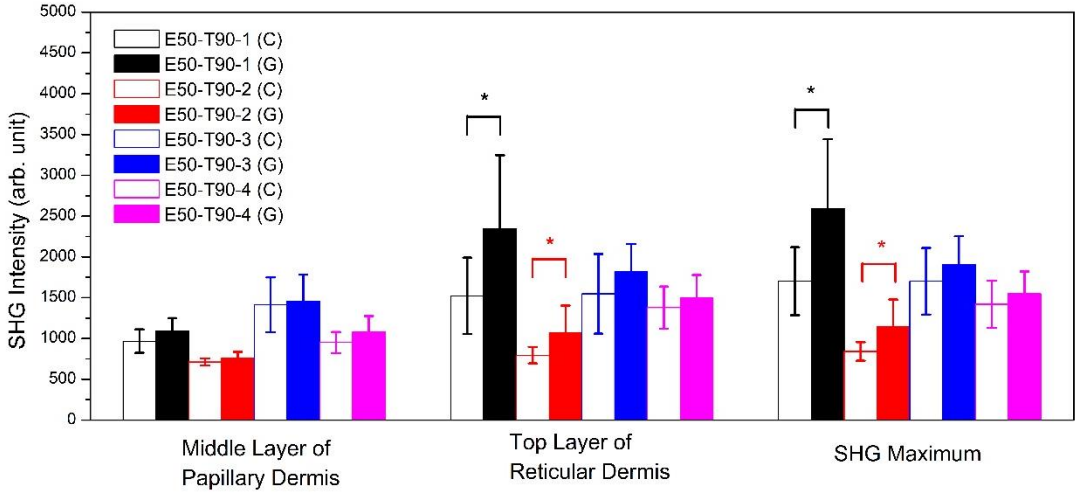

Fig. 4.16 Quantitative analysis and comparison of skin SHG intensities at three different depths. Black: Case E50-T90-1 (control: N=8, glycerol: N=8); Red: Case E50-T90-2 (control: N=10, glycerol: N=10). Blue: Case E50-T90-3 (control: N=9, glycerol: N=9). Magenta: Case E50-T90-4 (control: N=7, glycerol: N=7). *P <0.05; **P <0.01; *** P <0.001. C: control; G: glycerol.

From Table 4.8 to Table 4.11 show the relative lateral HGM images of Case E50-

doi:10.6342/NTU202000120

T90. The *en face* skin images were presented from Fig. 4.17 to Fig. 4.20.

Table 4.8 Case E50-T90-1: The lateral skin images of the control group and the glycerol group. Different skin layers images were presented. Red: THG (Contrast setting: 600~6000). Green: SHG (Contrast setting: 600~8000).

Case E50-T90-1				
	Glycerol	Glycerol	Control	Control
TOP	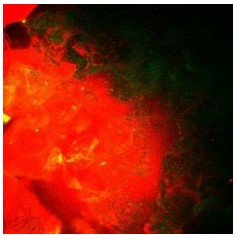	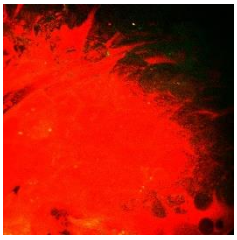	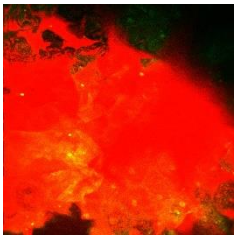	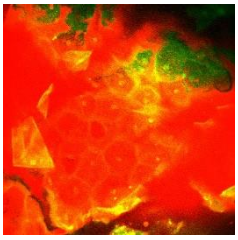
Bottom of SC	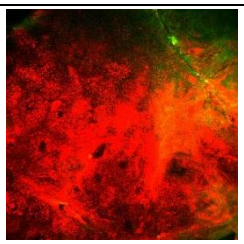	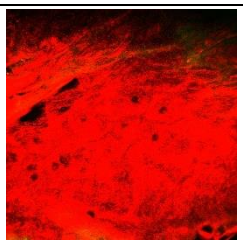	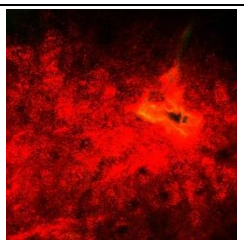	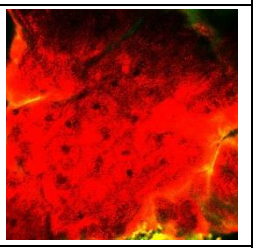
	14.4 μm	10.8 μm	19.8 μm	18 μm
Middle Layer of Viable Dermis	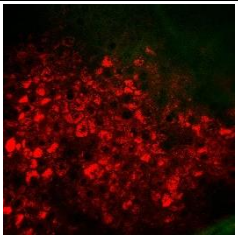	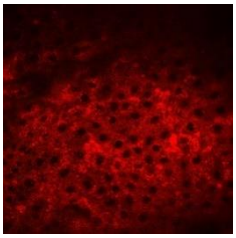	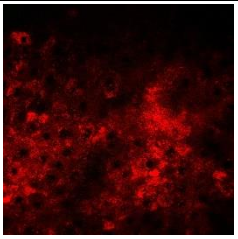	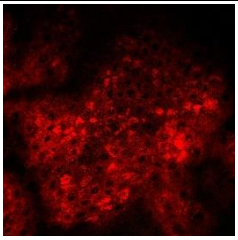
	36 μm	32.4 μm	34.2 μm	41.4 μm
Basal Layer	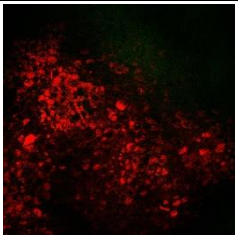	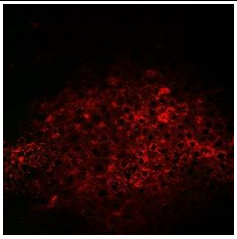	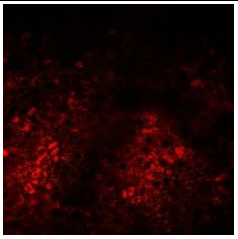	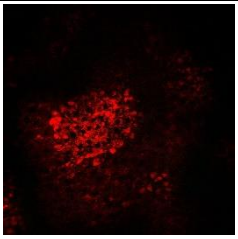
	55.8 μm	52.2 μm	48.6 μm	64.8 μm

doi:10.6342/NTU202000120

Middle Layer of Papillary Dermis	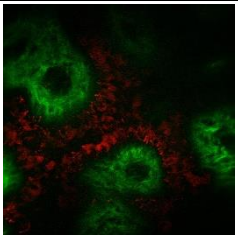	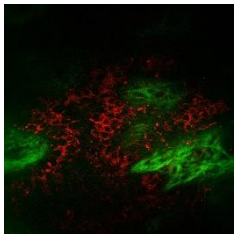	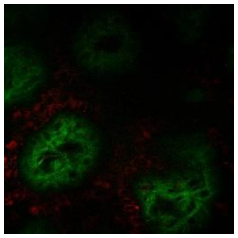	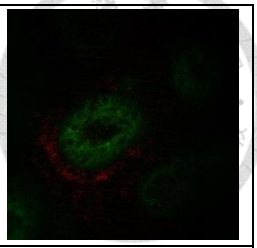
	118.8 μm	93.6 μm	120.6 μm	100.8 μm
Top Layer of Reticular Dermis	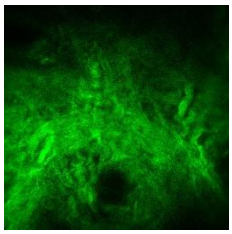	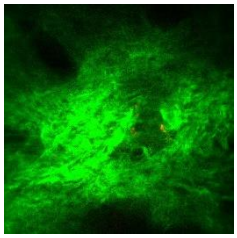	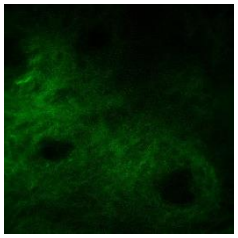	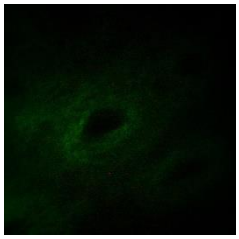
	142.2 μm	135 μm	156.6 μm	136.8 μm

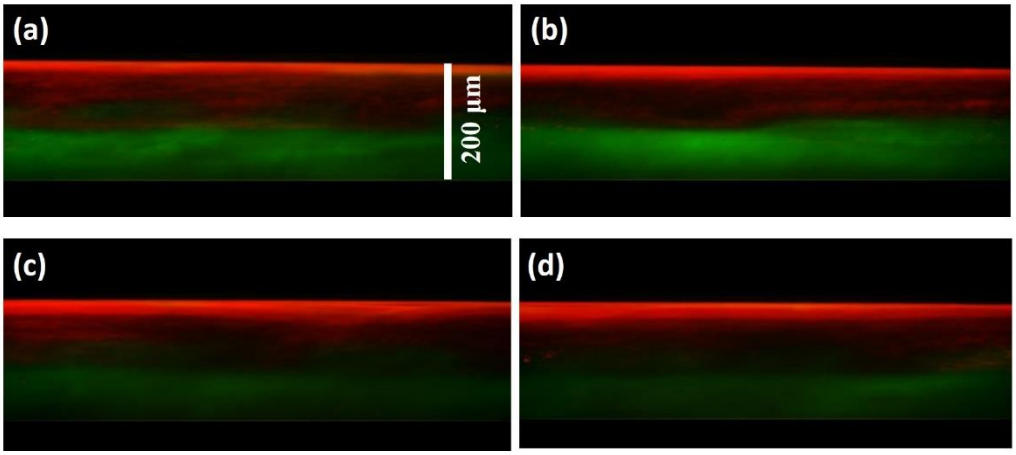

Fig. 4.17 *En face* skin image of Case E50-T90-1 (a) Glycerol-1 (b) Glycerol-2 (c) Control-1 (d) Control-2. Red: THG (Contrast setting: 600~6000). Green: SHG (Contrast setting: 600~8000).

Table 4.9 Case E50-T90-2: The lateral skin images of the control group and the glycerol group. Different skin layer images were presented. Red: THG (Contrast setting: 600~10000). Green: SHG (Contrast setting: 600~4500).

Case E50-T90-2				
	Glycerol	Glycerol	Control	Control

doi:10.6342/NTU202000120

TOP	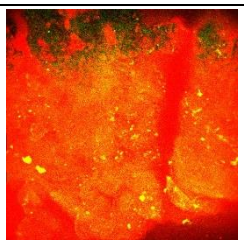		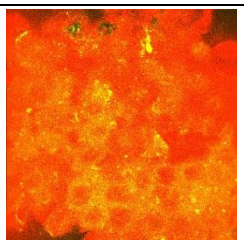	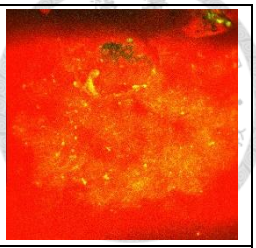
Bottom of SC		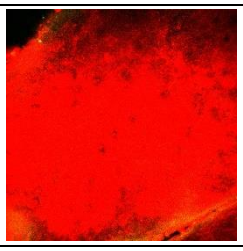	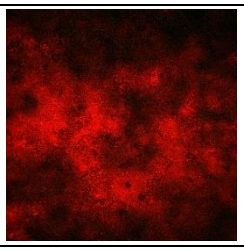	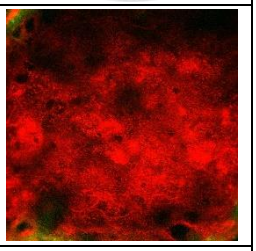
	19.8 μm	12.6 μm	36 μm	34.2 μm
Middle Layer of Viable Dermis	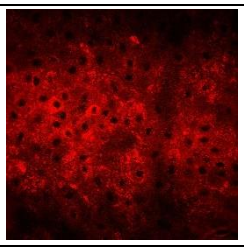	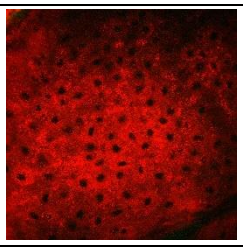	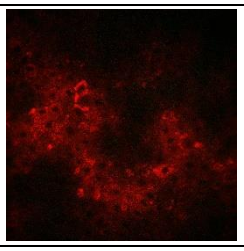	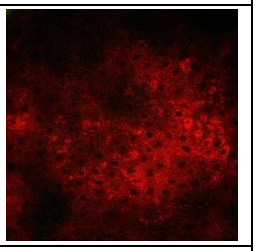
	39.6 μm	36 μm	54 μm	52.2 μm
Basal Layer	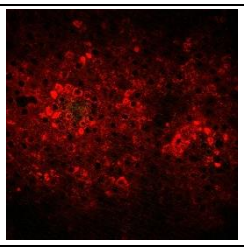	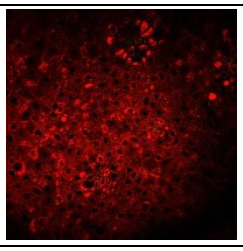	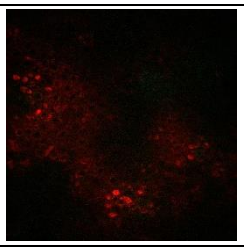	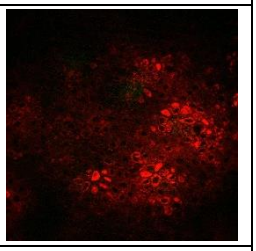
	57.6 μm	59.4 μm	70.2 μm	68.4 μm
Middle Layer of Papillary Dermis	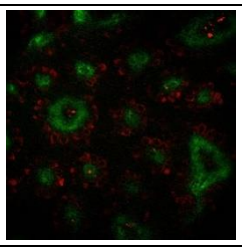	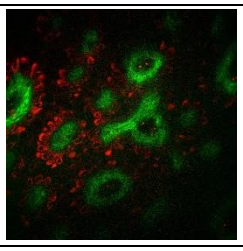	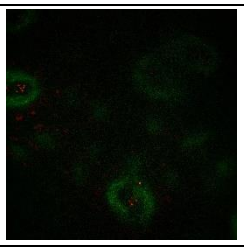	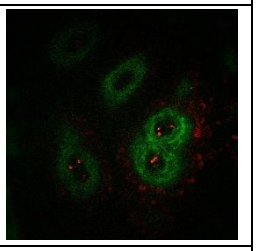
	122.4 μm	124.2 μm	117 μm	126 μm

doi:10.6342/NTU202000120

Top Layer of Reticular Dermis	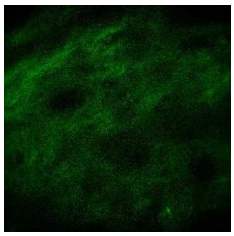	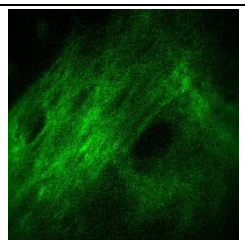	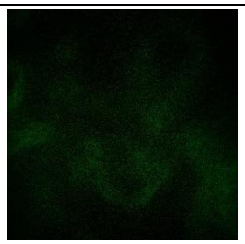	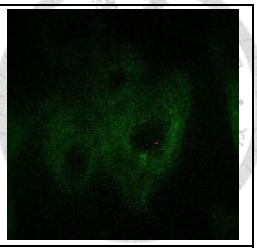
	185.4 μm	187.2 μm	162 μm	181.8 μm

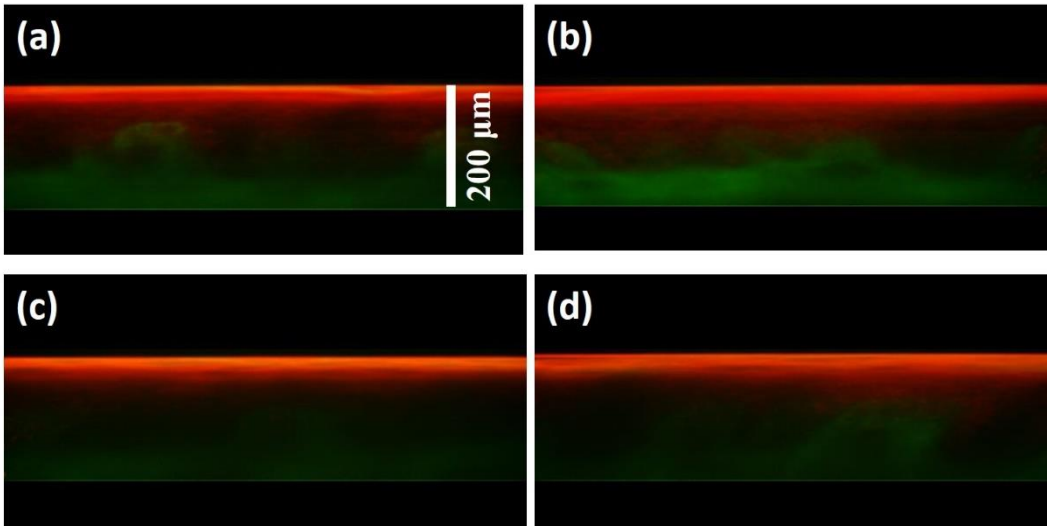

Fig. 4.18 *En face* skin image of Case E50-T90-2 (a) Glycerol-1 (b) Glycerol-2 (c) Control-1 (d) Control-2. Red: THG (Contrast setting: 600~10000). Green: SHG (Contrast setting: 600~4500).

Table 4.10 Case E50-T90-3: The lateral skin images of the control group and the glycerol group. Different skin layers images were presented. Red: THG (Contrast setting: 600~10000). Green: SHG (Contrast setting: 600~6000).

Case E50-T90-3				
	Glycerol	Glycerol	Control	Control
TOP	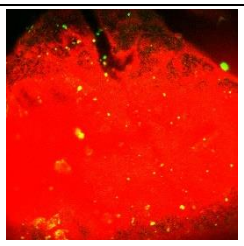	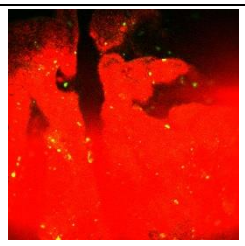	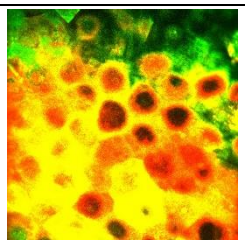	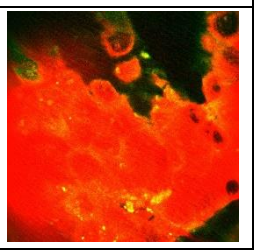

doi:10.6342/NTU202000120

Bottom of SC	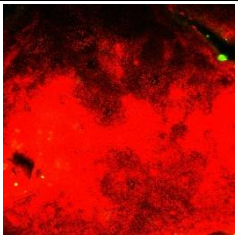	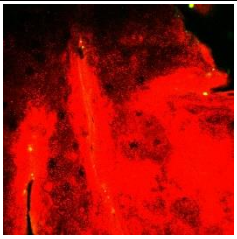	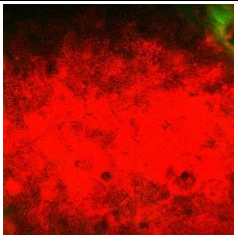	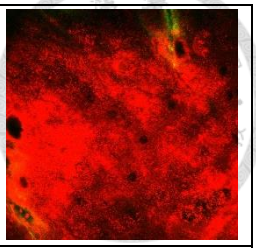
	10.8 μm	12.6 μm	14.4 μm	14.4 μm
Middle Layer of Viable Dermis	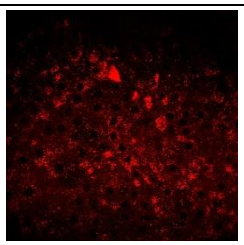	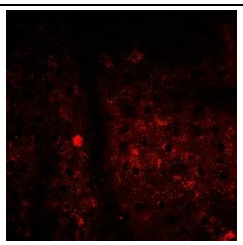	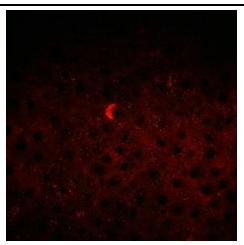	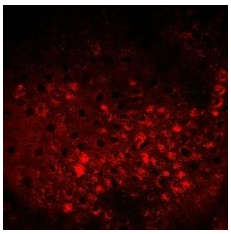
	34.2 μm	37.8 μm	39.6 μm	36 μm
Basal Layer	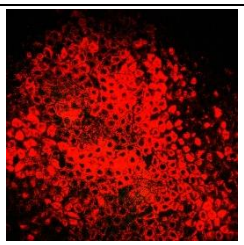	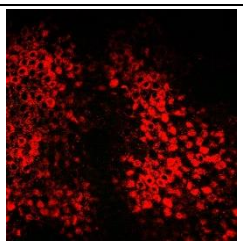	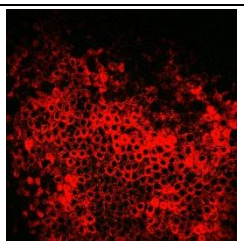	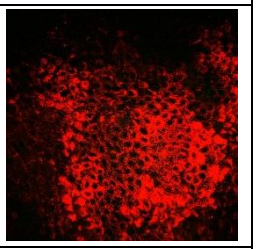
	57.6 μm	63 μm	63 μm	55.8 μm
Middle Layer of Papillary Dermis	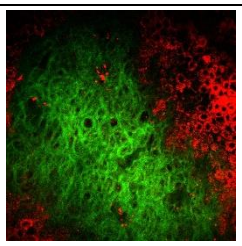	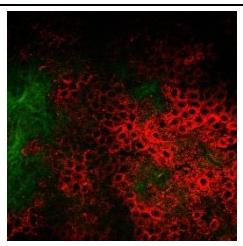	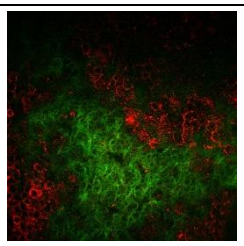	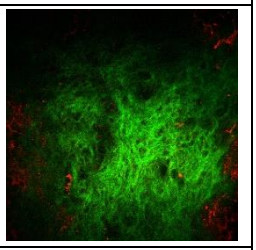
	72 μm	75.6μm	79.2 μm	73.8 μm
Top Layer of Reticular Dermis	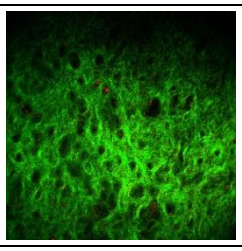	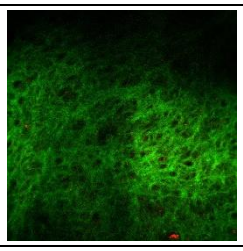	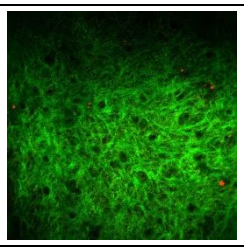	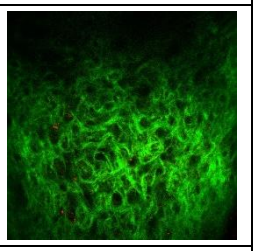
	86.4 μm	88.2 μm	93.6 μm	91.8 μm

doi:10.6342/NTU202000120

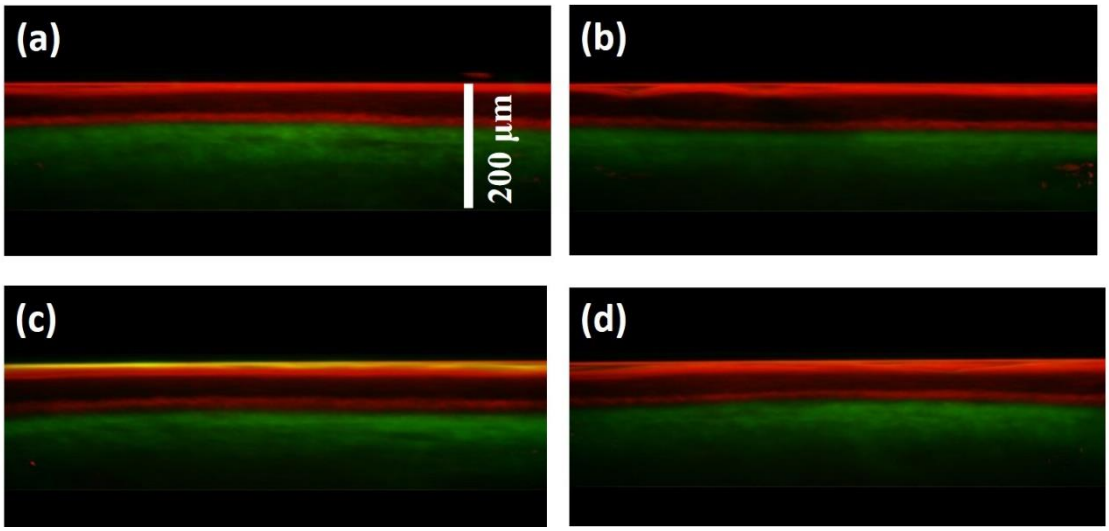

Fig. 4.19 *En face* skin image of Case E50-T90-3 (a) Glycerol-1 (b) Glycerol-2 (c) Control-1 (d) Control-2. Red: THG (Contrast setting: 600~10000). Green: SHG (Contrast setting: 600~6000).

Table 4.11 Case E50-T90-4: The lateral skin images of the control group and the glycerol group. Different skin layers images were presented. Red: THG (Contrast setting: 600~8000). Green: SHG (Contrast setting: 600~6000).

Case E50-T90-4				
	Glycerol	Glycerol	Control	Control
TOP	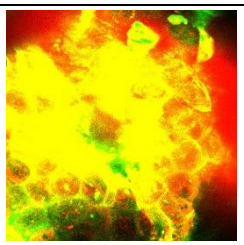	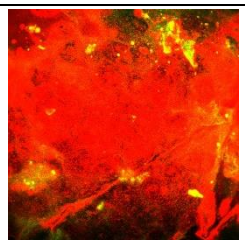	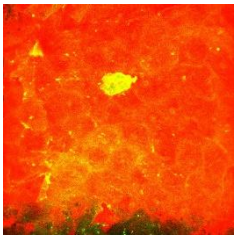	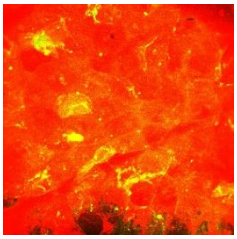
Bottom of SC	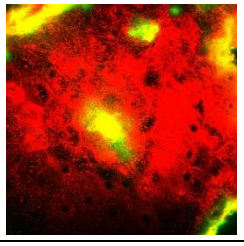	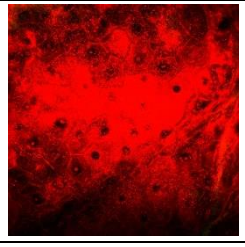	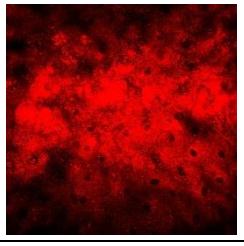	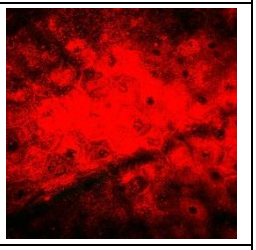
	16.2 μm	14.4 μm	30.6 μm	23.4 μm

doi:10.6342/NTU202000120

Middle Layer of Viable Dermis	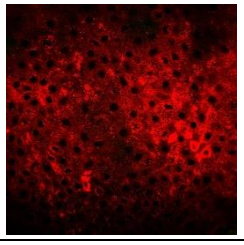	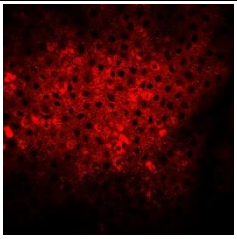	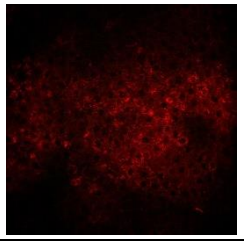	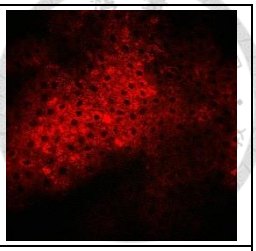
	45 μm	43.2 μm	61.2 μm	54 μm
Basal Layer	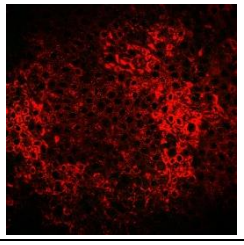	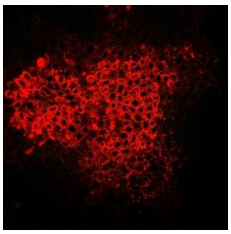	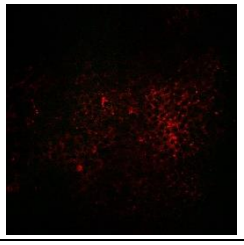	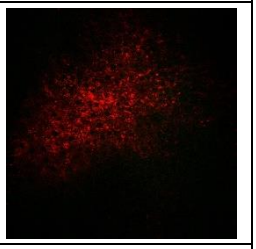
	73.8 μm	72 μm	91.8 μm	82.8 μm
Middle Layer of Papillary Dermis	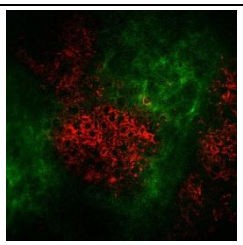	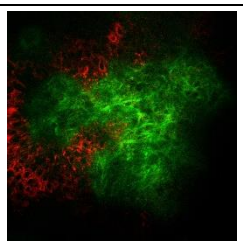	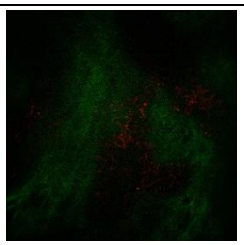	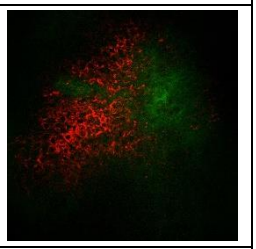
	108 μm	99 μm	115.2 μm	106.2 μm
Top Layer of Reticular Dermis	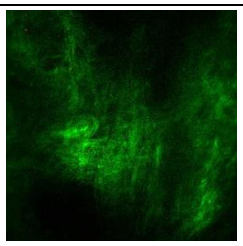	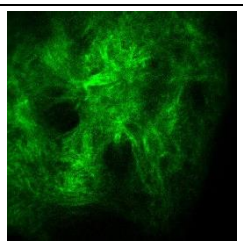	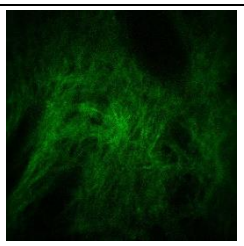	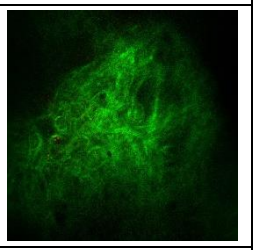
	140.4 μm	126 μm	136.8 μm	127.8 μm

doi:10.6342/NTU202000120

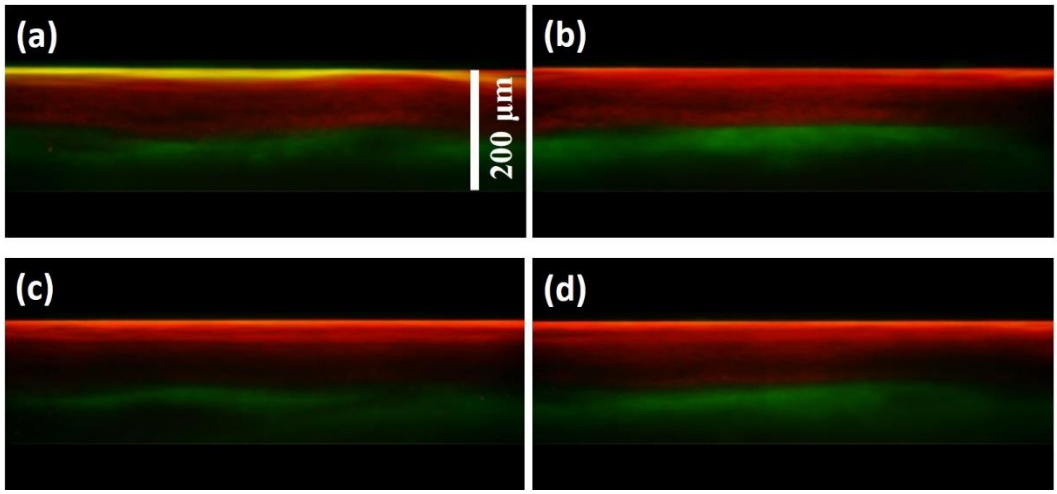

Fig. 4.20 *En face* skin image of Case E50-T90-4 (a) Glycerol-1 (b) Glycerol-2 (c) Control-1 (d) Control-2. Red: THG (Contrast setting: 600~8000). Green: SHG (Contrast setting: 600~6000).

4.4 Summary of the *Ex Vivo* Optical Clearing Results

Table 4.12 Skin structure analysis results of all studied cases. (*P <0.05, ** P <0.01, *** P <0.001)

	Depth or thickness change (μm)	Thickness of SC	Thickness of viable epidermis	Depth of basal layer	Depth of middle papillary dermis layer	Depth of top reticular dermis layer
			Case E100-I90			
1	Control (N=8)	13.7±4.6	54.9±13.4	68.6±13.0	113.0±9.1	156.6±8.8
	Glycerol (N=8)	12.6±4.6	50.6±7.5	63.2±11.6	116.1±7.8	168.5±13.4*
2	Control (N=9)	30.0±2.4	29.2±3.5	59.2±3.9	114.2±6.7	167.8±13.3
	Glycerol (N=9)	21.6±4.5***	20.4±5.3***	42.0±4.2***	87.0±5.2***	131.0±10.5***
			Case E50-I90			
1	C (N=6)	12.0±3.4	15.3±3.7	27.3±4.8	66.6±10.4	108.0±30.9
	G (N=6)	7.5±1.4*	15.0±5.7	22.5±5.4	66.0±16.9	105.0±16.1
2	C (N=12)	30.6±3.0	27.8±5.8	58.4±4.5	109.1±5.1	158.7±10.1
	G (N=12)	18.0±3.5***	35.1±6.8**	53.1±8.3	120.8±4.4***	187.7±6.0***
			Case E50-T90			
1	C (N=8)	22.1±4.8	33.8±6.1	55.8±6.3	95.4±5.4	134.1±12.7
	G (N=8)	13.3±1.6***	42.3±6.5*	55.6±7.0	94.1±9.0	132.3±12.6
2	C (N=10)	33.3±4.6	34.9±6.2	68.2±4.8	122.9±9.2	176.4±17.3
	G (N=10)	18.0±3.1***	40.1±6.0	58.1±5.8***	120.8±5.7	182.5±9.7
3	C (N=9)	12.2±2.0	53.8±12.4	66.0±10.8	93.4±15.1	120.4±13.7
	G (N=9)	13.0±1.5	57.2±7.8	70.2±8.3	92.2±12.2	113.4±17.6
4	C (N=7)	27.3±9.0	63.2±8.1	90.5±6.8	116.8±8.6	145.0±15.9
	G (N=7)	15.1±2.8***	55.5±7.0*	70.5±6.8***	102.6±7.8***	133.5±15.1

Table 4.13 Statistical analysis result on the THG intensity variation after the glycerol application. (-: no significant difference, △: Increased significantly, ▽: Decreased significantly, *P <0.05, ** P <0.01, *** P <0.001)

THG intensity	Bottom of SC	Middle viable epidermis layer	Basal layer	Middle papillary dermis layer	Top reticular dermis layer
Case			**E100-I90**		
1	▽ (**)	▽ (*)	-	-	△ (***)
2	▽ (**)	-	-	-	-
Case			**E50-I90**		

doi:10.6342/NTU202000120

1	-	-	-	△ (**)	△ (*)
2	△ (***)	△ (***)	△ (**)	△ (**)	-
Case			**E50-T90**		
1	-	-	-	-	-
2	△ (***)	△ (*)	△ (*)	△ (*)	-
3	-	-	-	△ (*)	-
4	△ (***)	△ (***)	△ (***)	-	-

Table 4.14 Statistical analysis result on the SHG intensity variation after the glycerol application. (-: no significant difference, △: Increased significantly, ▽: Decreased significantly, *P <0.05, ** P <0.01, *** P <0.001)

SHG intensity	Middle papillary dermis layer	Top reticular dermis layer	SHG Maximum
Case		**E100-I90**	
1	△ (**)	△ (*)	△ (*)
2	△ (**)	△ (**)	△ (***)
Case		**E50-I90**	
1	△ (*)	△ (*)	△ (*)
2	△ (*)	△ (***)	△ (***)
Case		**E50-T90**	
1	-	△ (*)	△ (*)
2	-	△ (*)	△ (*)
3	-	-	-
4	-	-	-

doi:10.6342/NTU202000120

Chapter 5 Discussion of the *Ex Vivo* Optical Clearing

5.1 Optical Clearing Effects and Mechanisms by Utilizing 100% Glycerol with the Tissue Immersion Technique

5.1.1 Bight-field Imaging

From bright-field images, we observed that after glycerol application the skin became transparent and the hair inside the deep area was more visible in both skin tissues (Fig. 4.4). Glycerol is with a higher refractive index (1.47) than extracellular and intracellular fluids (1.34-1.36). After immersion the skin tissues into anhydrous glycerol, glycerol diffused inside and filled all of the skin tissues to create a higher refractive index matching environment for the scattering particles (such as organelles, protein fibrils, membranes, protein globules, with refractive index 1.39-1.47 [49, 66]). Therefore, the light scattering was reduced and the image depth increased. This result is similar to and supported by the previous research of G. Vargas et al. in 1999, by observing the rat skin after the glycerol application [9]. By using spectrophotometer and OCT they proved that glycerol will diffuse into the skin to decrease the refractive index mismatch. This result also correlates with many previous studies [5, 26, 67].

5.1.2 HGM Imaging

With much-reduced scattering and higher transparency in the studied samples, we

doi:10.6342/NTU202000120

thus expect an increase of the SHG intensity at deeper dermis layers. Scattering in skin tissues will not only results in a decrease of excitation intensity, but also defocus the point spread function. The combined effect will not only cause SHG and THG signals to decrease, but will also degrade the system resolution and contrast with increased imaging depth [2]. As a result, in both samples of Case E100-I90, we witnessed that the SHG image intensity in the dermis was greatly enhanced after the optical clearing (Fig. 4.9 and Fig. 4.10). The excitation light was able to travel down to deep regions of the skin with less energy decrement and less wavefront distortion. Moreover, the reduction of scattering also makes it easier for SHG signals to travel back to the detector. Our SHG results correlate well with the bright-field images and with previous studies.

Besides excitation intensity and point spread function [2], THG intensities also strongly depend on the refractive index mismatch inside the excitation focus [68, 69]. After the glycerol application, the transparency effect will not only restore the excitation light and allow easier collection of the generated nonlinear signals, as been indicated by the SHG intensity recovery, but will also decrease the refractive index mismatch. These two different mechanisms will compete for the THG intensity. In Case E100-I90, THG intensity decreased at the epidermis while increased or remain the same at the dermis, indicating that refractive index matching is the dominant effect at the epidermis. Although glycerol will greatly enhance the homogeneity of the tissue and reduce the THG radiation,

doi:10.6342/NTU202000120

in the dermis, a strong reduction of scattering of the whole epidermis will result in a strong increment of excitation intensity and thus eventually the detected THG photons. Thus, the THG image intensity increased or remained the same in the dermis after optical clearing.

5.1.3 Skin Structure Analysis

The dehydration and shrinkage were proved two of the most important mechanisms of the optical clearing and well reported in previous illustrations [49, 70, 71]. In Case E100-I90-2, we found that the dehydration and shrinkage of tissue enhanced the SHG intensity and resulted in less reduction of THG image intensities at epidermis when compared to Case E100-I90-1 (Fig. 4.10). It is known that the thickness of skin tissues can be affected by glycerol application. First, the strong affinity of glycerol would make the water flux out tissues and lead to dehydration. Second, the permeability coefficients of water and glycerol are different, which are on the order of 10^{-2}cm/min and 10^{-5} cm/min. This difference made more water flux out than glycerol enter the skin, causing the tissue volume decrease [52]. By moving the skin structure toward the surface due to shrinkage, one thus expects to see further-improved image intensities.

5.2 100% Glycerol Immersion V.S. 50% Glycerol Immersion

In the case of 50% glycerol application with immersion, the SHG intensities at

doi:10.6342/NTU202000120

dermis were also greatly enhanced after the optical clearing (Fig. 4.14). Although with its lower refractive index (1.398)[72] and lower dehydration power compared to 100% glycerol, the 50% glycerol was also found able to decrease the scattering in the tissue by observing the significantly increased SHG intensity. In the bright light image, the transparency of the skin tissues was enhanced, showing a decrement of the scattering. However, the 50% glycerol could not introduce such a highly homogeneous environment inside the tissue as 100%. Under the bright light microscopy, the variation of the transparency by using 50% glycerol was less than 100% glycerol. The SHG images and bright images of Case E50-I90 were shown in section 4.3.2.

The most significant difference between these two different concentrations is the variation of the THG intensity. Different from the case of 100% glycerol immersion, of which the THG intensity greatly decreased in the epidermis after OC, the THG intensity of the 50% immersion cases increased or remained the same (

Table **4.13**). Although we observed significant reduction of light scattering in both concentrations through SHG and white light microscopy, the OC effect in THG intensity by using 50% glycerol showed the opposite consequences (Fig. 5.1). As discussed above, the THG intensity is affected by the refractive index mismatch inside the excitation focus [68, 69]. The 50% glycerol has a lower osmolarity than 100% glycerol [5, 72] and cannot

doi:10.6342/NTU202000120

introduce such a high homogeneous environment as the 100% glycerol. The optical clearing power of 50% glycerol is known to be less than the 100% glycerol. As a result, for 50% glycerol immersion, there was a compromise between the decrement of the light scattering and the decrement of the refractive index mismatch. The less decrement of refractive index mismatch and the recovery of the light intensity and quality made the THG intensity enhance or remain the same after the OC. Besides, in both two tissues of the 50% immersion cases, the thickness of the SC all greatly decreased by at least 37.5%. In the skin tissue with thicker SC, Case E50-I90-2, the THG intensity greatly increased at the dermis. To sum up, by immersed the skin tissue inside the 50% glycerol, we could enhance the THG intensity and the image at the epidermis can be better resolved.

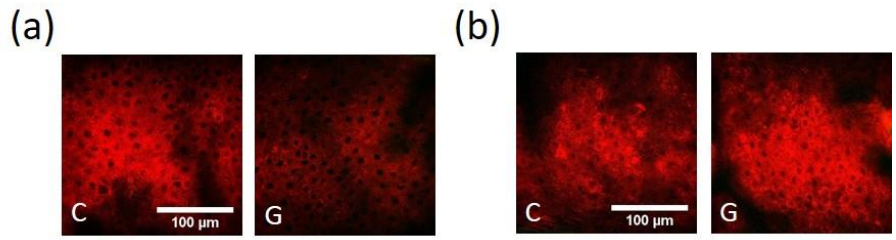

Fig. 5.1 The variation of the THG intensity at the middle epidermis layer. We presented and compared the THG intensity variation at the middle epidermis layer of Case E100-I90-1 and Case E50-I90-2. C: control; G: glycerol. (a) In the Case of 100% glycerol immersion (Case E100-I90-1), the THG intensity greatly reduced. (b) However, in the case of 50% glycerol immersion (Case E50-I90-2), the THG intensity greatly increased, opposite from (a). Scale bar = 100 μm.

5.3 50% Glycerol with Topical Application

To simulate and study the OC potential for *in vivo* clinical applications, we studied the OC of *ex vivo* human skin by using 50% glycerol with noninvasive topical application.

doi:10.6342/NTU202000120

Four tissues at different parts of the skin from different volunteers were included, which are the skin of forehead, buttock, chest, and temporal. After the glycerol application, only two tissues were found with the enhancement of the SHG intensity at the dermis (forehead, buttock; Table 4.14). In the bright light image, the transparency of all four skin tissues was slightly changed, showing less decrement of the scattering when compared to the immersion case (Fig. 4.6).

Compared to the immersion case, the clinical applicable topical application is with a less effective OC effect. In the case of topical application, the glycerol solution can only diffuse easily through the epidermis by considering the barrier function of SC, which greatly reduces the penetration of the glycerol solution. In the cases of chest and temporal samples, there was no observable enhancement of the SHG intensity. The reason might come from: (1) Variation of the SC permeability at different parts of the skin [37, 73, 74]; (2) Different skin conditions of different volunteers, therefore causing different skin barrier functions. Among all four tissues of this case type, three were found to be greatly decreased in SC thickness by at least 40%. In the Case E50-T90-2 and Case E50-T90-4, the THG intensity greatly increased in epidermis, accompanying with their greatly reduced SC thickness as compared to the other two cases. Combining all the results of the 50% glycerol cases, we found that the SC played a critical role for the observed THG enhancement. We proposed that if one can reduce the scattering in SC through OC, the

doi:10.6342/NTU202000120

THG intensity underneath the SC will surely increase.

5.4 The Relationship between the SC and the HGM Intensity Variation

In our studied cases by using 50% glycerol with either immersion or topical application, we found signal enhancement of epidermal THG image skin tissues with a SC layer thicker than 27 μm. This might be due to the fact that the skin tissue with a thicker SC layer suffers stronger light scattering so that the OC effect is more pronounced. Our observation also suggests the important role of SC to affect the epidermal THG signal after OC. To double-confirm the role of SC in OC effects, we further designed an experiment by using 100% glycerol with topical application. In previous studies, high concentration glycerol was proved to be with a slower permeation rate than lower concentration glycerol [5]. It can be described by the Fick's law, in which the skin permeability is inversely proportional to the glycerol concentration [25]. Based on the lower penetration rate with its higher viscosity and the higher OC power characteristic compared to 50% glycerol, the 100% glycerol was applied on the skin surface for 30 minutes, in contrast to the 90 minutes, to provide the OC effect in SC only (named: Case E100-T30). The results of the Case E100-T30 were presented in Table 5.1. Representative HGM skin images were presented in Table 5.2.

Table 5.1 Variation of skin structure, THG intensity, and SHG intensity after 100%

doi:10.6342/NTU202000120

glycerol topical application for 30 minutes.

Depth or thickness change (μm)	Thickness of SC	Thickness of viable epidermis	Depth of basal layer	Depth of middle papillary dermis layer	Depth of Top reticular dermis layer
Control (N=10)	13.5±0.9	17.3±4.3	30.8±4.7	60.1±6.0	88.7±13.2
Glycerol (N=10)	13.5±2.6	21.6±2.4*	35.1±3.3*	67.0±8.0*	98.1±16.9
THG intensity	**Bottom of SC**	**Middle viable epidermis layer**	**Basal layer**	**Middle papillary dermis layer**	**Top reticular dermis layer**
After the applying glycerol	△ (***)	△ (***)	△ (***)	△ (***)	-
SHG intensity	**Middle papillary dermis layer**		**Top reticular dermis layer**		**SHG Maximum**
After the applying glycerol	△ (*)		-		-

Table 5.2 The lateral skin images of the control group and the glycerol group at different depths. Red: THG (Contrast setting: 600~10000). Green: SHG (Contrast setting: 600~8000).

Case E100-T30-1				
	Glycerol	Glycerol	Control	Control
TOP	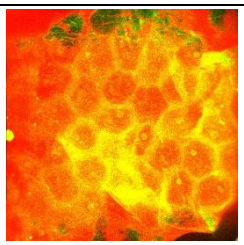	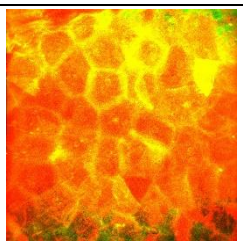	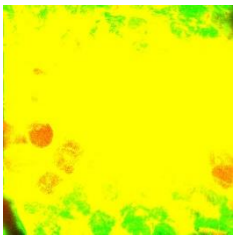	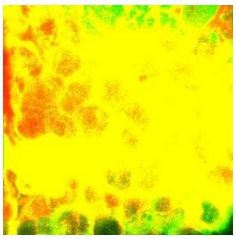
Bottom of SC	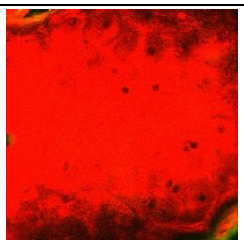		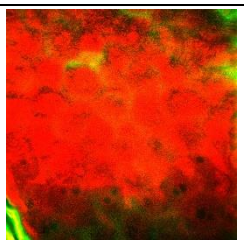	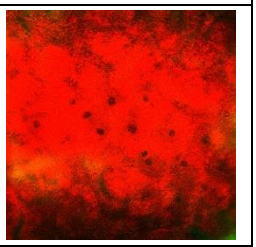
	14.4 μm	10.8 μm	12.6 μm	12.6 μm
Middle Layer of Viable Dermis	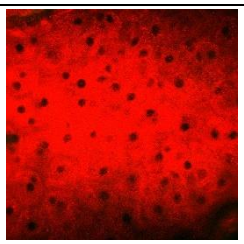	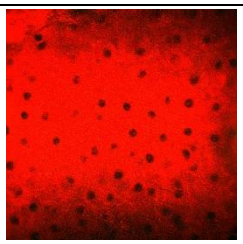	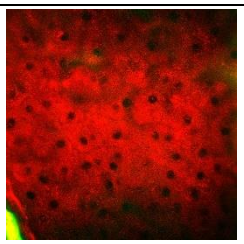	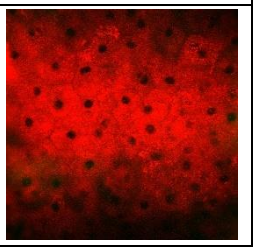
	23.4 μm	21.6 μm	21.6 μm	21.6 μm
Basal Layer	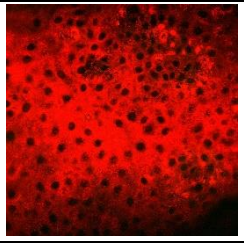	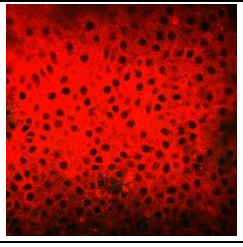	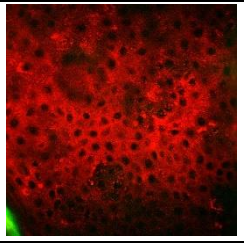	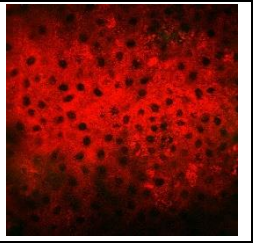

doi:10.6342/NTU202000120

	32.4 μm	32.4 μm	30.6 μm	30.6 μm
Middle Layer of Papillary Dermis	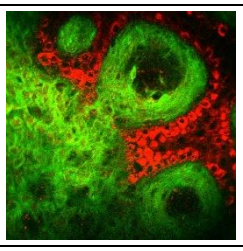	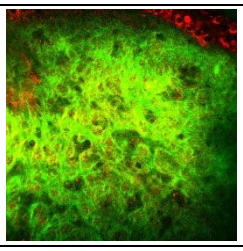	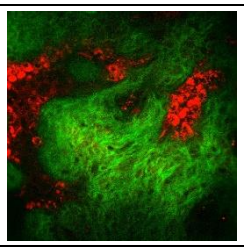	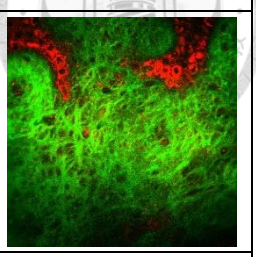
	72 μm	63 μm	70.2 μm	63 μm
Top Layer of Reticular Dermis	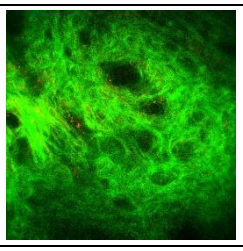	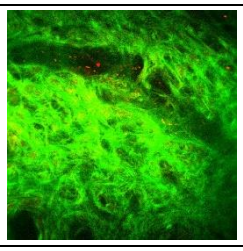	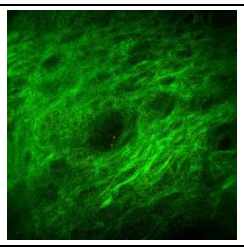	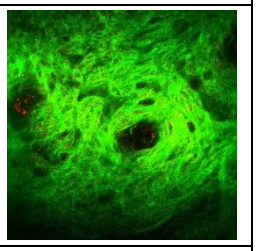
	109.8 μm	93.6 μm	109.8 μm	93.6 μm

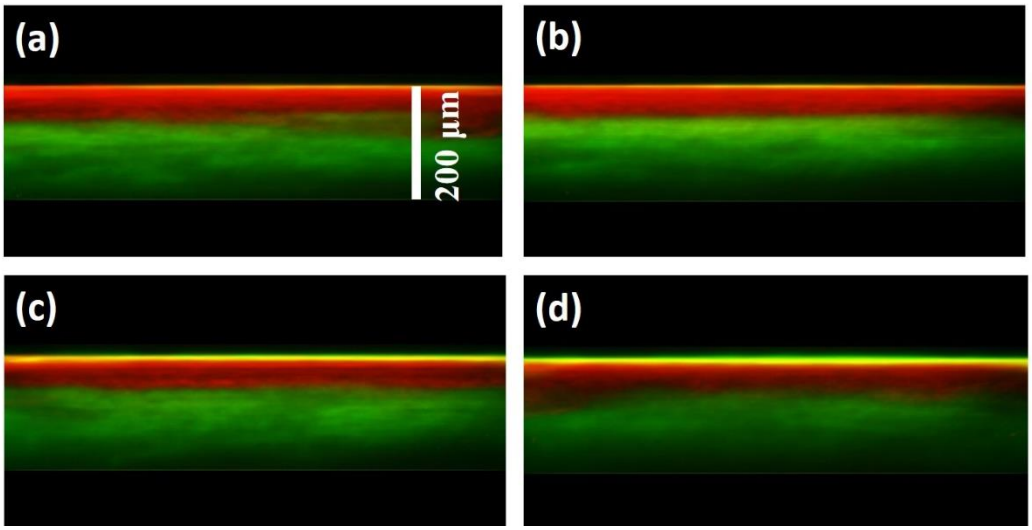

Fig. 5.2 *En face* skin image of Case E100-T30-1 (a) Glycerol-1 (b) Glycerol-2 (c) Control-1 (d) Control-2. Red: THG (Contrast setting: 600~10000). Green: SHG (Contrast setting: 600~8000).

The average THG intensities greatly increased at all skin layers except the top reticular dermis layer. For SHG, the average SHG intensity of the papillary dermis also showed significant increment (Table 5.2). The results of 100% glycerol topical

doi:10.6342/NTU202000120

application are quite different from the 100% glycerol tissue immersion. SC acts as a strong physical barrier and one of the main optical scatters of the skin, strongly decreasing the permeability of the glycerol and light penetration. With the method of the topical application and shorter applying time, glycerol solution cannot diffuse as far as the immersion case and the optical clearing is less effective at the deep dermis area. Instead, 100% glycerol diffuses into SC and reduced its optical scattering, thus increasing the laser excitation power in layers beneath as well as the back-reflection signals. The fact that glycerol did not reach the viable epidermis can be evidenced by the enhanced THG intensities through the viable epidermis.

Finally, it is noted that the mean SHG intensities all increase after OC at the middle papillary dermis layer, top reticular dermis layer, and SHG maximum layer in all studied 9 cases, even though some of increment might not be significant after statistical analysis. The mean SHG intensity of all studied cases is shown in Table 5.3.

Table 5.3 Mean SHG intensities (arbitrary unit) of all studied cases at the middle papillary dermis layer, top reticular dermis layer, and SHG maximum layer. *P <0.05, ** P <0.01, *** P <0.001.

Case number	Group	Middle papillary dermis layer	Top reticular dermis layer	SHG Maximum
		Case E100-I90		
1	Control (N=8)	691	756	839
	Glycerol (N=8)	810**	1210*	1434*
2	Control (N=9)	764	577	844
	Glycerol (N=9)	1258**	839**	1490***
		Case E50-I90		
1	Control (N=6)	1156	957	1246
	Glycerol (N=6)	2552*	3918*	4093*
2	Control (N=12)	768	930	1002
	Glycerol (N=12)	887*	1386***	1444***
		Case E50-T90		
1	Control (N=8)	966	1522	1702
	Glycerol (N=8)	1092	2346*	2594*
2	Control (N=10)	711	795	841
	Glycerol (N=10)	755	1070	1141
3	Control (N=9)	1411	1547*	1701*
	Glycerol (N=9)	1458	1819	1909

doi:10.6342/NTU202000120

4	Control (N=7)	949	1377	1419
	Glycerol (N=7)	1079	1493	1547
		Case E100-T30		
1	Control (N=10)	2366	3692	3789
	Glycerol (N=10)	3138*	4050	4362

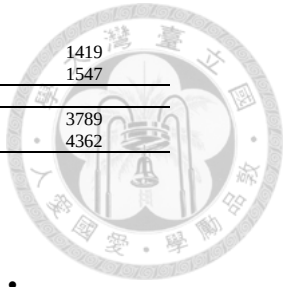

5.5 Conclusion of the *Ex Vivo* Optical Clearing

Although have been investigated by many previous studies, the effects and the mechanisms of OC in human skin are still not well understood. By utilizing the HGM microscopy, we first combined the SHG and THG microscopy images to study the OC effect. The informative image information of HGM provided more details regarding the skin OC effect. In this study, we establish a strict method to study the OC in skin precisely with statistical analysis.

In the case of 100% glycerol immersion, the glycerol diffused into the skin and made it more homogeneous to reduce the light scattering. The fact regarding the scattering reduction can be evidenced by the enhanced SHG intensities in dermis. On the other hand, the THG intensity depends strongly on refractive index mismatch and will vanish in homogeneous media. The 100% glycerol greatly enhanced the tissue homogeneity and the observed THG intensities were therefore decreased. We also studied the cases of the 50% glycerol by immersion or topical application since it is a safe concentration to apply on the human skin. In both methods, we observed the enhancement of the SHG intensities,

doi:10.6342/NTU202000120

but the OC is less effective by topical application. The 50% glycerol can also reduce the scattering inside the skin by observable SHG intensity increment in the dermis.

Three OC mechanisms were mentioned in previous studies: the refractive index matching [5, 26, 67], the dehydration [7, 8, 27, 49], and the shrinkage of the tissue [8, 52]. In our research, we found all these three mechanisms affecting the optical clearing efficacy. Besides, the stratum corneum also plays an important role to achieve the optical clearing. For THG signal enhancement in the epidermis, SC acts the most important role. It should be noted that after the topical applications with the 50% glycerol, we observed stronger OC effect in thicker SC skin tissues.

In our studies, we achieve the optical clearing by using the 50% glycerol with the topical application. The results of this study suggest the potential of 50% glycerol for future clinical OC topical applications, especially for skin with a thick SC layer.

doi:10.6342/NTU202000120

Chapter 6 Results of the *In Vivo* Optical Clearing

The skin is the outermost organ of human, which acts as the barrier between organism and environment. Many skin diseases can be diagnosed based on morphological changes in different skin layers. With these knowledge, early diagnosis of skin disease, studying age-related changes of morphology, and understanding drug delivery are then possible, which are essential in dermatology and cosmetology. However, skin is a high scattering tissue that comprises multiple layers with a variation of refractive index. The turbid nature of the skin strongly decreases the imaging depth of the optical microscopy and limit its *in vivo* applications in clinics [50]. In order to increase the depth of investigation, the *in vivo* optical clearing (OC) technique of human skin was proposed [1, 13-15, 18, 29-34, 48, 50, 51, 53-55].

For *in vivo* experiments, to reduce the strong barrier function of the stratum corneum, many physical methods such as injection [48, 51, 52] sonophoretic [33], electrophoretic [14], removal of SC [14, 29, 32, 53], laser ablation [18, 34, 54] and chemical methods such as chemical enhancer Thiazone [15, 29, 54, 55] were applied to accelerate penetration of optical clearing agents (OCAs) into the human skin. Most of these methods will damage the skin tissue and are usually combined high concentration OCAs which are less desirable for the *in vivo* human clinical examination due to the toxicity nature.

doi:10.6342/NTU202000120

For other *in vivo* human studies which used the noninvasive method with low concentration OCAs, the results are inconsistent [13, 30, 31, 33, 50]. When applied the glycerol on the volar forearm [50] and dorsal hand [33], no observable optical clearing effect was found. In contrast, when applied the glycerol on the palm [13, 30] and finger [31], the scattering of the skin was reduced and the image intensity was enhanced, indicating the possible clearing effect in SC. With a thick SC layer and with a strong scattering contribution from SC to reduce the image quality, the clearance of SC becomes more observable. Through topical application of the low concentration OCAs, which is the true noninvasive method, the optical clearing of the *in vivo* human skin still needs more exploitation, especially at the skin region with thin SC.

In our previous *ex vivo* human skin studies using third harmonic generation microscopy [60], we found that 100% glycerol was able to match the refractive index of the viable epidermis and significantly reduce the light scattering inside it. The THG intensity decreased within the depth of the glycerol diffusion, and both the THG and SHG intensity increased beyond the diffusion depth. Compared to the toxic 100% glycerol, for topical application of glycerol, $\leq$ 50% glycerol is biocompatible for *in vivo* human skin and has been allowed as human skincare products [75]. In previous experiment by using 50% glycerol with topical application [60], the OC was found less effective (3 of 4 cases) than using 100% glycerol. Instead of decreasing the THG intensity after 100% glycerol

doi:10.6342/NTU202000120

application, the THG intensity in epidermis increased or remained the same after the 50% glycerol application. The enhancement of the THG intensity was less effective in the skin area with thinner SC compared to thicker ones [60], indicating the OC of SC.

In the previous studies [33, 50], the *in vivo* human OC was found less effective in the region with thin SC, it could be accountable by the reduced OC effect of SC. However, the final goal of the OC is the clinical application, especially in thin SC region, the area where the light therapeutic and dermatological diagnosis often focus on [60]. The aim of this study is to investigate if the safe 50% glycerol can create the OC effect beyond SC. The OC effect and glycerol solution diffusion in different skin layers can be detected by THG image variation based on its homogeneous sensitivity, and the second harmonic generation (SHG) image intensity in the dermis is a beacon to confirm the reduction of the scattering in the epidermis layer [60]. The clearance of the viable epidermis *in vivo* will greatly increase the image depth and the image intensity of the deeper skin layer like the dermis will be enhanced. We studied and compared the OC by four different applying time (15, 30, 90, and 180 minutes) in volar forearm skin by using harmonic generation microscopy. For short application time, no OC effect can be observed, the result correlated to the previous study [50]. On the other hand, with 180 minutes application time, OC in the viable epidermis was observed for the first time by topically applying safe 50% glycerol, indicating the possibility to create OC effect with low concentration glycerol

doi:10.6342/NTU202000120

application which is widely used as skin care product.

6.1 System Calibration by Using Gallium Nitrite

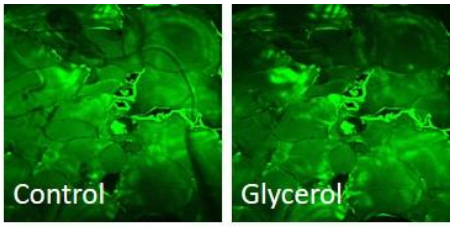

Fig. 6.1 SHG images of GaN for system calibration of Case I50-T15-1. Left: The reference SHG image before taking the HGM skin image of the control group. Right: The SHG image before taking the HGM skin image of the glycerol group. (PMT setting: 400 Volt, Contrast: 400~4500, Illuminate power: 20 mW). It is only a little difference and indicates that the system condition remained the same.

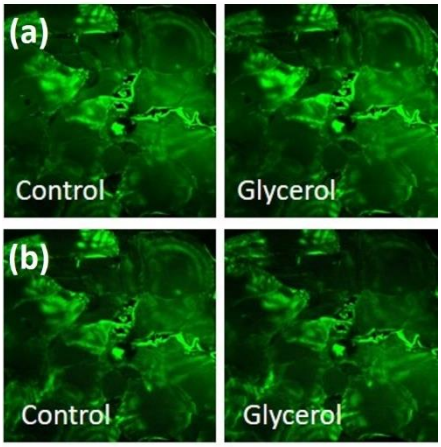

Fig. 6.2 SHG images of GaN for system calibration. Left: The reference SHG image before taking the HGM skin image of the control group. Right: The SHG image before taking the HGM skin image of the glycerol group. (PMT setting: 400 Volt, Contrast: 400~4500, Illuminate power: 20 mW). It is only a little difference and indicates that the system condition remained the same. (a) Case I50-T30-1 (b) Case I50-T30-2

doi:10.6342/NTU202000120

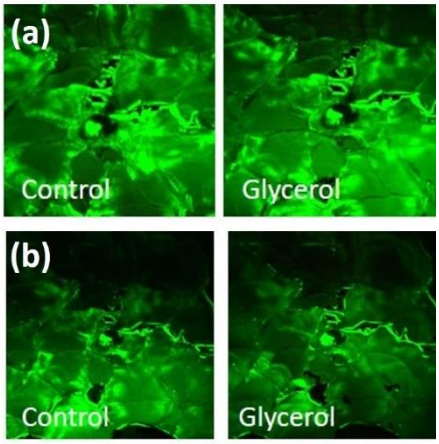

Fig. 6.3 SHG images of GaN for system calibration. Left: The reference SHG image before taking the HGM skin image of the control group. Right: The SHG image before taking the HGM skin image of the glycerol group. (PMT setting: 400 Volt, Contrast: 400~4500, Illuminate power: 20 mW). It is only a little difference and indicates that the system condition remains the same. (a) Case I50-T90-1 (b) Case I50-T90-2

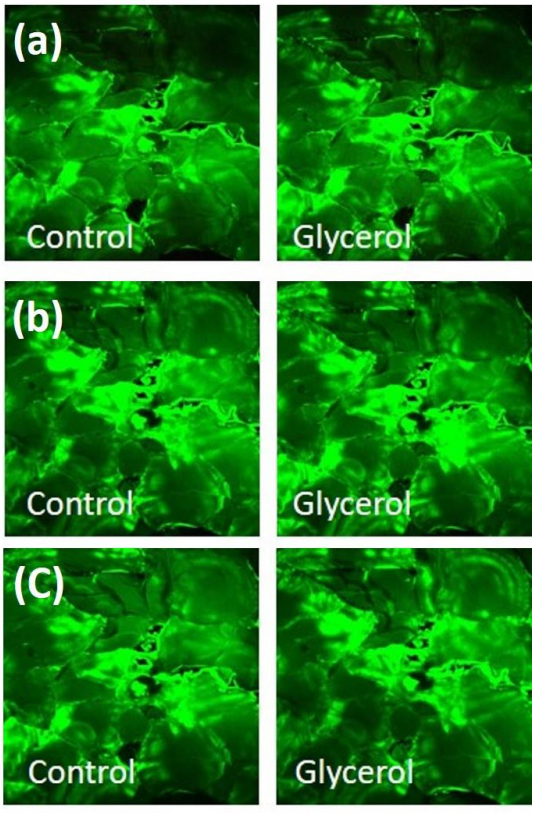

Fig. 6.4 SHG images of GaN for system calibration. Left: The reference SHG image before taking the HGM skin image of the control group. Right: The SHG image before taking the HGM skin image of the glycerol group. (PMT setting: 400 Volt, Contrast: 400~4500, Illuminate power: 20 mW). It is only a little difference and indicates that the system condition remained the same. (a) Case I50-T180-1 (b) Case I50-T180-2 (c) Case

doi:10.6342/NTU202000120

6.2 Statistical Analysis of HGM Image and Representative HGM Images

In this section, we presented the analysis of HGM *in vivo* skin images. The optical clearing effects of the SHG and THG image were discussed. We took the stack images randomly on the volar forearm skin surface to analyze effect of the optical clearing statistically. For each volunteer, at least six image stacks acquired at different points of the skin were collected.

6.2.1 Structure and HGM Intensity Analysis of Case I50-T15

Table 6.1 shows the skin structure analysis before and after the glycerol application. Only the average depth of basal layer significantly increased by nearly 10% (from 45.18 μm to 49.86 μm). In this case, no significant difference in HGM intensity was observed (Fig. 6.5 and Fig. 6.6). Table 6.2 and Fig. 6.7 presents HGM skin images of Case I50-T15-1. The HGM images changed little after the glycerol application. It might not be a sufficient time for 50% glycerol to achieve the optical clearing within 15 minutes.

Table 6.1 Skin structure analysis results of all studied cases. (*p<0.05, **p<0.01, ***p<0.001)

	Depth or thickness change (μm)	Thickness of SC	Thickness of viable epidermis	Depth of basal layer	Depth of middle papillary dermis layer	Depth of Top reticular dermis layer
1	Control (N=10)	17.6±2.0	27.5±5.4	45.2±4.8	78.3±5.8	110.9±10.3
	Glycerol (N=10)	18.4±2.8	31.5±3.4	**49.9±4.0***	80.3±5.1	109.6±11.2

doi:10.6342/NTU202000120

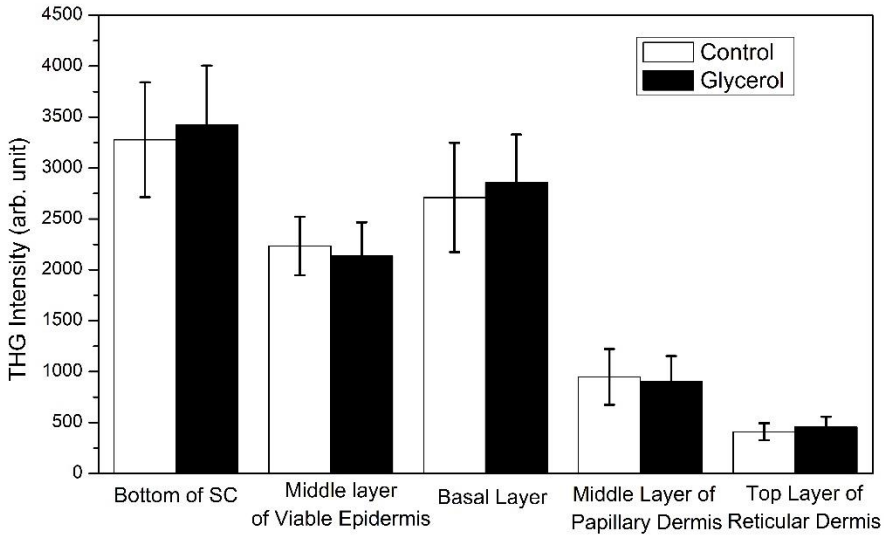

Fig. 6.5 Quantitative analysis and comparison of skin THG intensities at five different depths. Black (control: N=10, glycerol: N=10).

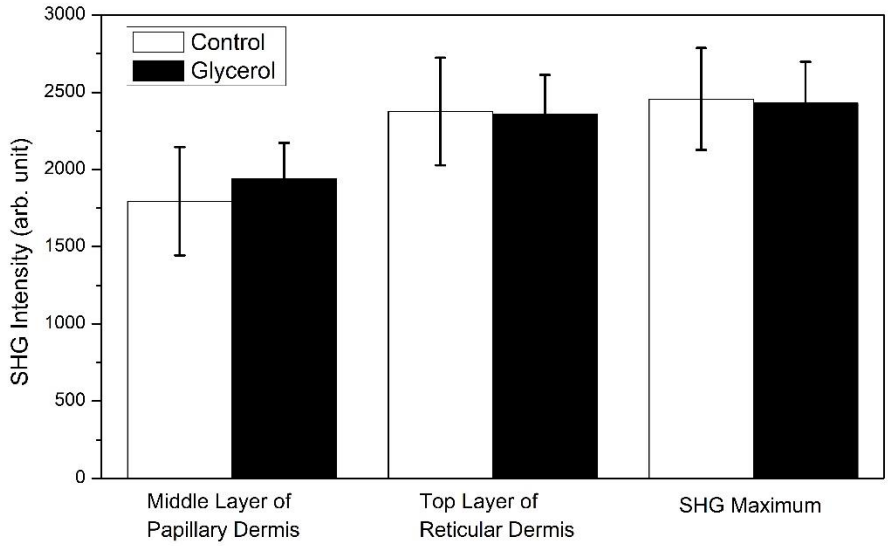

Fig. 6.6 Quantitative analysis and comparison of skin SHG intensities at three different depths. Black (control: N=10, glycerol: N=10).

Table 6.2 Case I50-T15-1: The lateral skin images at different skin layers of the control group and the glycerol group. Red: THG (Contrast setting: 600~10000). Green: SHG (Contrast setting: 600~8000).

Case I50-T15-1

doi:10.6342/NTU202000120

	Glycerol	Glycerol	Control	Control
TOP	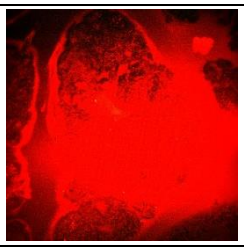	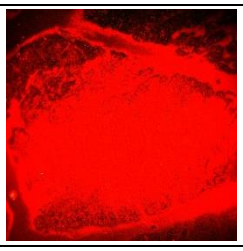	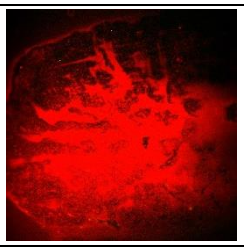	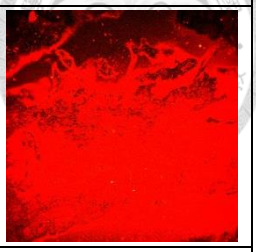
Bottom of SC	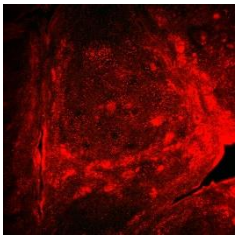	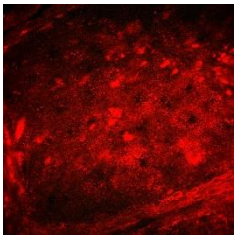	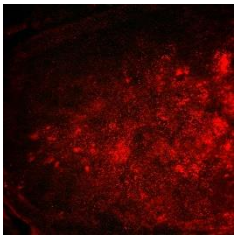	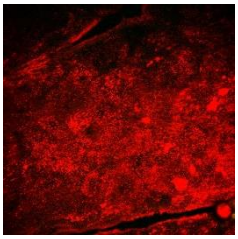
	16.2 μm	16.2 μm	18 μm	16.2 μm
Middle Layer of Viable Dermis	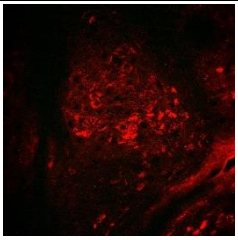	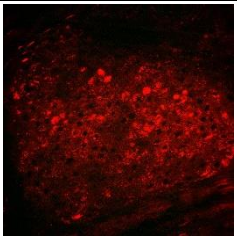	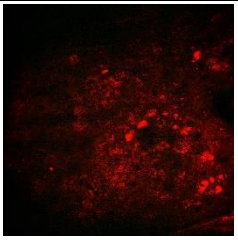	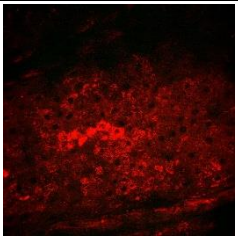
	32.4 μm	34.2 μm	34.2 μm	34.2 μm
Basal Layer	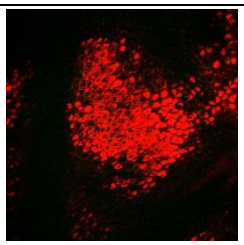	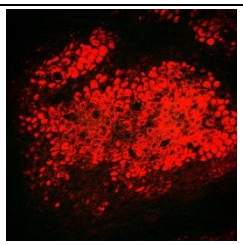	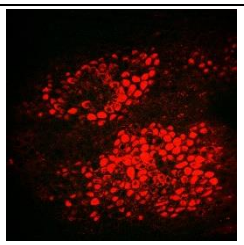	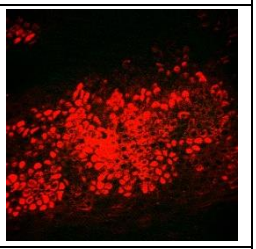
	48.6 μm	52.2 μm	48.6 μm	50.4 μm
Middle Layer of Papillary Dermis	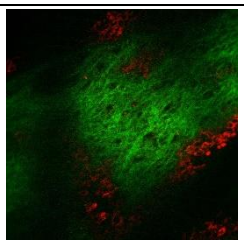	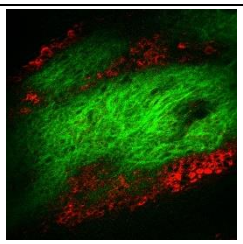	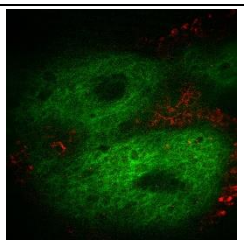	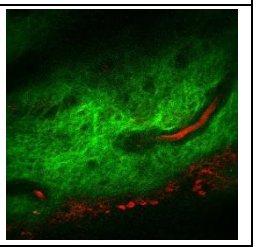
	75.6 μm	79.2 μm	77.4 μm	79.2 μm

doi:10.6342/NTU202000120

Top Layer of Reticular Dermis	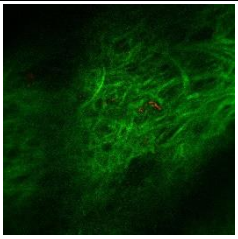	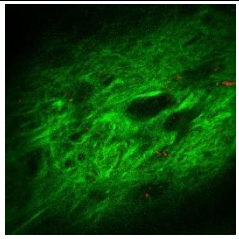	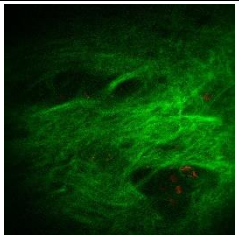	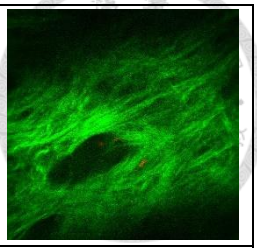
	100.8 μm	104.4 μm	104.4 μm	106.2 μm

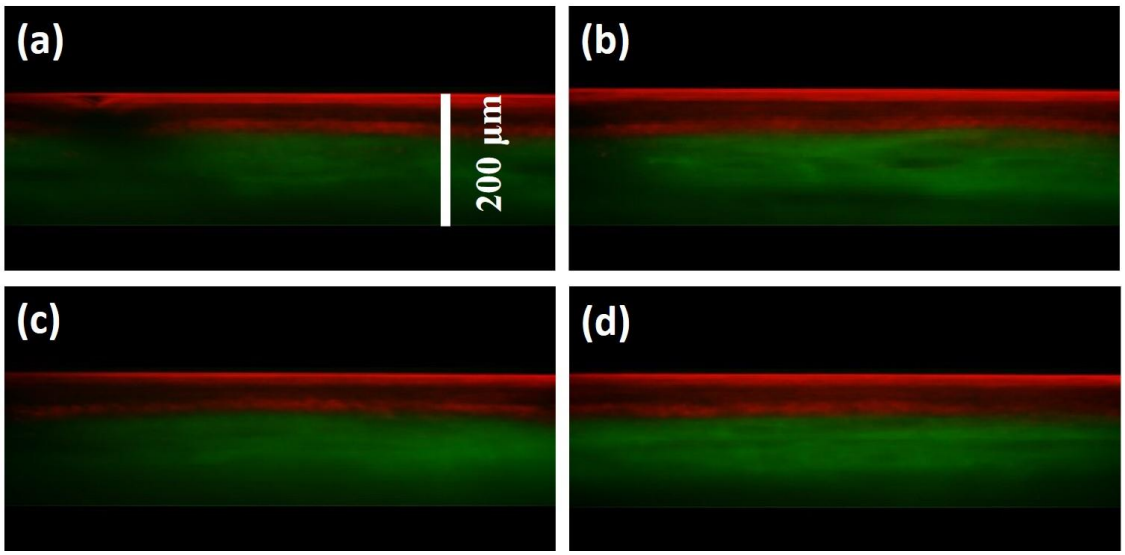

Fig. 6.7 *En face* skin image of Case I50-T15-1 (a) Glycerol-1 (b) Glycerol-2 (c) Control-1 (d) Control-2. Red: THG (Contrast setting: 600~10000). Green: SHG (Contrast setting: 600~8000).

6.2.2 Structure and HGM Intensity Analysis of Case I50-T30

For the case of I50-T30, two volunteers were studied. For Case I50-T30-1, after the 50% glycerol application for 30 minutes, the average thickness of viable epidermis and depth of basal layer decreased significantly by nearly 11% (from 26.82 μm to 24.12 μm) and nearly 7% (from 43.92 μm to 40.86 μm) (Table 6.3). While for Case I50-T30-2, no variation of the skin thickness was observed.

In the Case I50-T30-1, we achieve the optical clearing after the glycerol application (Fig. 6.8 and Fig. 6.9). However, in Case I50-T30-2, we did not observe the effect of the

doi:10.6342/NTU202000120

optical clearing (Fig. 6.8 and Fig. 6.9).

Table 6.4 and Fig. 6.10 show the HGM skin images of Case I50-T30-1. The average THG intensities and SHG intensities all significantly increased by at least 30% at different positions except the bottom of SC (only 17% increment with no significant difference). The HGM intensity of the skin image increased a lot. However, in Case I50-T90-2, we did not observe the effect of the optical clearing (Table 6.5 and Fig. 6.11).

Table 6.3 Skin structure analysis results of Case I50-T30. (*p<0.05, **p<0.01, ***p<0.001)

	Depth or thickness change (μm)	Thickness of SC	Thickness of viable epidermis	Depth of basal layer	Depth of middle papillary dermis layer	Depth of Top reticular dermis layer
1	C (N=10)	17.1±1.7	26.8±1.3	43.9±2.1	87.3±6.1	130.1±12.1
	G (N=10)	16.7±2.9	**24.1±2.8****	**40.9±4.2***	84.1±4.9	126.4±7.3
2	C (N=10)	16.2±2.2	35.8±4.8	52.0±4.2	95.2±6.5	137.2±13.4
	G (N=10)	16.2±1.5	34.6±4.1	50.8±4.1	91.1±5.6	130.7±11.9

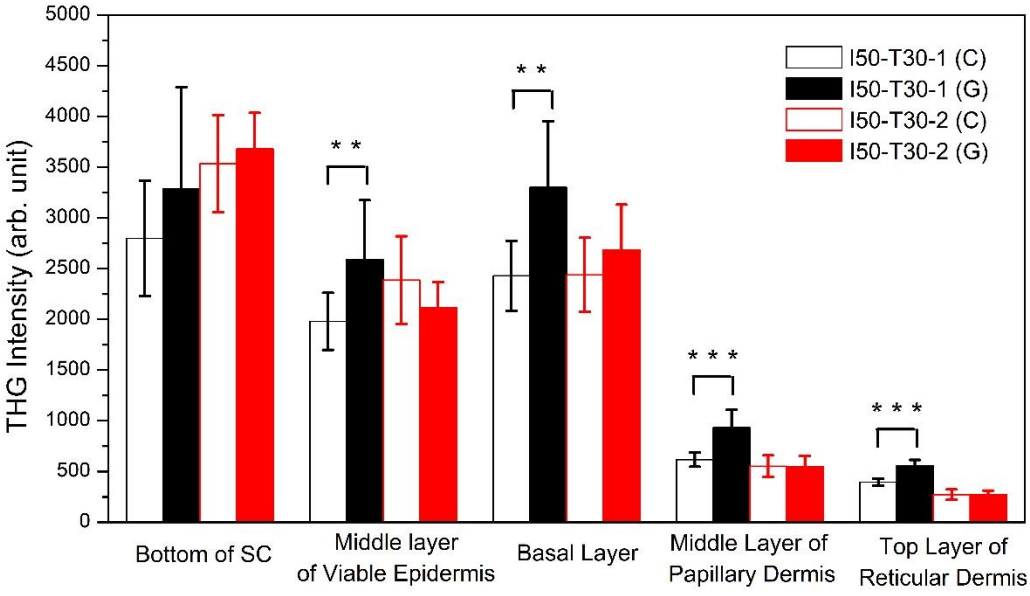

Fig. 6.8 Quantitative analysis and comparison of skin THG intensities at five different depths. Black: Case I50-T30-1 (control: N=10, glycerol: N=10); Red: Case I50-T30-2 (control: N=10, glycerol: N=10). **P <0.01; *** P <0.001. C: control; G: glycerol.

doi:10.6342/NTU202000120

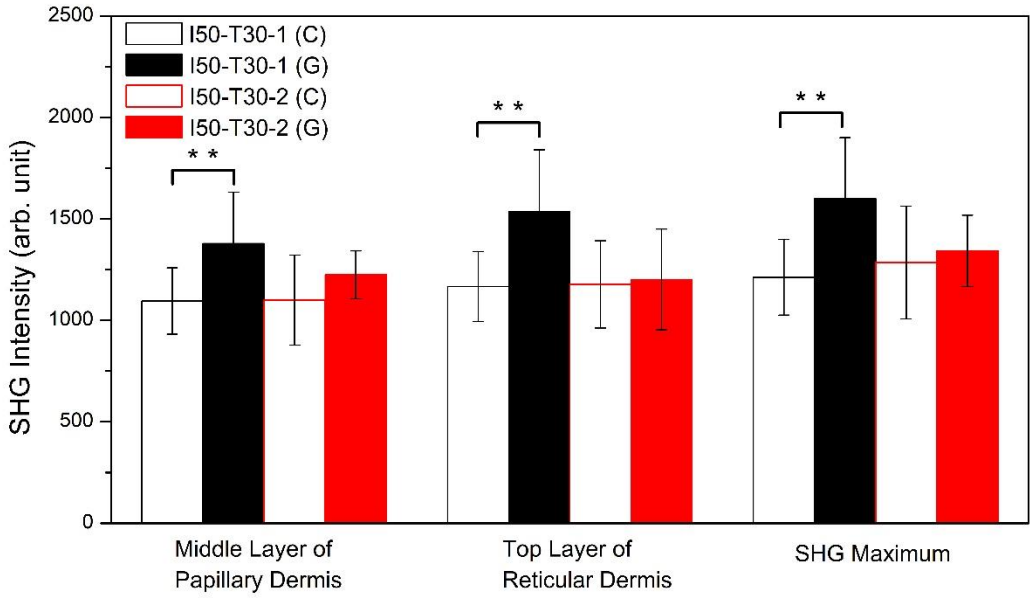

Fig. 6.9 Quantitative analysis and comparison of skin SHG intensities at three different depths. Black: Case I50-T30-1 (control: N=10, glycerol: N=10); Red: Case I50-T30-2 (control: N=10, glycerol: N=10). ** P <0.01. C: control; G: glycerol.

Table 6.4 Case I50-T30-1: The lateral skin images at different skin layers of the control group and the glycerol group. Red: THG (Contrast setting: 600~15000). Green: SHG (Contrast setting: 600~10000).

Case I50-T30-1				
	Glycerol	Glycerol	Control	Control
TOP	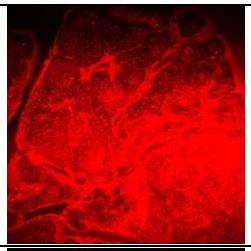	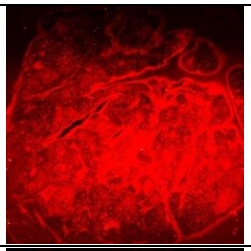	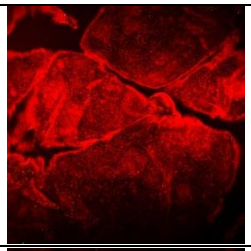	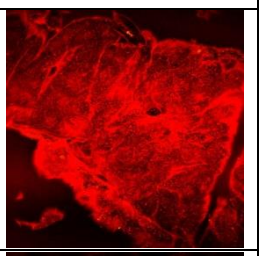
Bottom of SC	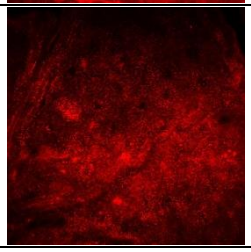	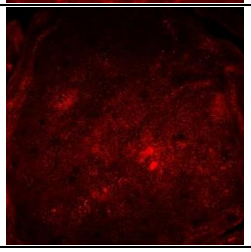	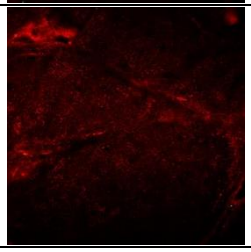	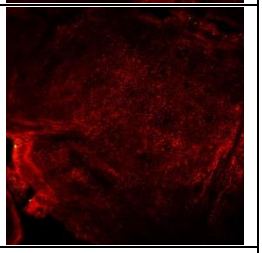
	14.4 μm	16.2 μm	14.4 μm	16.2 μm

doi:10.6342/NTU202000120

Middle Layer of Viable Dermis	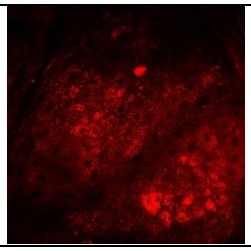	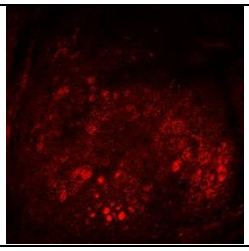	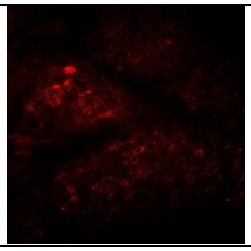	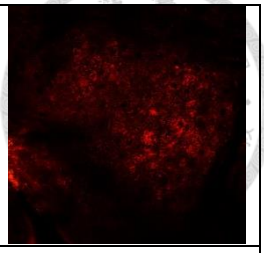
	27 μm	28.8 μm	28.8 μm	30.6 μm
Basal Layer	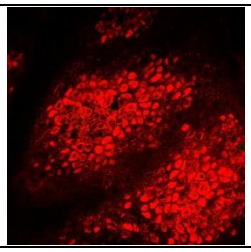	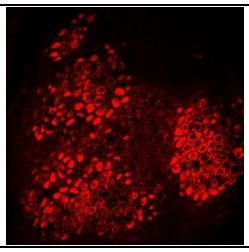	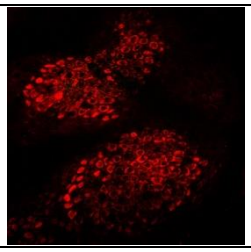	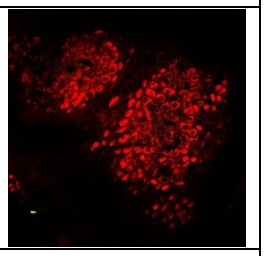
	39.6 μm	39.6 μm	41.4 μm	45 μm
Middle Layer of Papillary Dermis	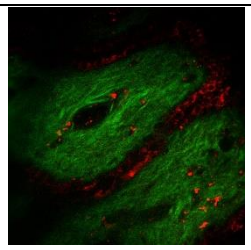	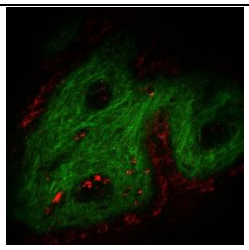	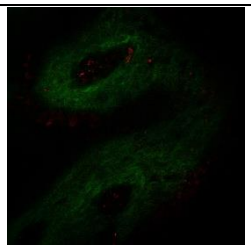	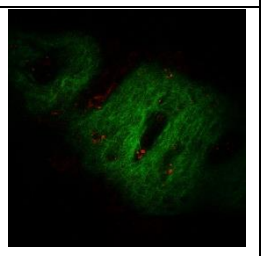
	84.6 μm	82.8 μm	84.6 μm	86.4 μm
Top Layer of Reticular Dermis	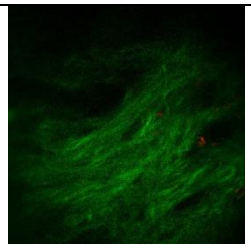	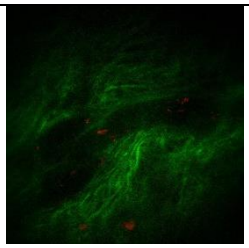	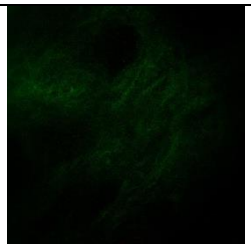	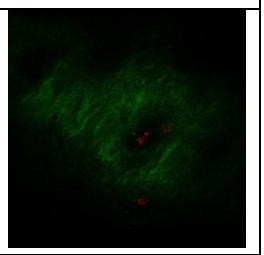
	127.8 μm	124.2 μm	127.8 μm	127.8 μm

doi:10.6342/NTU202000120

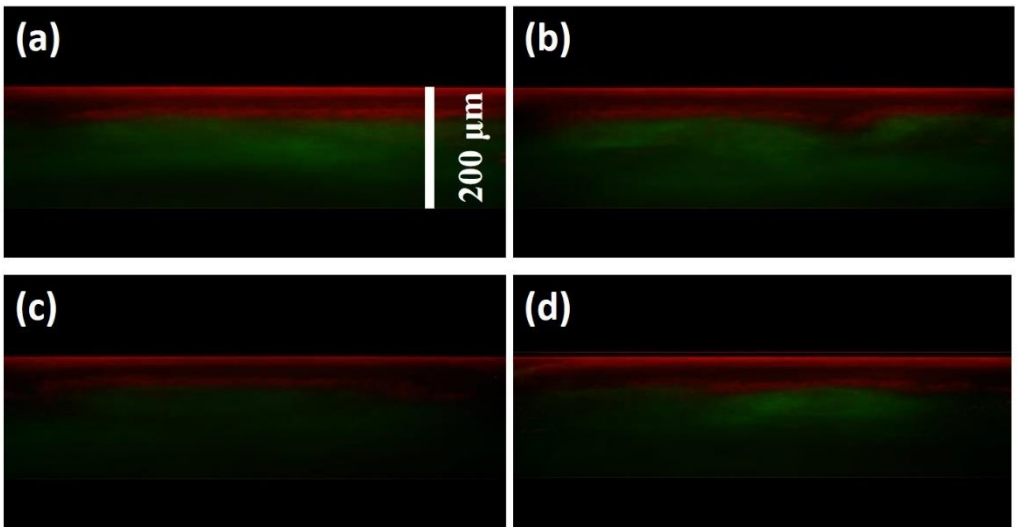

Fig. 6.10 *En face* skin image of Case I50-T30-1 (a) Glycerol-1 (b) Glycerol-2 (c) Control-1 (d) Control-2. Red: THG (Contrast setting: 600~15000). Green: SHG (Contrast setting: 600~10000).

Table 6.5 Case I50-T30-2: The skin images at different skin depths of the control group and the glycerol group. Red: THG (Contrast setting: 600~10000). Green: SHG (Contrast setting: 600~8000).

Case I50-T30-2				
	Glycerol	Glycerol	Control	Control
TOP	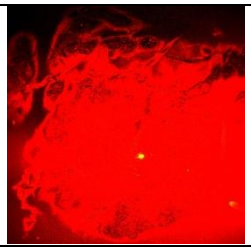	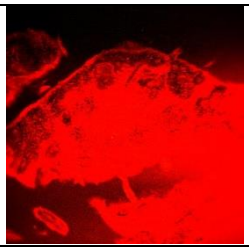	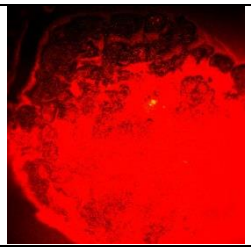	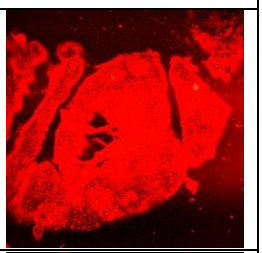
Bottom of SC	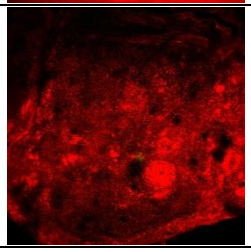	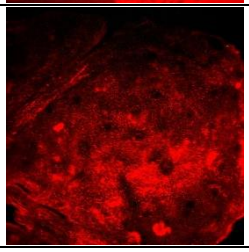	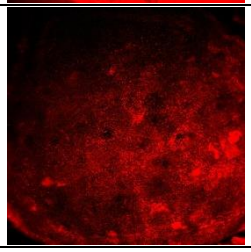	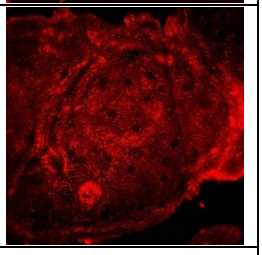
	16.2 μm	16.2 μm	18 μm	16.2 μm

doi:10.6342/NTU202000120

Middle Layer of Viable Dermis	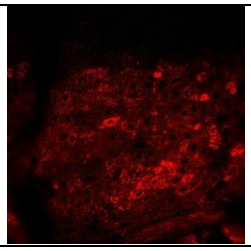	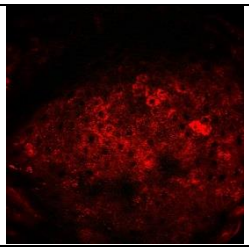	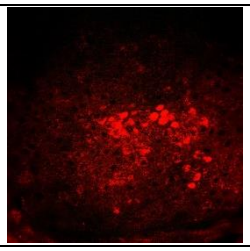	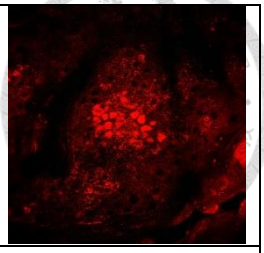
	34.2 μm	32.4 μm	36 μm	34.2 μm
Basal Layer	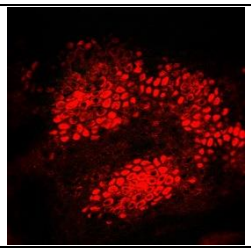	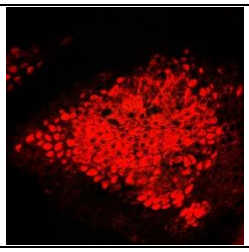	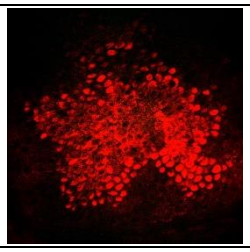	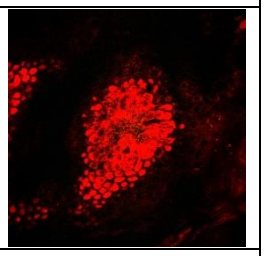
	50.4 μm	46.8 μm	52.5 μm	50.4 μm
Middle Layer of Papillary Dermis	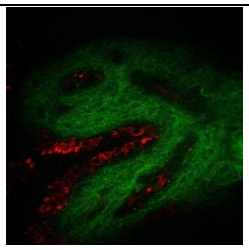	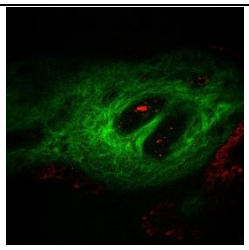	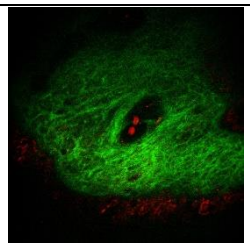	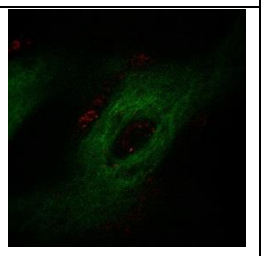
	90 μm	90 μm	93.6 μm	88.2 μm
Top Layer of Reticular Dermis	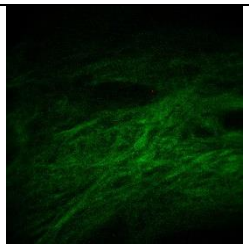	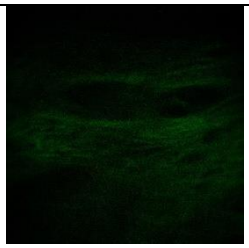	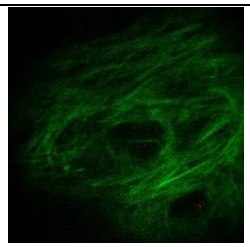	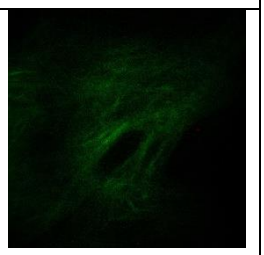
	129.6 μm	131.4 μm	133.2 μm	124.2 μm

doi:10.6342/NTU202000120

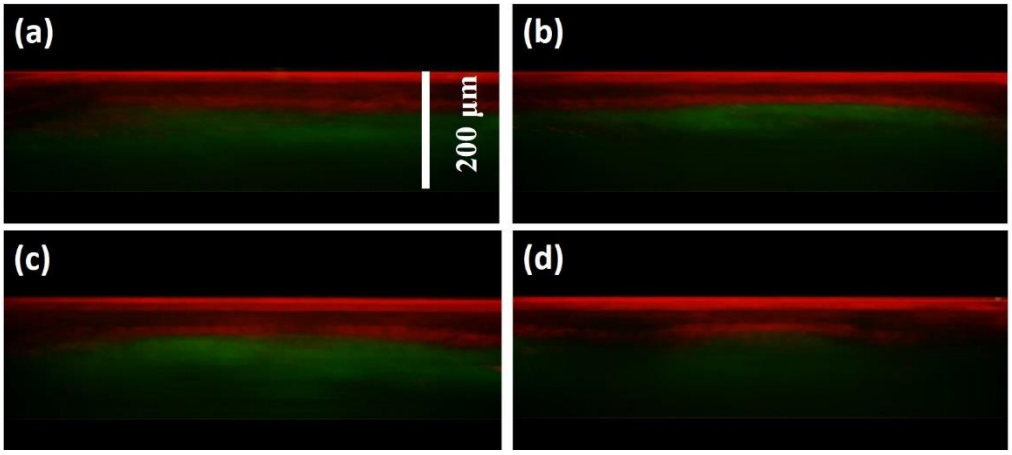

Fig. 6.11 *En face* skin image of Case I50-T30-2 (a) Glycerol-1 (b) Glycerol-2 (c) Control-1 (d) Control-2. Red: THG (Contrast setting: 600~10000). Green: SHG (Contrast setting: 600~8000).

6.2.3 Structure and HGM Intensity Analysis of Case I50-T90

For the case of I50-T90, two volunteers were studied. In both cases (I50-T90-1 and I50-T90-2), no thickness variation and effect of the optical clearing was found. Table 6.6 shows the analysis of the skin structure. No significant difference was found in both volunteers. Fig. 6.12 and Fig. 6.13 show the image intensity analysis. Table 6.7and Fig. 6.14 show the representative HGM images of Case I50-T90-1. Table 6.8 and Fig. 6.15 show the representative HGM images of Case I50-T90-2.

Table 6.6 Skin structure analysis results of all studied cases. (*p<0.05, **p<0.01, ***p<0.001)

	Depth or thickness change (μm)	Thickness of SC	Thickness of viable epidermis	Depth of basal layer	Depth of middle papillary dermis layer	Depth of Top reticular dermis layer
1	C (N=6)	17.7±3.5	28.8±3.6	46.5±2.4	89.1±12.3	131.1±23.7
	G (N=6)	20.7±1.9	26.7±1.4	47.4±1.9	92.4±5.9	136.8±10.6
2	C (N=6)	18.3±2.6	28.5±5.7	46.8±5.9	86.4±9.5	127.2±11.4
	G (N=6)	18.9±1.9	29.7±4.8	48.6±4.6	92.4±4.1	135.6±7.6

doi:10.6342/NTU202000120

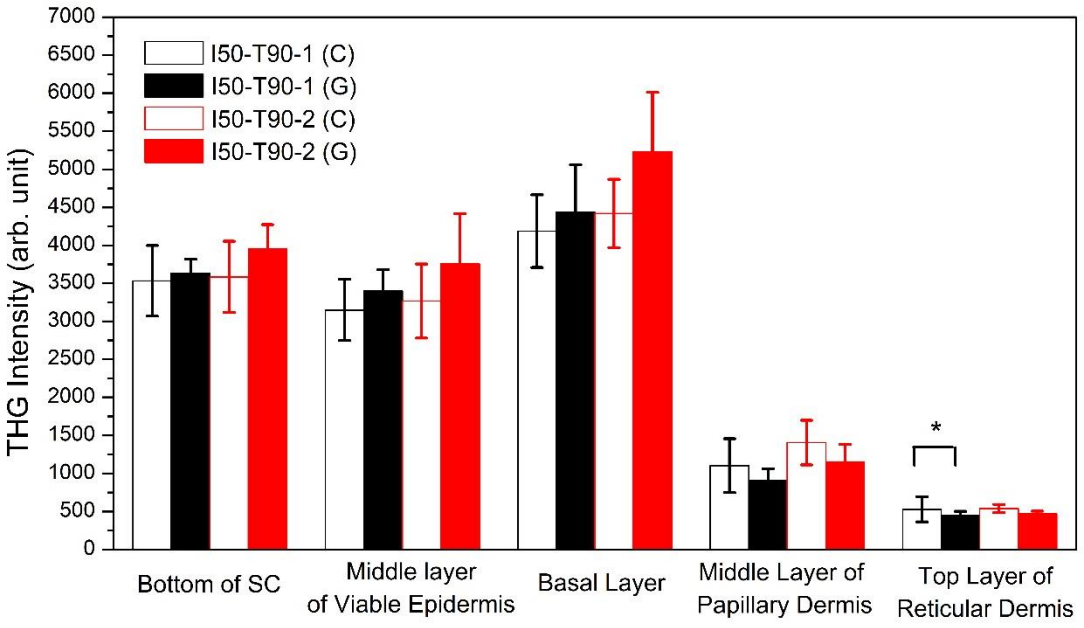

Fig. 6.12 Quantitative analysis and comparison of skin THG intensities at five different depths. Black: Case I50-T90-1 (control: N=6, glycerol: N=6); Red: Case I50-T90-2 (control: N=6, glycerol: N=6). *P <0.05. C: control; G: glycerol.

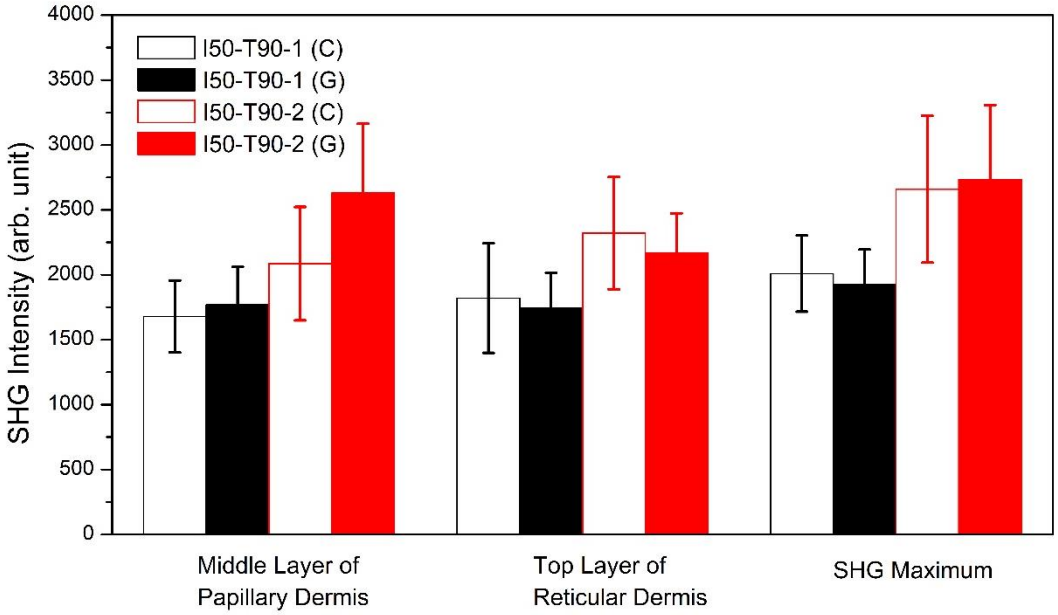

Fig. 6.13 Quantitative analysis and comparison of skin SHG intensities at three different depths. Black: Case I50-T90-1 (control: N=8, glycerol: N=8); Red: Case I50-T90-2 (control: N=9, glycerol: N=9). C: control; G: glycerol.

doi:10.6342/NTU202000120

Table 6.7 Case I50-T90-1: The skin images at different depths of the control group and the glycerol group. Red: THG (Contrast setting: 600~15000). Green: SHG (Contrast setting: 600~8000)

Case I50-T90-1				
	Glycerol	Glycerol	Control	Control
TOP	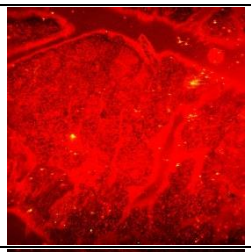	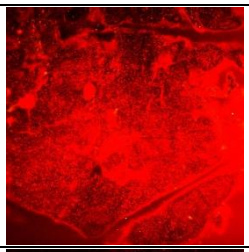	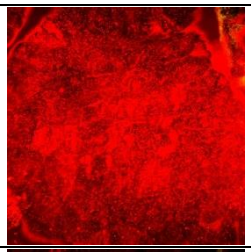	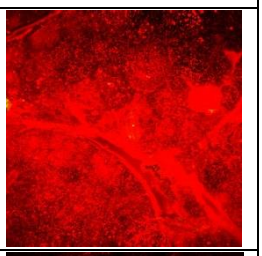
Bottom of SC	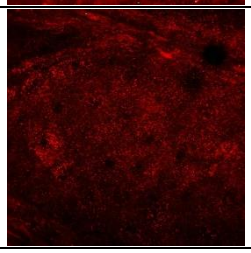	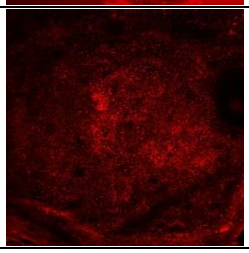	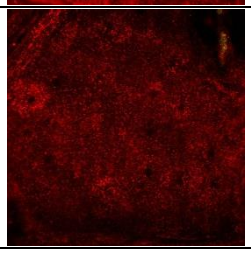	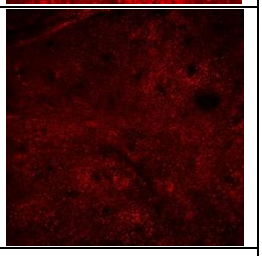
	21.6 μm	21.6 μm	19.8 μm	18 μm
Middle Layer of Viable Dermis	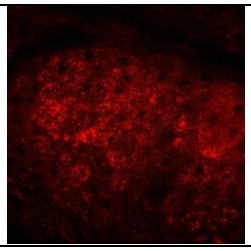	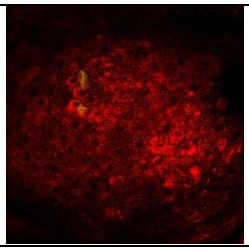	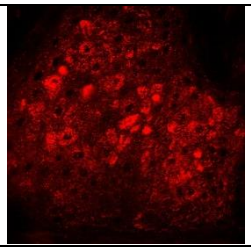	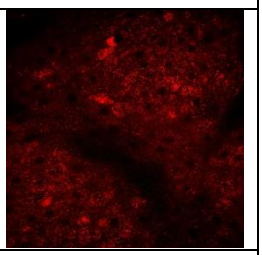
	34.2 μm	36 μm	36 μm	32.4 μm
Basal Layer	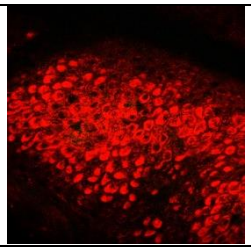	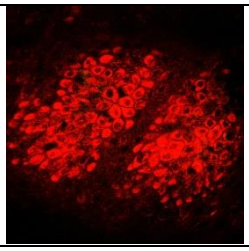	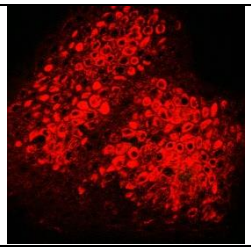	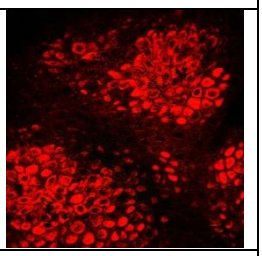
	46.8 μm	48.6 μm	50.4 μm	46.8 μm
Middle Layer of Papillary Dermis	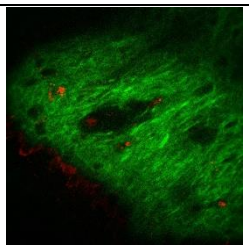	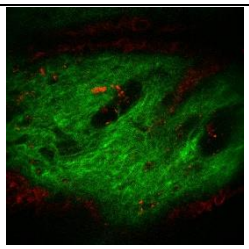	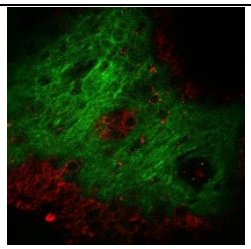	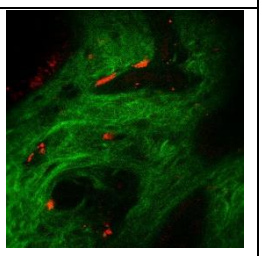

doi:10.6342/NTU202000120

	93.6 μm	84.6 μm	84.6 μm	102.6 μm
Top Layer of Reticular Dermis	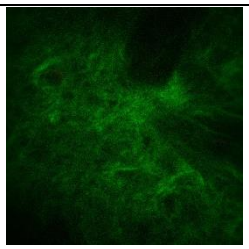	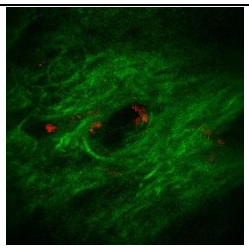	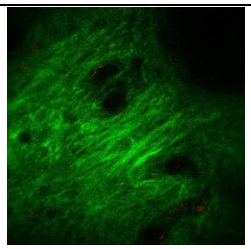	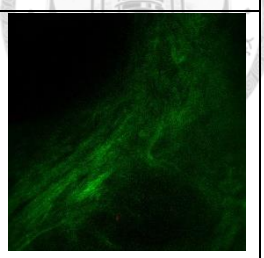
	140.4 μm	120.6 μm	118.8 μm	158.4 μm

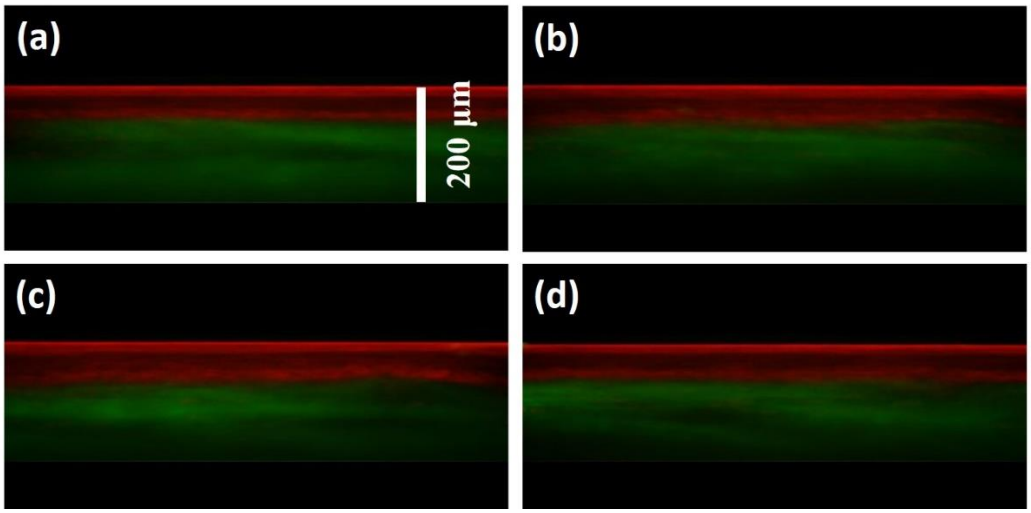

Fig. 6.14 *En face* skin image of Case I50-T90-1 (a) Glycerol-1 (b) Glycerol-2 (c) Control-1 (d) Control-2. Red: THG (Contrast setting: 600~15000). Green: SHG (Contrast setting: 600~8000)

Table 6.8 Case I50-T90-2: The skin images at different depths of the control group and the glycerol group. Red: THG (Contrast setting: 600~10000). Green: SHG (Contrast setting: 600~8000)

Case I50-T90-2				
	Glycerol	Glycerol	Control	Control
TOP	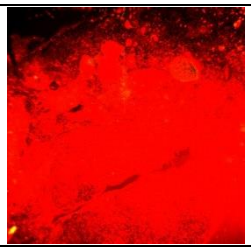	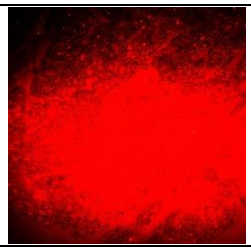	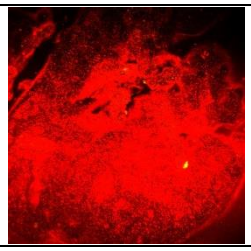	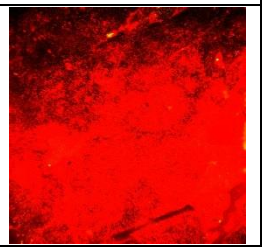

doi:10.6342/NTU202000120

Bottom of SC	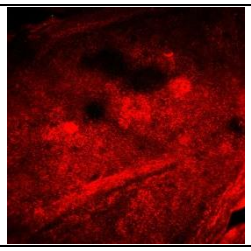	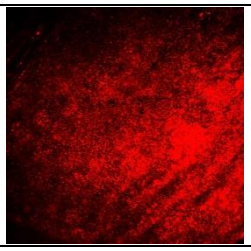	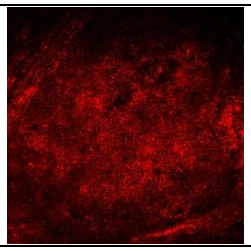	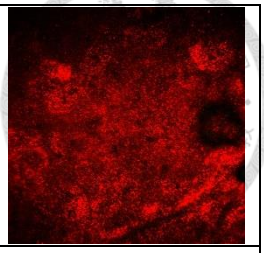
	18 μm	16.2 μm	18 μm	16.2 μm
Middle Layer of Viable Dermis	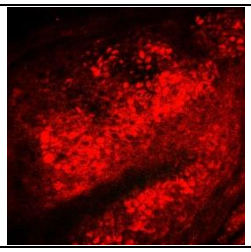	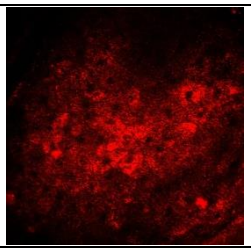	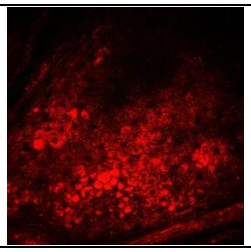	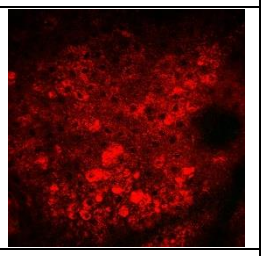
	32.4 μm	32.4 μm	30.6 μm	34.2 μm
Basal Layer	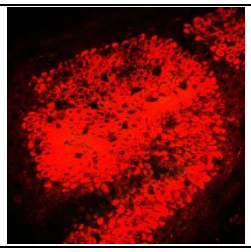	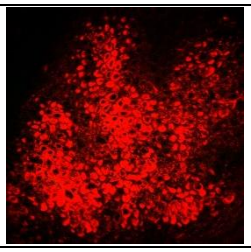	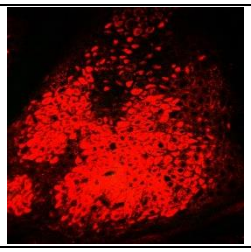	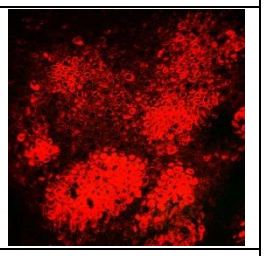
	45 μm	46.8 μm	43.2 μm	50.4 μm
Middle Layer of Papillary Dermis	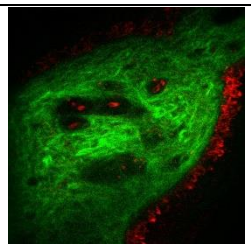	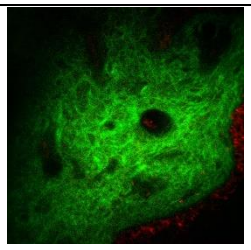	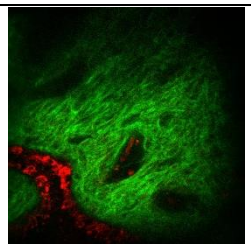	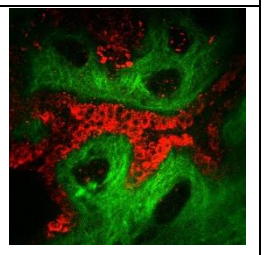
	95.4 μm	93.6 μm	82.8 μm	95.4 μm
Top Layer of Reticular Dermis	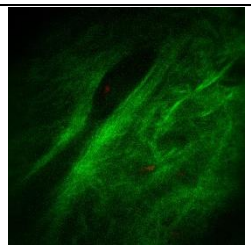	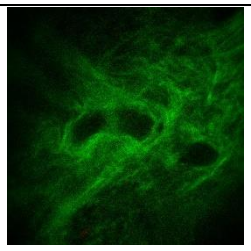	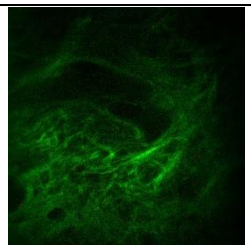	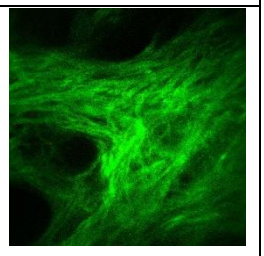
	145.8 μm	140.4 μm	122.4 μm	138.6 μm

doi:10.6342/NTU202000120

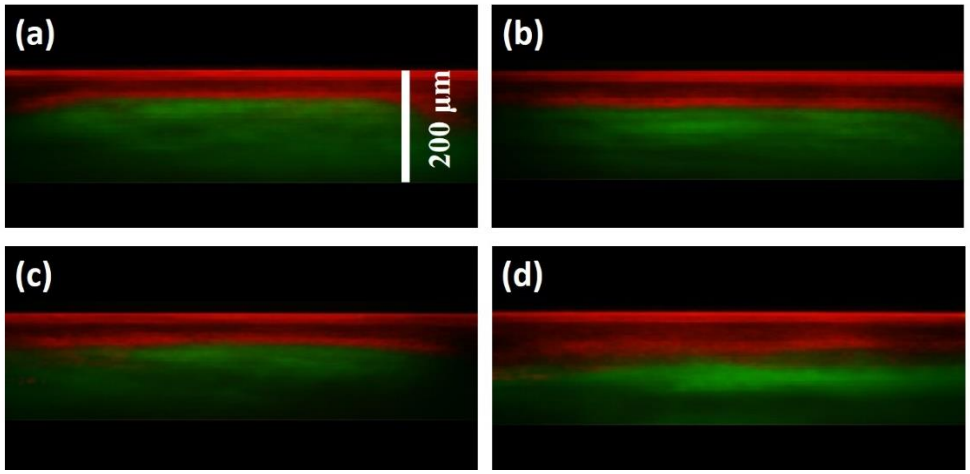

Fig. 6.15 *En face* skin image of Case I50-T90-2 (a) Glycerol-1 (b) Glycerol-2 (c) Control-1 (d) Control-2. Red: THG (Contrast setting: 600~10000). Green: SHG (Contrast setting: 600~8000)

6.2.4 Structure and HGM Intensity Analysis of Case I50-T180

In Case I50-T180, we did not find the variation of the skin structure, except at the epidermis of the Case I50-T180-3. In which the thickness of the viable increased significantly (Table 6.9).

Besides, the HGM intensity analysis data was recorded in Fig. 6.16 and Fig. 6.17. In Case I50-T180-1, the THG intensities of the skin significant decreased at the bottom of SC and the middle layer of the viable epidermis after the glycerol application. The average intensity significantly reduced by nearly 12% at the bottom of SC and nearly 9% at the middle layer of viable epidermis. When looking forward into the deeper area: basal layer, papillary dermis, and reticular dermis, we found that the average HGM intensities increased or remained the same. In Case I50-T180-2, there was no significant difference in HGM intensity. It is hard to tell the difference between the image before and after the

doi:10.6342/NTU202000120

glycerol application. Although we found the effect of the optical clearing in the Case I50-T180-1, in Case I50-T180-2, the effect of optical clearing is indistinct. In Case I50-T180-3, the THG intensity increased significantly by nearly 14% at the middle layer of the viable epidermis and nearly 20% at the bottom of SC. While for the SHG intensities, no significant difference was found.

Table 6.10 and Fig. 6.18 show the representative HGM images of Case I50-T180-1. Table 6.11 and Fig. 6.19 show the representative HGM images of Case I50-T180-2. Table 6.12 and Fig. 6.20 show the representative HGM images of Case I50-T180-3.

Table 6.9 Skin structure analysis results of all studied cases. (*p<0.05, **p<0.01, ***p<0.001)

	Depth or thickness change (μm)	Thickness of SC	Thickness of viable epidermis	Depth of basal layer	Depth of middle papillary dermis layer	Depth of Top reticular dermis layer
1	C (N=7)	18.3±2.4	24.7±3.1	42.9±3.0	80.2±8.2	117.3±14.1
	G (N=7)	17.5±0.9	24.2±2.5	41.7±3.2	75.1±2.5	107.5±8.2
2	C (N=9)	16.4±1.9	29.0±2.3	45.4±2.7	87.8±4.2	129.4±9.7
	G (N=9)	16.0±2.5	27.8±3.4	43.8±3.6	84.8±9.5	124.6±18.4
3	C (N=10)	19.1±2.3	30.1±2.6	49.1±2.7	93.1±6.8	136.1±13.0
	G (N=10)	17.8±2.7	**33.3±3.5***	51.1±3.9	97.2±4.6	142.2±9.2

doi:10.6342/NTU202000120

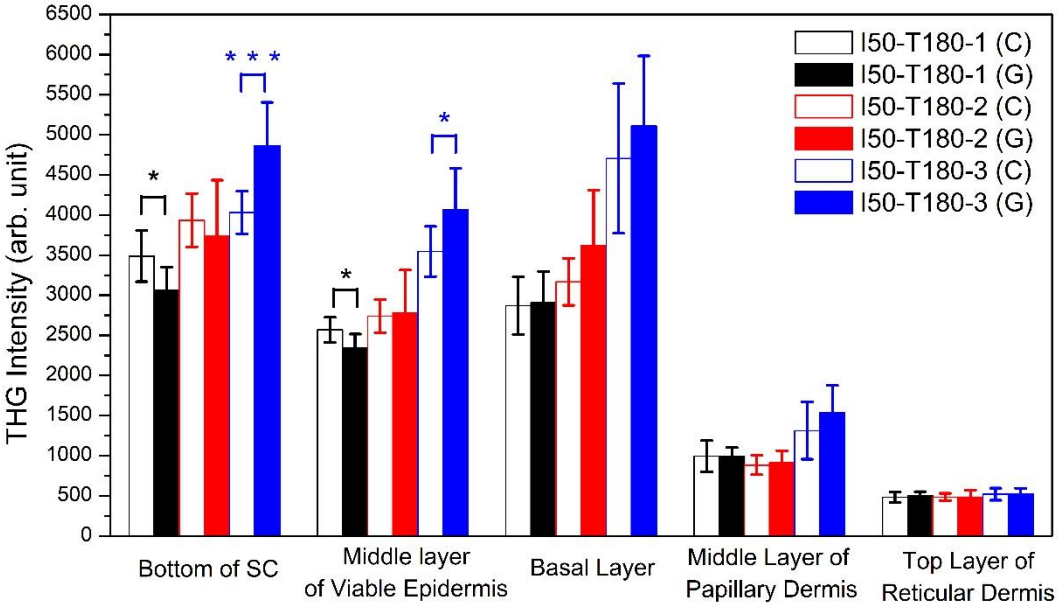

Fig. 6.16 Quantitative analysis and comparison of skin THG intensities at five different depths. Black: Case I50-T180-1 (control: N=7, glycerol: N=7); Red: Case I50-T180-2 (control: N=9, glycerol: N=9). Blue: Case I50-T180-3 (control: N=10, glycerol: N=10). *P <0.05; *** P <0.001. C: control; G: glycerol

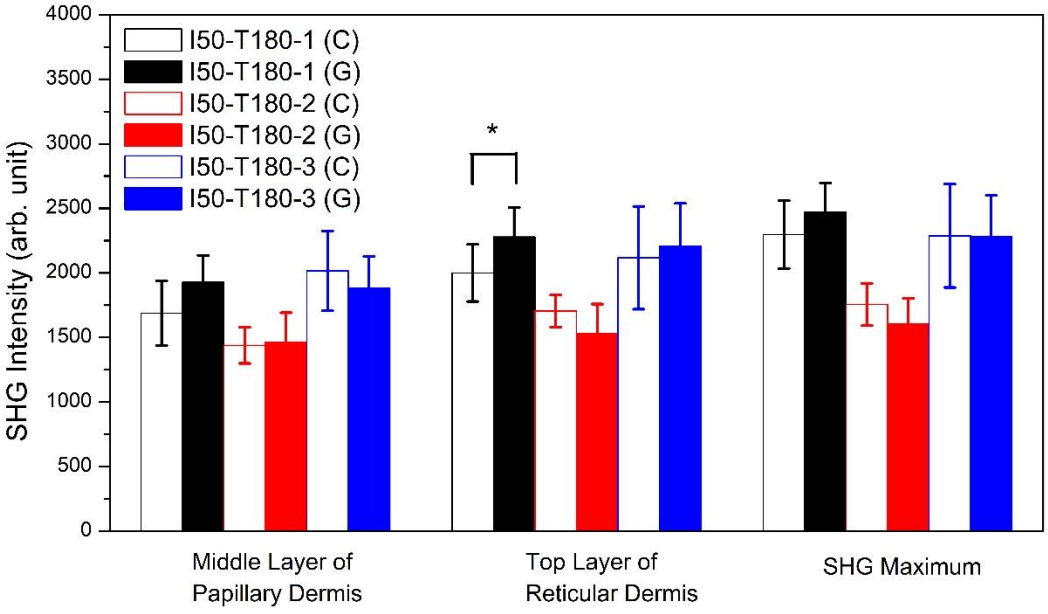

Fig. 6.17 Quantitative analysis and comparison of skin SHG intensities at three different depths. Black: Case I50-T180-1 (control: N=7, glycerol: N=7); Red: Case I50-T180-2 (control: N=9, glycerol: N=9). Blue: Case I50-T180-3 (control: N=10, glycerol: N=10). *P

doi:10.6342/NTU202000120

<0.05. C: control; G: glycerol.

Table 6.10 Case I50-T180-1: The skin images at different depths of the control group and the glycerol group. Red: THG (Contrast setting: 600~10000). Green: SHG (Contrast setting: 600~8000)

Case I50-T180-1				
	Glycerol	Glycerol	Control	Control
TOP		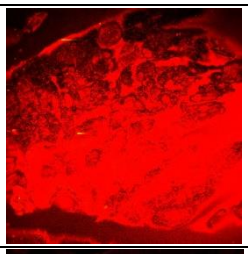	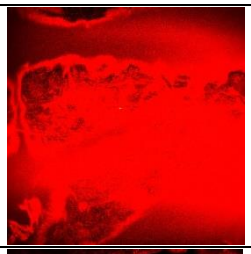	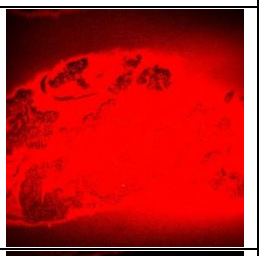
Bottom of SC	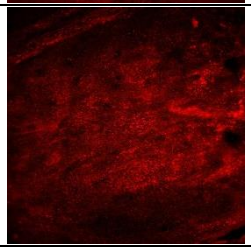	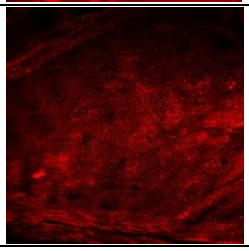	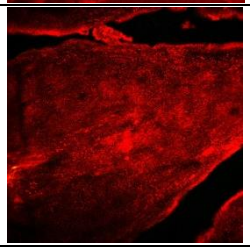	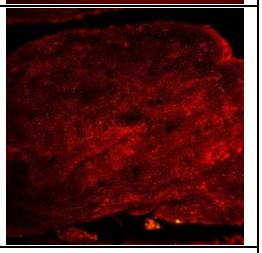
	16.2 μm	18 μm	18 μm	19.8 μm
Middle Layer of Viable Dermis	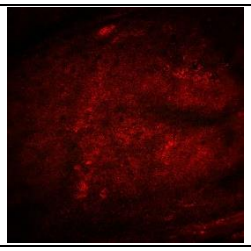	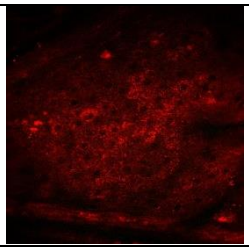	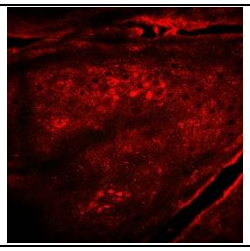	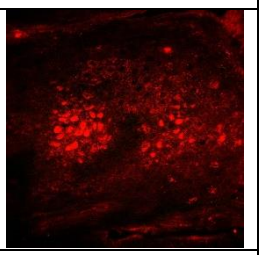
	28.8 μm	32.4 μm	30.6 μm	32.4 μm
Basal Layer	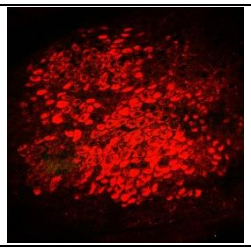	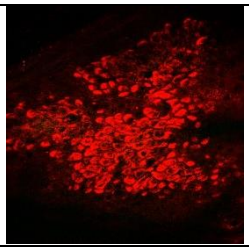	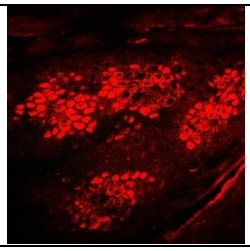	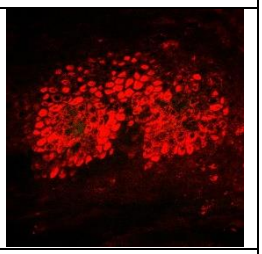
	39.6 μm	45 μm	43.2 μm	45 μm

doi:10.6342/NTU202000120

Middle Layer of Papillary Dermis	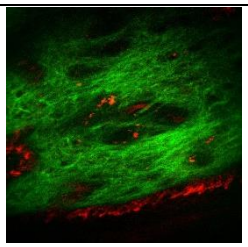	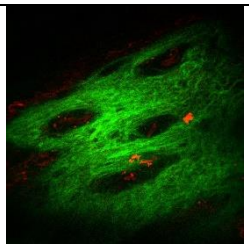	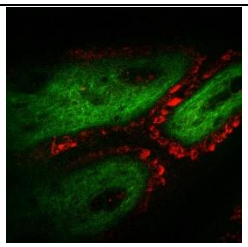	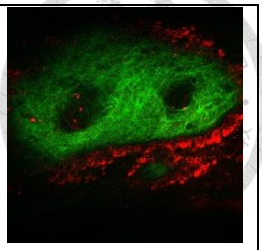
	75.6 μm	73.8 μm	84.6 μm	75.6 μm
Top Layer of Reticular Dermis	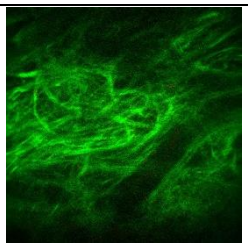	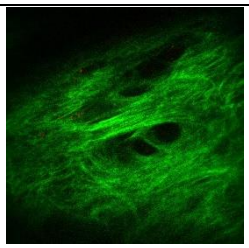	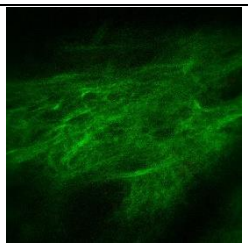	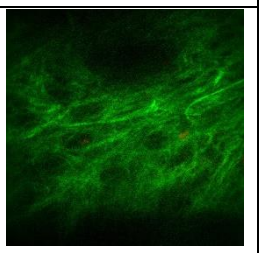
	111.6 μm	100.8 μm	124.2 μm	106.2 μm

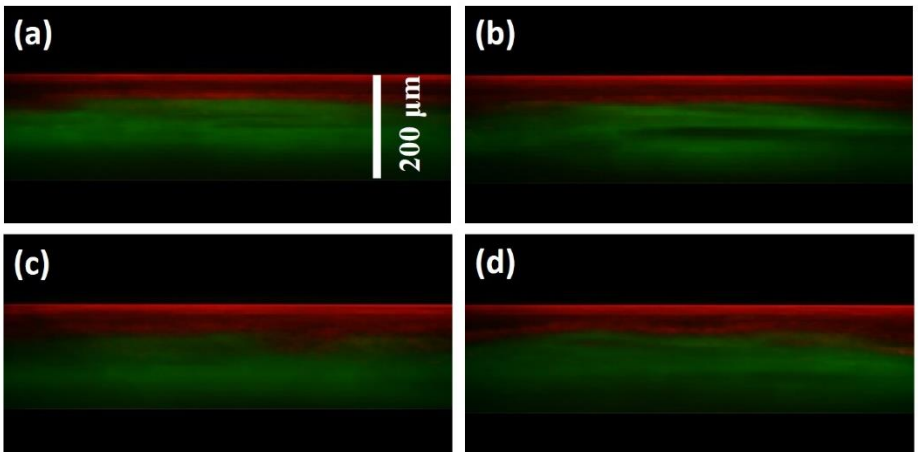

Fig. 6.18 *En face* skin image of Case I50-T180-1 (a) Glycerol-1 (b) Glycerol-2 (c) Control-1 (d) Control-2. Red: THG (Contrast setting: 600~10000). Green: SHG (Contrast setting: 600~8000)

Table 6.11 Case I50-T180-2: The skin images at different depths of the control group and the glycerol group. Red: THG (Contrast setting: 600~15000). Green: SHG (Contrast setting: 600~8000)

Case I50-T180-2				
	Glycerol	Glycerol	Control	Control

doi:10.6342/NTU202000120

TOP	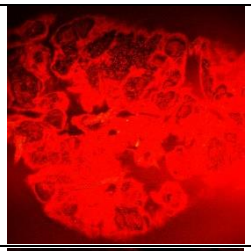	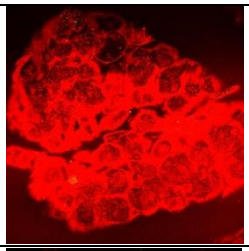	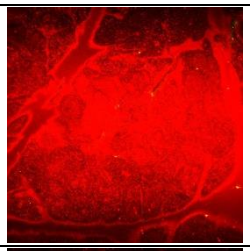	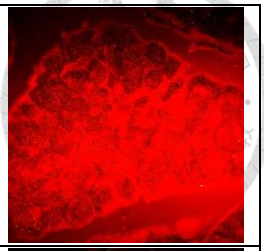
Bottom of SC	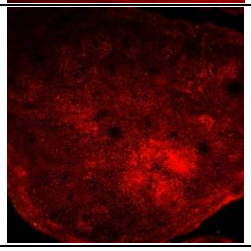	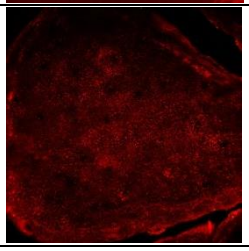	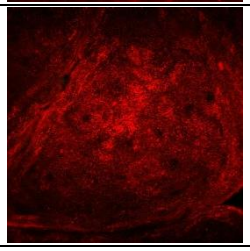	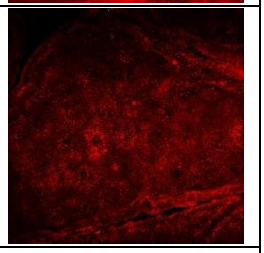
	16.2 μm	18 μm	16.2 μm	14.4 μm
Middle Layer of Viable Dermis	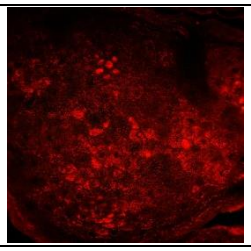	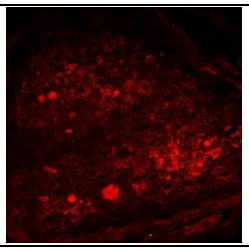	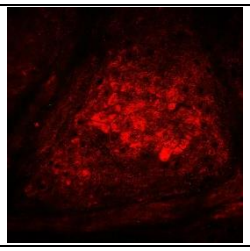	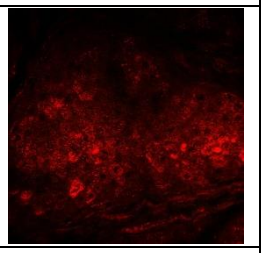
	30.6 μm	30.6 μm	30.6 μm	28.8 μm
Basal Layer	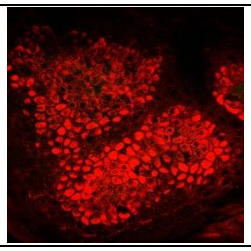	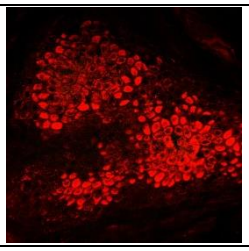	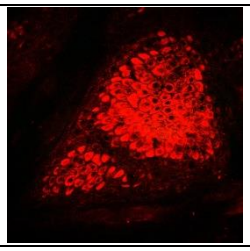	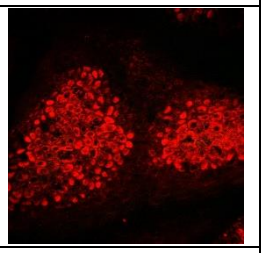
	43.2 μm	41.4 μm	45 μm	43.2 μm
Middle Layer of Papillary Dermis	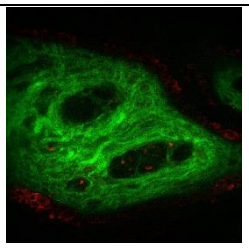	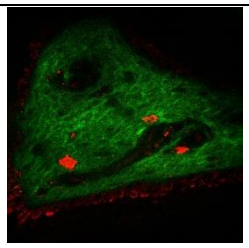	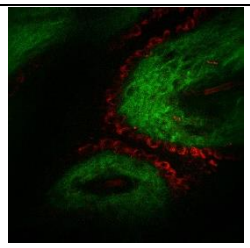	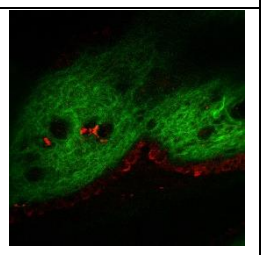
	95.4 μm	90 μm	88.2 μm	88.2 μm

doi:10.6342/NTU202000120

Top Layer of Reticular Dermis	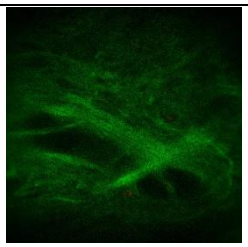	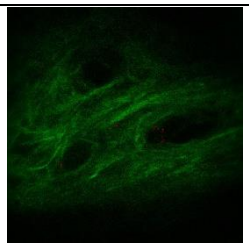	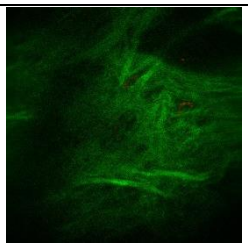	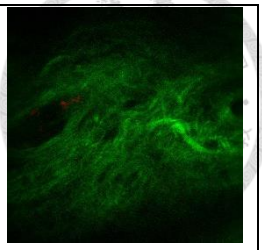
	145.8 μm	136.8 μm	129.6 μm	133.2 μm

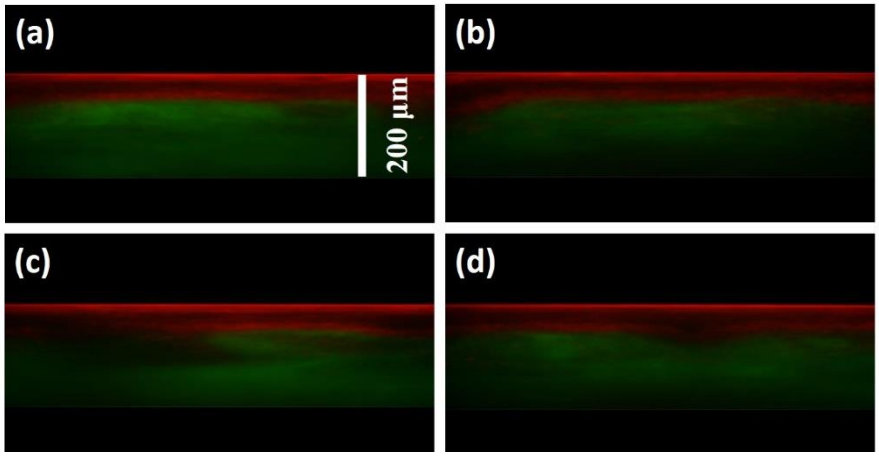

Fig. 6.19 *En face* skin image of Case I50-T180-2 (a) Glycerol-1 (b) Glycerol-2 (c) Control-1 (d) Control-2. Red: THG (Contrast setting: 600~15000). Green: SHG (Contrast setting: 600~8000)

Table 6.12 Case I50-T180-3: The skin images at different depths of the control group and the glycerol group. Red: THG (Contrast setting: 600~15000). Green: SHG (Contrast setting: 600~8000)

Case I50-T180-3				
	Glycerol	Glycerol	Control	Control
TOP	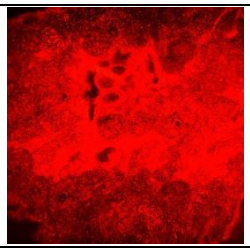	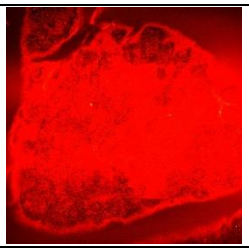	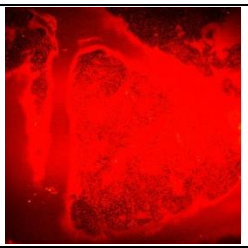	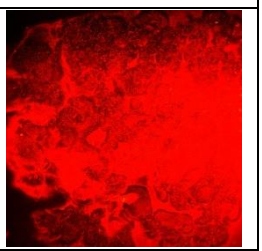
Bottom of SC		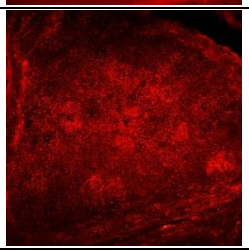	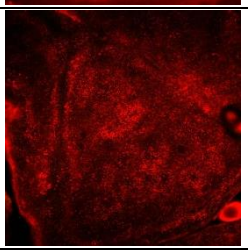	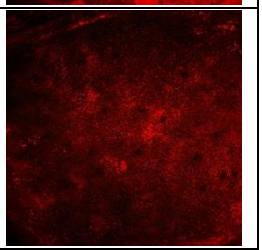

doi:10.6342/NTU202000120

	16.2 μm	16.2 μm	18 μm	21.6 μm
Middle Layer of Viable Dermis	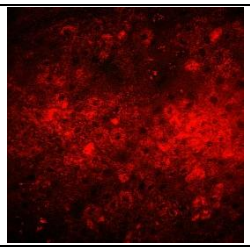	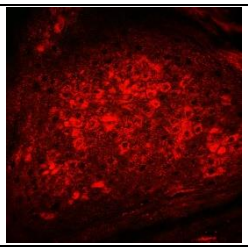	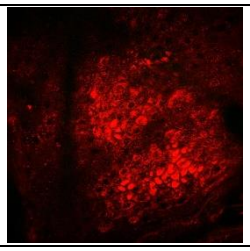	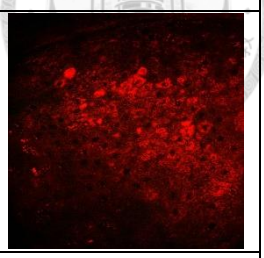
	32.4 μm	32.4 μm	32.4 μm	37.8 μm
Basal Layer	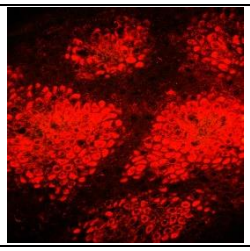	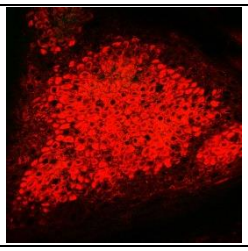	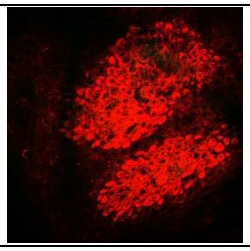	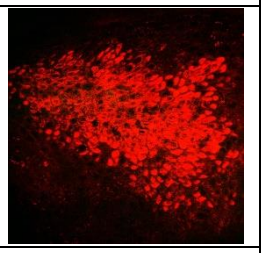
	48.6 μm	48.6 μm	46.8 μm	52.2 μm
Middle Layer of Papillary Dermis	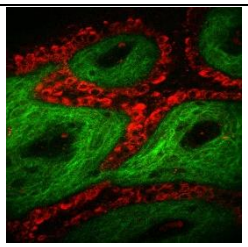	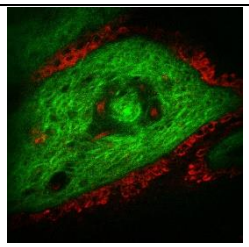	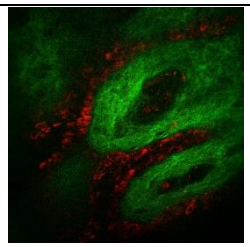	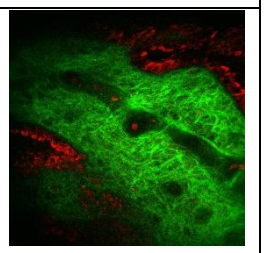
	90 μm	93.6 μm	88.2 μm	93.6 μm
Top Layer of Reticular Dermis	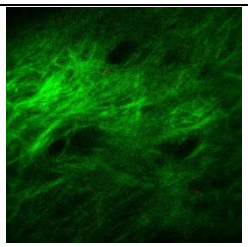	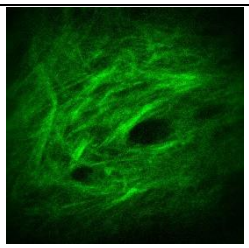	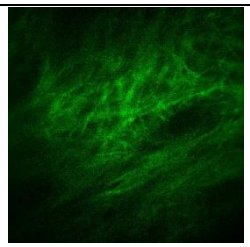	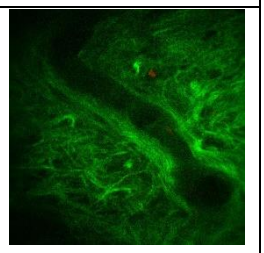
	131.4 μm	138.6μm	129.6 μm	135 μm

doi:10.6342/NTU202000120

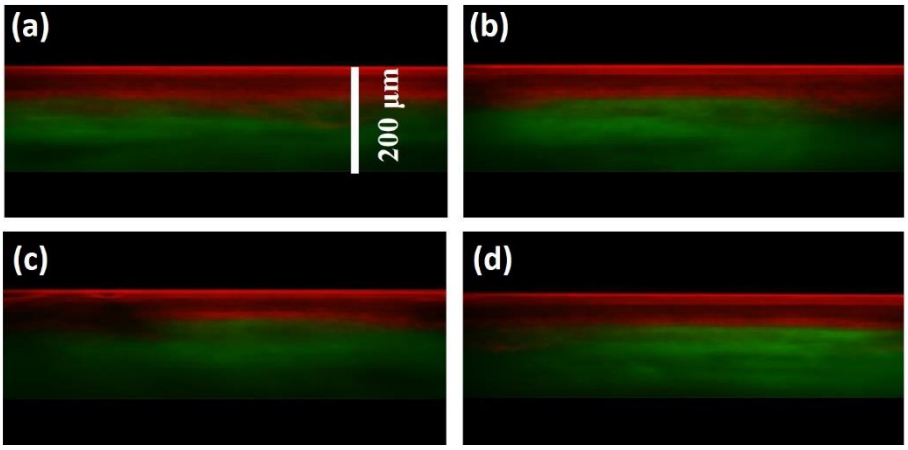

Fig. 6.20 *En face* skin image of Case I50-T180-3 (a) Glycerol-1 (b) Glycerol-2 (c) Control-1 (d) Control-2. Red: THG (Contrast setting: 600~15000). Green: SHG (Contrast setting: 600~8000)

6.3 Summary of the *In Vivo* Optical Clearing Results

Table 6.13 Skin structure analysis results of all studied cases. (*p<0.05, **p<0.01, ***p<0.001)

	Depth or thickness change (μm)	Thickness of SC	Thickness of viable epidermis	Depth of basal layer	Depth of middle papillary dermis layer	Depth of Top reticular dermis layer
			Case I50-T15			
1	Control (N=10)	17.6±2.0	27.5±5.4	45.2±4.8	78.3±5.8	110.9±10.3
	Glycerol (N=10)	18.4±2.8	31.5±3.4	**49.9±4.0***	80.3±5.1	109.6±11.2
			Case I50-T30			
1	C (N=10)	17.1±1.7	26.8±1.3	43.9±2.1	87.3±6.1	130.1±12.1
	G (N=10)	16.7±2.9	**24.1±2.8****	**40.9±4.2***	84.1±4.9	126.4±7.3
2	C (N=10)	16.2±2.2	35.8±4.8	52.0±4.2	95.2±6.5	137.2±13.4
	G (N=10)	16.2±1.5	34.6±4.1	50.8±4.1	91.1±5.6	130.7±11.9
			Case I50-T90			
1	C (N=6)	17.7±3.5	28.8±3.6	46.5±2.4	89.1±12.3	131.1±23.7
	G (N=6)	20.7±1.9	26.7±1.4	47.4±1.9	92.4±5.9	136.8±10.6
2	C (N=6)	18.3±2.6	28.5±5.7	46.8±5.9	86.4±9.5	127.2±11.4
	G (N=6)	18.9±1.9	29.7±4.8	48.6±4.6	92.4±4.1	135.6±7.6
			Case I50-T180			
1	C (N=7)	18.3±2.4	24.7±3.1	42.9±3.0	80.2±8.2	117.3±14.1
	G (N=7)	17.5±0.9	24.2±2.5	41.7±3.2	75.1±2.5	107.5±8.2
2	C (N=9)	16.4±1.9	29.0±2.3	45.4±2.7	87.8±4.2	129.4±9.7
	G (N=9)	16.0±2.5	27.8±3.4	43.8±3.6	84.8±9.5	124.6±18.4
3	C (N=10)	19.1±2.3	30.1±2.6	49.1±2.7	93.1±6.8	136.1±13.0
	G (N=10)	17.8±2.7	**33.3±3.5***	51.1±3.9	97.2±4.6	142.2±9.2

Table 6.14 Statistical analysis result on the THG intensity variation after the glycerol application. (-: no significant difference, △: Increased significantly, ▽: Decreased significantly, *p<0.05, **p<0.01, ***p<0.001)

THG intensity	Bottom of SC	Middle viable epidermis layer	Basal layer	Middle papillary dermis layer	Top reticular dermis layer
Case			**I50-T15**		
1	-	-	-	-	-
Case			**I50-T30**		
1	-	△ (**)	△ (**)	△ (***)	△ (***)
2	-	-	-	-	-

doi:10.6342/NTU202000120

Case					
			I50-T90		
1	-	-	-	-	-
2	-	-	-	-	▽ (*)
Case			**I50-T180**		
1	▽ (*)	▽ (*)	-	-	-
2	-	-	-	-	-
3	△ (***)	△ (*)	-	-	-

Table 6.15 Statistical analysis result on the SHG intensity variation after the glycerol application. (-: no significant difference, △: Increased significantly, ▽: Decreased significantly, *p<0.05, **p<0.01, ***p<0.001)

SHG intensity	Middle papillary dermis layer	Top reticular dermis layer	SHG Maximum
Case		**I50-T15**	
1	-	-	-
Case		**I50-T30**	
1	△ (**)	△ (**)	△ (**)
2	-	-	-
Case		**I50-T90**	
1	-	-	-
2	-	-	-
Case		**I50-T180**	
1	-	△ (*)	-
2	-	-	-
3	-	-	-

doi:10.6342/NTU202000120

Chapter 7 Discussion of the *Ex Vivo* Optical Clearing

Within 90-minutes glycerol application (Case I50-T15, Case I50-T30, and Case I50-T90), most of the volunteers showed no significant difference except Case I50-T30-1. The optical clearing was less effective within 90 minutes application. This result correlates well with the previous studies on the volar forearm by 60- and 120-minutes topical application [33, 50] and on the dorsal hand by 60-minutes application [33]. The only case showing the OC effect can be attributed to the skin shrinkage, and will be discussed separately below.

However, in a case type of 180-minutes application, two of three volunteers (Case I50-T180-1 and Case I50-T180-3) were found with the optical clearing effect, on the skin area with a thin SC. The thickness of SC was all lower than 20 μm (Table 6.13). This indicates that even with a thin SC, it is with a higher probability to witness the optical clearing after a longer applying time. It is further noted that these two cases show different trends in the HGM image, indicating that the optical clearing mechanisms were different between these two cases.

7.1 Case I50-T180-1

There were enhancements of the SHG intensities in the dermis (Table 6.15), indicating that the light scattering in the epidermal skin was reduced [60, 61]. This is

doi:10.6342/NTU202000120

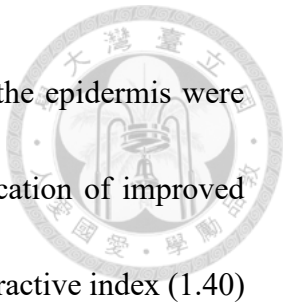

further evidenced by the fact that the THG intensity at the SC and the epidermis were both decreased (Table 6.14). Decrease of THG intensity is the indication of improved optical homogeneity [61, 68, 69]. A 50 % glycerol is with a higher refractive index (1.40) [72] than extracellular and intracellular fluids (1.34-1.36) [66] . After immersion the skin tissues into anhydrous glycerol, glycerol diffused inside and filled all of the skin tissues to create a higher refractive index matching environment for the scattering particles (such as organelles, protein fibrils, membranes, protein globules, with refractive index 1.39-1.47 [49, 66]). Our result supports that fact that the 50% glycerol solution diffused into the epidermal skin, created a higher homogeneous environment, and resulted in reduction of the light scattering as well as the THG intensity [60]. The skin became transparent in the superficial skin layers and there were more photons travelling in/out the tissue, so as to enhance the image intensity in the deep skin. The results were similar to our *ex vivo* study by 100% glycerol immersion. Similar conclusion was also suggested in the study of Wen et al. [29] by introducing thiazone-PEG400 *in vivo* on rat skin, and in the study of Fox et al. [32] by introducing 100% glycerol with SC removal and low pressure transdermal device on *in vivo* human skin. The correlated HGM images of Case I50-T180-1 have shown in section 6.2.4.

doi:10.6342/NTU202000120

7.2 Case I50-T180-3

In this case, the THG intensity increased greatly at the bottom of the SC and the middle layer of the viable epidermis (Table 6.14). However, the optical clearing effect was not found in the dermis (Table 6.15). The reason might be that the glycerol solution did not penetrate far enough into the epidermis as the above-mentioned case to introduce an optical clearing effect at the dermis. The results of this volunteer were similar to our another previous *ex vivo* study by 100% glycerol topical application. The glycerol diffused into the SC and reduced its optical scattering, thus increasing the laser excitation power in layers beneath as well as the back-reflection signals. The relationship of the OCAs diffusion and the optical clearing effect at the deep area was also noted by Tuchin in 2017 [5]

7.3 Case I50-T30-1

In this case, we found the strongest OC effects, and it was the only case the optical clearing effect found with application within 90 minutes. The average THG and SHG intensities were all greatly enhanced (Table 6.4 and Fig. 6.10 in section 6.2.2). The 50% glycerol diffused into the skin within 30 minutes and this is the only tissue that was found to shrink after the glycerol application (Table 6.13). In our previous *ex vivo* study, 50% glycerol was found to be able to dehydrate and shrink the skin. The dehydration and shrinkage of the tissue were both proved to benefit the OC efficacy, and to enhance the

doi:10.6342/NTU202000120

image intensities [49, 70, 71]. It might be the main reason that the optical clearing effect was pronounced in this case. Similar results were also found in our previous *ex vivo* study by 50% glycerol topical application, and in the study of Zhong et al. by introducing thiazone-PEG400 with ultrasonic on *in vivo* human skin [15] in which the OCT image intensity increased at all detected depths.

7.4 Conclusion

In this study, we investigated the optical clearing of the human volar forearm. The results showed that the optical clearing was less effective with topical application within 90 minutes. Only one case was found the effect of the optical clearing accompanied with its significant decrements of the skin thickness. For 180 minutes topical application, two of three cases were found the effect of the optical clearing. In the skin area with thinner SC, there was a higher probability to witness the optical clearing after a longer applying time.

In general, topical application by introducing 50% glycerol cannot provide a promising optical clearing effect in the *in vivo* human skin. For most of the cases, the skin structure and the HGM intensity remained the same after the glycerol application. Optical clearing agents cannot introduce the same optical clearing effect on the skin *in vivo* as that of *ex vivo*. We believe the main reason might be the hydration effect, while

doi:10.6342/NTU202000120

dehydration has been proved as one of the most important factors for the optical clearing [49, 52, 71]. The metabolism and blood circulation of the human body prevented the skin from dehydration and thus decreased the optical clearing efficacy. Besides, in our previous *ex vivo* study, SC played a critical role for the observed THG enhancement. We found signal enhancement in THG imaged epidermal tissues with a SC layer thicker than 27 μm. Skin tissue with a thicker SC layer suffers stronger light scattering in SC so that the OC effect is more pronounced after topical applications. In other previous studies, the optical clearing of *in vivo* human skin was found effective in *in vivo* human palm [13, 30] and finger [31], in which the thickness of SC is thicker than the volar forearm. In this studies, the SC thicknesses of the inner side of forearm were all thinner than 21 μm. Weaker scattering in the thin SC might make the OC effect less observable after application.

Still, we successfully achieved the optical clearing of the *in vivo* human skin by using topical application with 50% glycerol after long application time. After the glycerol application, no photodamage or the destruction of the skin structure was observed. This true noninvasive method with low concentration glycerol (50%) is safer than other methods in previous studies which adopted invasive methods that made the skin suppurate, necrose, or develop erythema [14, 48, 51]. Furthermore, in case I50-T180-1, the glycerol diffused into the viable epidermis and enhanced the image intensity at the dermis, proved

doi:10.6342/NTU202000120

the possibility OC effect beyond the SC. We found different effects of the optical clearing in different volunteers, indicating that the optical clearing efficacy strongly depends on human factor and mainly depends on the individual difference of each volunteer.

doi:10.6342/NTU202000120

Chapter 8 Summary

In the previous studies, the mechanisms of the skin optical clearing still not be well-understood. In this study, the mechanisms and effects of the *ex vivo* and *in vivo* optical clearing were investigated by HGM which combined both SHG and THG. The optical clearing was first studied by combined these two different image techniques. SHG is a beacon to accumulate the reduction of the scattering. On the other hand, the THG intensity variation strongly based on its homogeneity sensitivity. We investigated the optical clearing by this unprecedented approach with a statistic analysis, to reveal the detail mechanisms of the optical clearing.

In *ex vivo* experiments, nine different volunteers were separated into four different case types to study the OC. Based on the different refractive indices between 100% and 50% glycerol, the THG intensity variation showed different consequences. We first addressed the optical clearing by using THG. It was also a new approach to provide information of OCAs diffusion. The topical application with the 50% glycerol, which was a safe method for the clinical, showed minimal optical efficacy. In the skin area with a thicker SC, the more enhancement of the THG intensity at the epidermis. The thickness of the skin and the diffusion depth of the glycerol played a critical role in the optical clearing.

doi:10.6342/NTU202000120

Based on the results of the ex vivo experiments, we further studied the *in vivo* optical clearing, especially at the skin area with a thin SC, volar forearm. In *in vivo* experiments, eight volunteers were separated into four different applying time to study the OC. In most volunteers, the effect of the optical clearing was not obvious. With and within 90 minutes application, only one case was found the optical clearing with significant shrinkage of the skin. After 180 minutes application, two of three cases were found the effect of the OC. There was a higher probability to witness the optical clearing after a longer applying time. Although it was not obvious OC effect in *in vivo* experiment, we still found OC effect beyond the SC in one of the volunteers. We supposed that the metabolism and blood circulation would decrease the OC efficacy, and it also strongly depended on the individual difference of the volunteers. The *in vivo* OC in the skin area with a thin SC still needs more exploitation.

Overall, in this study, the optical clearing effects were obvious in the *ex vivo* experiments. We studied many different skin areas to reveal the mechanisms of the OC. The OC was effective at different skin areas *ex vivo*. However, we didn't study the OC effect at the same site continuously. It was challenging to observe the effect of the OC continuously at one same skin site, especially for the human in vivo with such a long experiment time. The next step of this research is to observe the OC continuously at the

doi:10.6342/NTU202000120

same skin site. The most detail information of the OC, and its relationship between the image intensity variation and the OCAs diffusion can be better revealed and studied.

doi:10.6342/NTU202000120

References

1. A. Forli, D. Vecchia, N. Binini, F. Succol, S. Bovetti, C. Moretti, F. Nespoli, M. Mahn, C. A. Baker, M. M. Bolton, O. Yizhar, and T. Fellin, “Two-photon bidirectional control and imaging of neuronal excitability with high spatial resolution in vivo,” Cell Rep. **22**, 3087-3098 (2018).
2. T. H. Tsai, S. P. Tai, W. J. Lee, H. Y. Huang, Y. H. Liao, and C. K. Sun, “Optical signal degradation study in fixed human skin using confocal microscopy and higher-harmonic optical microscopy,” Opt. Express **14**, 749-758 (2006).
3. V. V. Tuchin, I. L. Maksimova, D. A. Zimnyakov, I. L. Kon, A. H. Mavlyutov, and A. A. Mishin, “Light propagation in tissues with controlled optical properties,” J. Biomed. Opt. **2**, 401-417 (1997).
4. H. Zhong, Z. Guo, H. Wei, C. Zeng, H. Xiong, Y. He, and S. Liu, “In vitro study of ultrasound and different-concentration glycerol-induced changes in human skin optical attenuation assessed with optical coherence tomography,” J. Biomed. Opt. **15**, 036012 (2010).
5. A. Sdobnov, M. E. Darvin, J. Lademann, and V. Tuchin, “A comparative study of ex vivo skin optical clearing using two-photon microscopy,” J Biophotonics **10**, 1115-1123 (2017).
6. Z. Mao, D. Zhu, Y. Hu, X. Wen, and Z. Han, “Influence of alcohols on the optical clearing effect of skin in vitro,” J. Biomed. Opt. **13**, 1-6 (2008).
7. T. Yu, X. Wen, V. V. Tuchin, Q. Luo, and D. Zhu, “Quantitative analysis of dehydration in porcine skin for assessing mechanism of optical clearing,” J. Biomed. Opt. **16**, 095002 (2011).
8. V. Genin, D. Tuchina, A. J. Sadeq, E. Genina, V. Tuchin, and A. Bashkatov, “Ex vivo

doi:10.6342/NTU202000120

investigation of glycerol diffusion in skin tissue," Journal of Biomedical Photonics & Engineering **2**, 010303 (2016).

9. O. Vargas, E. K. Chan, J. K. Barton, H. G. Rylander, and A. J. Welch, "Use of an agent to reduce scattering in skin," Lasers Surg. Med. **24**, 133-141 (1999).
10. M. Kohl, M. Cope, M. Essenpreis, and D. Böcker, "Influence of glucose concentration on light scattering in tissue-simulating phantoms," Opt. Lett. **19**, 2170-2172 (1994).
11. J. S. Maier, S. A. Walker, S. Fantini, M. A. Franceschini, and E. Gratton, "Possible correlation between blood glucose concentration and the reduced scattering coefficient of tissues in the near infrared," Opt. Lett. **19**, 2062-2064 (1994).
12. H. Liu, B. Beauvoit, M. Kimura, and B. Chance, "Dependence of tissue optical properties on solute-induced changes in refractive index and osmolarity," J. Biomed. Opt. **1**, 200-211 (1996).
13. R. K. Wang, X. Xu, Y. He, S. G. Proskurin, R. K. Wang, J. B. Elder, J. C. Hebden, A. V. Priezzhev, and V. V. Tuchin, "Optical clearing of in vivo human skin with hyperosmotic chemicals investigated by optical coherence tomography and near-infrared reflectance spectroscopy," presented at the Proc. SPIE 5486,129-135 (2004).
14. V. V. Tuchin, S. P. Chernova, N. y. V. Kuznetsova, A. B. Pravdin, and V. V. Tuchin, "Dynamics of optical clearing of human skin in vivo," presented at the Proc. SPIE 4162,227-235 (2000).
15. H. Zhong, Z. Guo, H. Wei, L. Guo, C. Wang, Y. He, H. Xiong, and S. Liu, "Synergistic effect of ultrasound and thiazone-peg 400 on human skin optical clearing in vivo," Photochem. Photobiol. **86**, 732-737 (2010).
16. X. Xu, and Q. Zhu, "Feasibility of sonophoretic delivery for effective skin optical

doi:10.6342/NTU202000120

clearing," IEEE Trans. Biomed. Eng. **55**, 1432-1437 (2008).

17. V. V. Tuchin, G. B. Altshuler, A. A. Gavrilova, A. B. Pravdin, D. Tabatadze, J. Childs, and I. V. Yaroslavsky, "Optical clearing of skin using flash lamp-induced enhancement of epidermal permeability," Lasers Surg. Med. **38**, 824-836 (2006).
18. C. Liu, Z. Zhi, V. V. Tuchin, Q. Luo, and D. Zhu, "Enhancement of skin optical clearing efficacy using photo-irradiation," Lasers Surg. Med. **42**, 132-140 (2010).
19. I. V. Meglinskii, E. A. Genina, D. Y. Churmakov and V. V. Tuchin, "Study of the possibility of increasing the probing depth by the method of reflection confocal microscopy upon immersion clearing of near-surface human skin layers," Quantum Electronics **32**, 875-882 (2002).
20. A. Majdzadeh, Z. Wu, H. Lui, D. I. McLean, and H. Zeng, "Investigation of optically cleared human skin in combined multiphoton and reflectance confocal microscopy," Optics in the Life Sciences, NM4C.6 (2015).
21. E. Song, Y. Ahn, J. Ahn, S. Ahn, C. Kim, S. Choi, R. M. Boutilier, Y. Lee, P. Kim, and H. Lee, "Optical clearing assisted confocal microscopy of ex vivo transgenic mouse skin," Optics & Laser Technology **73**, 69-76 (2015).
22. R. Cicchi, F. S. Pavone, D. Massi, and D. D. Sampson, "Contrast and depth enhancement in two-photon microscopy of human skin ex vivo by use of optical clearing agents," Opt. Express **13** (2005).
23. V. Hovhannisyan, P. S. Hu, S. J. Chen, C. S. Kim, and C. Y. Dong, "Elucidation of the mechanisms of optical clearing in collagen tissue with multiphoton imaging," J. Biomed. Opt. **18**, 046004 (2013).
24. B. Choi, N. Kollias, H. Zeng, H. W. Kang, B. J. F. Wong, J. F. Ilgner, G. J. Tearney, K. W. Gregory, L. Marcu, M. C. Skala, P. J. Campagnola, A. Mandelis, M. D. Morris, R. Samatham, N. K. Wang, and S. L. Jacques, "Investigation of the effect of hydration

doi:10.6342/NTU202000120

on dermal collagen in ex vivo human skin tissue using second harmonic generation microscopy," presented at the Photonic Therapeutics and Diagnostics XII (2016).

25. T. Son, and B. Jung, “Cross-evaluation of optimal glycerol concentration to enhance optical tissue clearing efficacy,” Skin Res. Technol. **21**, 327-332 (2015).

26. R. K. Wang, X. Xu, V. V. Tuchin, and J. B. Elder, “Concurrent enhancement of imaging depth and contrast for optical coherence tomography by hyperosmotic agents,” J. Opt. Soc. Am. B **18**, 948-953 (2001).

27. C. G. Rylander, O. F. Stumpp, T. E. Milner, N. J. Kemp, J. M. Mendenhall, K. R. Diller, and A. J. Welch, “Dehydration mechanism of optical clearing in tissue,” J. Biomed. Opt. **11**, 041117 (2006).

28. K. V. Larin, M. G. Ghosn, A. N. Bashkatov, E. A. Genina, N. A. Trunina, and V. V. Tuchin, “Optical clearing for oct image enhancement and in-depth monitoring of molecular diffusion,” IEEE Journal of Selected Topics in Quantum Electronics **18**, 1244-1259 (2012).

29. X. Wen, S. L. Jacques, V. V. Tuchin, and D. Zhu, “Enhanced optical clearing of skin in vivo and optical coherence tomography in-depth imaging,” J. Biomed. Opt. **17**, 066022 (2012).

30. X. Guo, Z. Guo, H. Wei, H. Yang, Y. He, S. Xie, G. Wu, X. Deng, Q. Zhao, and L. Li, “In vivo comparison of the optical clearing efficacy of optical clearing agents in human skin by quantifying permeability using optical coherence tomography,” Photochem. Photobiol. **87**, 734-740 (2011).

31. S. G. Proskurin, and I. V. Meglinski, “Optical coherence tomography imaging depth enhancement by superficial skin optical clearing,” Laser Physics Letters **4**, 824-826 (2007).

doi:10.6342/NTU202000120

32. M. A. Fox, D. G. Diven, K. Sra, A. Boretsky, T. Poonawalla, A. Readinger, M. Motamedi, and R. J. McNichols, “Dermal scatter reduction in human skin: A method using controlled application of glycerol,” Lasers Surg. Med. **41**, 251-255 (2009).

33. X. X. Q. Zhu, “Sonophoretic delivery for contrast and depth improvement in skin optical coherence tomography,” IEEE Journal of Selected Topics in Quantum Electronics **14**, 56 - 61 (2008).

34. E. A. Genina, N. S. Ksenofontova, A. N. Bashkatov, G. S. Terentyuk, and V. V. Tuchin, “Study of the epidermis ablation effect on the efficiency of optical clearing of skin in vivo,” Quantum Electronics **47**, 561-566 (2017).

35. A. Y. Sdobnov, V. V. Tuchin, J. Lademann, and M. E. Darvin, “Confocal raman microscopy supported by optical clearing treatment of the skin—influence on collagen hydration,” J. Phys. D: Appl. Phys. **50** (2017).

36. R. F. Rushmer, K. J. K. Buettner, J. M. Short, and G. F. Odland, “The skin,” Science **154**, 343-348 (1966).

37. M. A. Lampe, A. L. Burlingame, J. Whitney, M. L. Williams, B. E. Brown, E. Roitman, and P. M. Elias, “Human stratum corneum lipids: Characterization and regional variations,” J. Lipid Res. **24**, 120-130 (1983).

38. R. R. Wickett, and M. O. Visscher, “Structure and function of the epidermal barrier,” Am. J. Infect. Control **34**, S98-S110 (2006).

39. M. B. Brown, G. P. Martin, S. A. Jones, and F. K. Akomeah, “Dermal and transdermal drug delivery systems: Current and future prospects,” Drug Deliv. **13**, 175-187 (2006).

40. G. J. Tearney, M. E. Brezinski, J. F. Southern, B. E. Bouma, M. R. Hee, and J. G. Fujimoto, “Determination of the refractive index of highly scattering human

doi:10.6342/NTU202000120

tissue by optical coherence tomography," Opt. Lett. **20**, 2258-2260 (1995).

41. J. W. Fluhr, M. Gloor, L. Lehmann, S. Lazzerini, F. Distante, and E. Berardesca, "Glycerol accelerates recovery of barrier function in vivo," Acta Derm. Venereol. **79**, 418-421 (1999).

42. D. L. Bissett, and J. F. Mcbride, "Skin conditioning with glycerol," J. Soc. Cosmet. Chem. **35**, 345-350 (1984).

43. R. L. Evans, G. A. Turner, S. Bates, T. Robinson, D. Arnold, R. E. Marriott, P. D. A. Pudney, E. Y. M. Bonnist, and D. Green, "Human axillary skin condition is improved following incorporation of glycerol into the stratum corneum from an antiperspirant formulation," Arch. Dermatol. Res. **309**, 739-748 (2017).

44. C. E. Rommel, C. Dierker, L. Schmidt, S. Przibilla, G. von Bally, B. Kemper, and J. Schnekenburger, "Contrast-enhanced digital holographic imaging of cellular structures by manipulating the intracellular refractive index," J. Biomed. Opt. **15**, 041509 (2010).

45. S. Plotnikov, V. Juneja, A. B. Isaacson, W. A. Mohler, and P. J. Campagnola, "Optical clearing for improved contrast in second harmonic generation imaging of skeletal muscle," Biophys. J. **90**, 328-339 (2006).

46. B. Choi, L. Tsu, E. Chen, T. S. Ishak, S. M. Iskandar, S. Chess, and J. S. Nelson, "Determination of chemical agent optical clearing potential using in vitro human skin," Lasers Surg. Med. **36**, 72-75 (2005).

47. G. Vargas, K. F. Chan, S. L. Thomsen, and A. J. Welch, "Use of osmotically active agents to alter optical properties of tissue: Effects on the detected fluorescence signal measured through skin," Lasers Surg. Med. **29**, 213-220 (2001).

48. D. S. Jäger, Z. Mao, D. Liu, Z. Han, X. Wen, P. Shum, Q. Luo, and D. Zhu, "Influence of glycerol with different concentrations on skin optical clearing and

doi:10.6342/NTU202000120

morphological changes in vivo," presented at the Proc. SPIE 7278(2008).

49. X. Xu, and R. K. Wang, “The role of water desorption on optical clearing of biotissue: Studied with near infrared reflectance spectroscopy,” Med. Phys. **30**, 1246-1253 (2003).

50. M. H. Khan, B. Choi, S. Chess, K. M. Kristen, J. McCullough, and J. S. Nelson, “Optical clearing of in vivo human skin: Implications for light-based diagnostic imaging and therapeutics,” Lasers Surg. Med. **34**, 83-85 (2004).

51. E. I. Galanzha, V. V. Tuchin, A. V. Solovieva, T. V. Stepanova, Q. Luo, and H. Cheng, “Skin backreflectance and microvascular system functioning at the action of osmotic agents,” J Phys D Appl Phys **36**, 1739-1746 (2003).

52. X. Wen, Z. Mao, Z. Han, V. V. Tuchin, and D. Zhu, “In vivo skin optical clearing by glycerol solutions: Mechanism,” J Biophotonics **3**, 44-52 (2010).

53. Y. Gu, Y. Tang, X. Li, Q. Luo, L. Deng, D. Zhu, T. Yu, and W. Feng, "In vivo monitoring optical clearing process of skin using two-photon microscopy," presented at the Proc. SPIE 10820 (2018).

54. X. Liu, and B. Chen, “In vivo experimental study on the enhancement of optical clearing effect by laser irradiation in conjunction with a chemical penetration enhancer,” Applied Sciences **9**, 542 (2019).

55. D. Zhu, J. Wang, Z. Zhi, X. Wen, and Q. Luo, “Imaging dermal blood flow through the intact rat skin with an optical clearing method,” J. Biomed. Opt. **15**, 026008 (2010).

56. J. Squier, and M. Müller, “High resolution nonlinear microscopy: A review of sources and methods for achieving optimal imaging,” Rev. Sci. Instrum. **72**, 2855-2867 (2001).

57. Y. Barad, H. Eisenberg, M. Horowitz, and Y. Silberberg, “Nonlinear scanning laser

doi:10.6342/NTU202000120

microscopy by third harmonic generation," Appl. Phys. Lett. **70**, 922-924 (1997).

58. C. K. Sun, C. T. Kao, M. L. Wei, S. H. Chia, F. X. Kärtner, A. Ivanov, and Y. H. Liao, "Slide-free imaging of hematoxylin-eosin stained whole-mount tissues using combined third-harmonic generation and three-photon fluorescence microscopy," Journal of Biophotonics **12**, e201800341 (2019).

59. C. K. Sun, S. W. Chu, S. P. Tai, S. Keller, A. Abare, U. K. Mishra, and S. P. Denbaars, "Mapping piezoelectric-field distribution in gallium nitride with scanning second-harmonic generation microscopy," Scanning **23**, 182-192 (2001).

60. J. H. Lai, Y. H. Liao, and C. K. Sun, "Investigating the optical clearing effects and mechanisms in ex vivo human skin by harmonic generation microscopy," Subittmed to Biomedical Optical Express (2020), Manuscript ID: 385788.

61. S. Y. Chen, S. U. Chen, H. Y. Wu, W. J. Lee, Y. H. Liao, and C. K. Sun, "In vivo virtual biopsy of human skin by using noninvasive higher harmonic generation microscopy," IEEE Journal of Selected Topics in Quantum Electronics **16**, 478-492 (2010).

62. Y. H. Liao, Y. H. Su, Y. T. Shih, W. S. Chen, S. H. Jee, and C. K. Sun, "In vivo third-harmonic generation microscopy study on vitiligo patients," J. Biomed. Opt. **25**, 014504 (2019).

63. M. R. Tsai, Y. H. Cheng, J. S. Chen, Y. S. Sheen, Y. H. Liao, and C. K. Sun, "Differential diagnosis of nonmelanoma pigmented skin lesions based on harmonic generation microscopy," J. Biomed. Opt. **19**, 036001 (2014).

64. M. R. Tsai, S. Y. Chen, D. B. Shieh, P. J. Lou, and C. K. Sun, "In vivo optical virtual biopsy of human oral cavity with harmonic generation microscopy," Biomed. Opt. Express **2**, 2317-2328 (2011).

65. Y. H. Liao, S. Y. Chen, S. Y. Chou, P. H. Wang, M. R. Tsai, and C. K. Sun,

doi:10.6342/NTU202000120

"Determination of chronological aging parameters in epidermal keratinocytes by in vivo harmonic generation microscopy," Biomed. Opt. Express **4**, 77-88 (2013).

66. Z. Gajinov, M. Matić, S. Prćić, and V. Đuran, "Optical properties of the human skin / optičke osobine ljudske kože," Serbian Journal of Dermatology and Venerology **2**, 131-136 (2010).

67. L. Guo, R. Shi, C. Zhang, D. Zhu, Z. Ding, and P. Li, "Optical coherence tomography angiography offers comprehensive evaluation of skin optical clearing in vivo by quantifying optical properties and blood flow imaging simultaneously," J. Biomed. Opt. **21**, 081202 (2016).

68. D. Yelin, and Y. Silberberg, "Laser scanning third-harmonic-generation microscopy in biology," Opt. Express **5**, 169-175 (1999).

69. J. A. Squier, M. Müller, G. J. Brakenhoff, and K. R. Wilson, "Third harmonic generation microscopy," Opt. Express **3**, 315-324 (1998).

70. I. F. Çilesiz, and A. J. Welch, "Light dosimetry: Effects of dehydration and thermal damage on the optical properties of the human aorta," Appl. Opt. **32**, 477-487 (1993).

71. E. A. Genina, A. N. Bashkatov, and V. V. Tuchin, "Tissue optical immersion clearing," Expert Rev. Med. Devices **7**, 825-842 (2010).

72. G. P. Association, *Physical properties of glycerine and its solutions* (1963).

73. R. J. Scheuplein, and I. H. Blank, "Permeability of the skin," Physiol. Rev. **51**, 702-747 (1971).

74. P. M. Elias, E. R. Cooper, A. Korc, and B. E. Brown, "Percutaneous transport in relation to stratum corneum structure and lipid composition," J. Invest. Dermatol. **76**, 297-301 (1981).

75. GLYSOLID, "Http://www.Glysolid.Com/about-glysolid.Html."

doi:10.6342/NTU202000120

doi:10.6342/NTU202000120